DURBAN UNIVERSITY OF TECHNOLOGY
INYUVESI YASETHEKWINI YEZOBUCHWEPHESHE

Oxidative dehydrogenation of n-octane using dealuminated faujasite zeolites

Submitted in fulfilment of the academic requirements for the Master of Applied Science degree in the Faculty of Applied Sciences at the Durban University of Technology

Archie Sifundo Mpotulo

APRIL 2024

Supervisor: Prof HB Friedrich Date: 22/4/2024

Co-Supervisor: Dr SS Ndlela Date: 22/4/2024

ABSTRACT

Commercially obtained NaY was modified by a dealumination process using different solutions containing specific concentrations of citric acid, ethylenediaminetetraacetic acid disodium (EDTA-2Na), and a mixture of both EDTA-2Na and citric acid. The three prepared catalysts were then used to study the effect of dealumination on oxidative dehydrogenation (ODH) of n-octane. Dealumination was carried out to strengthen the zeolites acid sites, which will lead to an increased activity towards the oxidation of n-octane. Results from these showed that removing the framework and extra framework aluminium in the NaY zeolites increases the intrinsic acidity, which then led to increased conversion in the ODH of n-octane, with the catalyst prepared by the mixture of both EDTA-2Na and citric acid recording the highest conversion of just above 10 %. The conversion was ascribed to the removal of both the non- and framework aluminium, which leads to improved pore volumes and surface area. All the three prepared catalysts were mostly selective towards the carbon oxides (CO_x) products which was due to the absence of the ODH promoting metal.

To induce the ODH promoting properties on the prepared catalysts (NaY[AL] for acid leaching using citric acid, NaY[CAT] for chelating agent treatment using EDTA-2Na and NaY[CT] for complex treatment using citric acid and EDTA-2Na), they were then further modified by introducing gallium using a modified ionic exchange procedure. Gallium has been shown by previous studies to be a promising ODH active metal. All the prepared catalysts were exchanged by 2 %wt of gallium which contributed to the increase of about 2 % for all the prepared catalysts when they tested were under similar ODH conditions with the first three batches of dealuminated NaY. The introduction of framework gallium also decreased side reactions such as the cyclization and cracking reactions, due to the reduction in medium to strong acid sites. The CO_x selectivity for the catalysts decreased from above 90 % to just below 85 %. This was not the case for the highest acidic NaY[AL], which showed no decrease in the CO_x selectivity. Though there was a slight improvement on the olefins selectivity after gallium introduction, CO_x production was still favoured by the catalysts. To mitigate this, barium, a basic metal was also introduced into the prepared Ga-NaY catalysts. Barium was also introduced using ionic exchange, and 1.5 %wt was introduced. Barium is known for inducing basic sites which facilitates the quick desorption of ODH products, leading to suppressed overoxidation. Due to subsequent ionic exchange procedures done on the catalysts, the morphology of the catalysts was altered, with the NaY zeolites losing their cubic shape and also clustering. The effect of Ba for all the catalysts was not much, as only BaGa-NaY[CT]

showed a 4 % decrease in the CO_x activity. All the catalysts showed increased cracked products and oxygenates, but not much improvement in the olefins and aromatic products.

The findings of this study showed that the behavior of the zeolite catalysts in the ODH of alkanes depends both on the physical and chemical properties of the catalyst. Acidity is a big factor when dealing with zeolites, as the activity and selectivity of the catalysts depends on the alteration of this feature. A high concentration of strong acid sites alone can activate the paraffin of interest, however Lewis acid sites induced by a reducible gallium metal are responsible for improved octene activity, selectivity and stability of the catalysts through the facilitation of coke burning on the surface of the catalyst.

ACKNOWLEDGEMENTS

1. Dr. S.S. Ndlela and Prof. H.B. Friedrich, my supervisors, for their assistance and guidance.
2. My financial sponsor, National Research Foundation (NRF).
3. Durban University of Technology, Department of chemistry for giving me a platform to further my studies.
4. Catalysis Research Group for their support and assistance with the experimental aspect of the project. (UKZN)
5. EM unit at University of KwaZulu-Natal (Westville Campus) for SEM analysis and Clariant (Richards Bay) for XRF analysis.

PREFACE

All the experimental work described in this thesis was performed at University of KwaZulu Natal in the School of Chemistry & Physics, Westville Campus, Durban. The experimental work was done from July 2022 to November 2023 under the supervision of Dr S.S. Ndlela and Prof. H.B. Friedrich.

The work presented in this thesis represents original work by the author that has not been done or published elsewhere by others. The work of others that has been used in this work is fully acknowledged.

Archie S. Mpotulo

PLAGIARISM DECLARATION

I, Archie Sifundo Mpotulo declare that:

1. The research reported in this dissertation, except where otherwise indicated, is my original research.
2. This dissertation has not been submitted for any degree or examination at any other university.
3. This dissertation does not contain other persons' data, pictures, graphs, or other information unless specifically acknowledged as being sourced from other persons.
4. This dissertation does not contain other persons' writing unless specifically acknowledged as being sourced from other researchers. Where other written sources have been quoted, then:

a. Their words have been re-written, but the general information attributed to them has been referenced.

b. Where their exact words have been used, then their writing has been placed in italics and inside quotation marks and referenced.

5. This thesis does not contain text, graphics, or tables copied and pasted from the Internet unless specifically acknowledged, and the source being detailed in the thesis and the References sections.

_____

Signature

ARCHIE SIFUNDO MPOTULO

Name (in capital letters)

21937067

Student number

Signed:_____ Name: HB Friedrich Date: 22/04/24

Signed: Name: SS Ndlela Date: 22/04/24

CONFERENCE CONTRIBUTION

The following conferences have been attended where part of this work was presented:

1. CATSA Conference 2022, Drakensburg, presented a poster entitled “The effect of dealumination on the physicochemical properties of NaY zeolite”.

2. Faculty of Applied Sciences Research Day 2022, Durban (DUT), presented a poster entitled “Oxidative dehydrogenation of n-octane using gallium containing dealuminated NaY zeolites”.

ABBREVIATIONS

BET	Brunauer-Emmett-Teller
C-H	Carbon – hydrogen bond
CHA	Chabazite
C:O	Carbon to oxygen ration
CO_x	Carbon oxides
CVD	Chemical vapour deposition
DH	Dehydrogenation
FAU	Faujasite
FT	Fischer-Tropsch
FT-IR	Fourier-transform infrared spectroscopy
GHSV	Gas hourly space velocity
IE	Ion-exchange
IS	Isomorphic substitution
MCM	Mobil composition of matter
LTA	Linde Type A
MFI	Mobil type five
MOF	Meta organic framework
MR	Membered Ring of a zeolite
MvK	Mars and van Krevelen
$O^-/O^{\delta-}$	Electrophilic oxygen species derived from O_2
O^{2-}	Nucleophilic metal oxide lattice oxygen anion
ODH	Oxidative dehydrogenation
P-XRD	Powder X-ray diffraction

XRF	X-ray fluorescence
REDOX	Reduction and oxidation
SBA	Santa Barbara Amorphous type material
SEM-EDX	Scanning electron microscopy, energy dispersive X-ray analysis
Sil	Silicalite
SOD	Sodalite
TCD	Thermal conductivity detector
TPD	Temperature programmed desorption
TPR	Temperature programmed reduction
ZSM-5	Zeolite socony mobil number 5
Å	Angstroms

LIST OF FIGURES

LIST OF SCHEMES

LIST OF TABLES

TABLE OF CONTENTS

Chapter 1

Introduction

1.1 Catalysis

1.1.1 Definition of Catalysis

Catalysis is the process of increasing the speed of a chemical reaction through the use of a catalyst. A catalyst on the other hand refers to a substance designed to increase the rate of a chemical reaction without it being consumed in a process. As a result, the catalyst is acceptable for repeated cycles in its application in a chemical process. In a catalytic reaction, an uncatalyzed reaction pathway is replaced by a new one that has a lower activation energy. As a result, the reaction can proceed more easily, which frequently leads to higher reaction rates and efficiency. [1]

1.1.2 Categories of Catalysis

Homogeneous and heterogeneous catalysis are the two most prevalent and often utilized forms of catalysis. The phrase "homogeneous catalysis" refers to a catalytic system in which the catalyst and reactants are both in the same phase and most often in solution. Contrarily, heterogeneous catalysis refers to the system in which the substrate and catalyst are in dissimilar phases, most often solid and gaseous phase. [2] The ease of the catalyst and the products separation results in lower operating costs and quicker chemical processes, when heterogeneous catalysis is carried out, and this is important in the production of industrial chemicals. [3,4] Heterogeneously catalysed reactions in industry fall into four categories: organic and inorganic product production, petrochemical and crude oil refining, environmental protection, and energy transformation processes. [5] Hydrogenation reactions, like aldehydes and ketones to alcohols using nickel, platinum, and nickel based catalysts, and methanol synthesis which uses copper supported on zinc oxide catalysts, hydrocracking of fuels on zeolites and nickel aluminosilicates, steam reforming and methanation which uses nickel supported on alumina catalysts are all examples of categories of inorganic and organic chemicals. [5-9]

Platinum and copper catalysts based on alumina are commonly used in the dehydrogenation (DH) of hydrocarbons, whereas palladium and copper chloride catalysts are used in the oxidation of ethylene to acetaldehyde. In the Fischer-Tropsch (FT) process, iron and cobalt-based catalysts are utilized to produce linear paraffins. [10] Mineral oil, which is a mixture of high carbon number alkanes, is a kind of liquid paraffin and is among the substances that are most prevalent in the world. Paraffins are also present in natural gas as methane. Most importantly, paraffins may be manufactured utilizing a range of technologies and processes as either a by-product or the main products. [11-13] For this reason, research on the activation of inert paraffins has increased over the years. There are now two well-established industrial procedures for the activation of paraffins: (hydro) cracking or reforming, and dehydrogenation. [14,15] These procedures have a number of drawbacks, including high energy requirements, selectivity control, coke formation, and thermodynamic limitations. [15,16] Due to its capacity to circumvent the difficulties associated with dehydrogenation reactions, oxidative dehydrogenation (ODH) has over the years received attention as a potential substitute method for the production of olefins. [17] In oxidative dehydrogenation, oxygen is used as the oxidant, making the reaction exothermic (**equation 1**), which in turn leads to reduced carbon deposition on the catalyst surface and thermodynamic limitations. [18]

$$\mathbf{C_nH_{2n+2} + \frac{1}{2}O_2 \rightarrow C_nH_{2n} + H_2O + heat} \qquad \mathbf{(1)}$$

In the subject of oxidative dehydrogenation (ODH), there are several well-established and well-acknowledged reaction mechanisms. The most often mentioned mechanism for the oxidative dehydrogenation reaction is the Mars van Krevelen (MvK) mechanism, in which the activity and selectivity of the catalyst is related to the reducibility of the catalyst. [19-21]

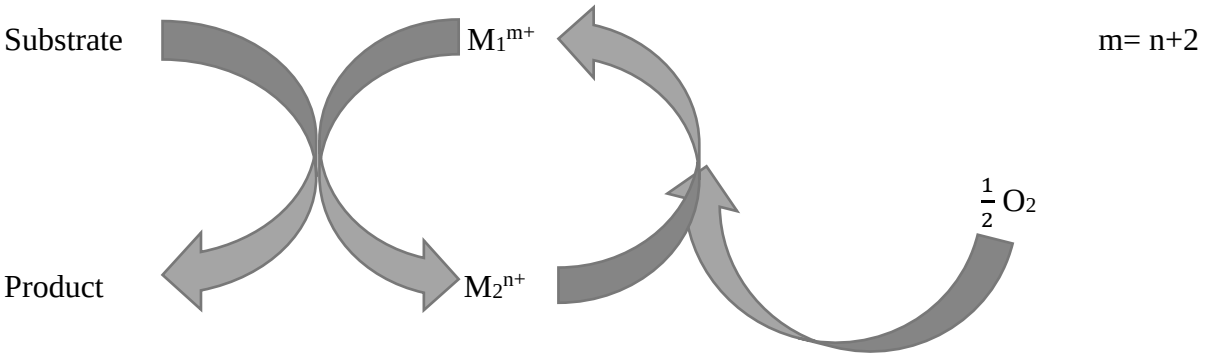

Figure 1.1. The Mars van Krevelen (MvK) mechanism, where oxygen is used as the oxidant in the reaction

Paraffins (feedstocks), in accordance with the MvK mechanism, reduce the catalyst by absorbing lattice oxygen, which is then reoxidized by the oxidant supplied along with the paraffin, (**Figure 1.1**). [19] Hence, ODH using a metal oxide catalysts is considered to proceed via the MvK mechanism. Two oxygen species may be formed during the ODH reaction: electron-deficient oxygen (O^-, O_2^- and O_2^{2-}) species and electron-rich oxygen species. The electron-rich lattice oxygen (O^{2-}) species that attacks the paraffin molecule, leading in the production of olefin and water, supports the MvK mechanism concept. The employment of an oxidant causes the creation of electron-deficient oxygen species, which causes the olefins to be overoxidized, resulting in the formation of carbon oxides (CO_x) and water. [22-24]

1.2 Zeolites

The material of interest for this study is a zeolite material which offers different chemistry compared to the metal oxide catalysts discussed above. In ODH reactions, zeolites are known to trigger the activation of the alkane's C-H bond via a surface oxide, yielding a metal-alkoxide and a surface hydroxyl. Subsequently, a β-hydrogen abstraction occurs, resulting in the formation of an alkene. To supply the oxidized metal site, the reduced metal oxide is oxidized by molecular oxygen to complete the catalytic cycle (**Scheme 1.1**). [25,26]

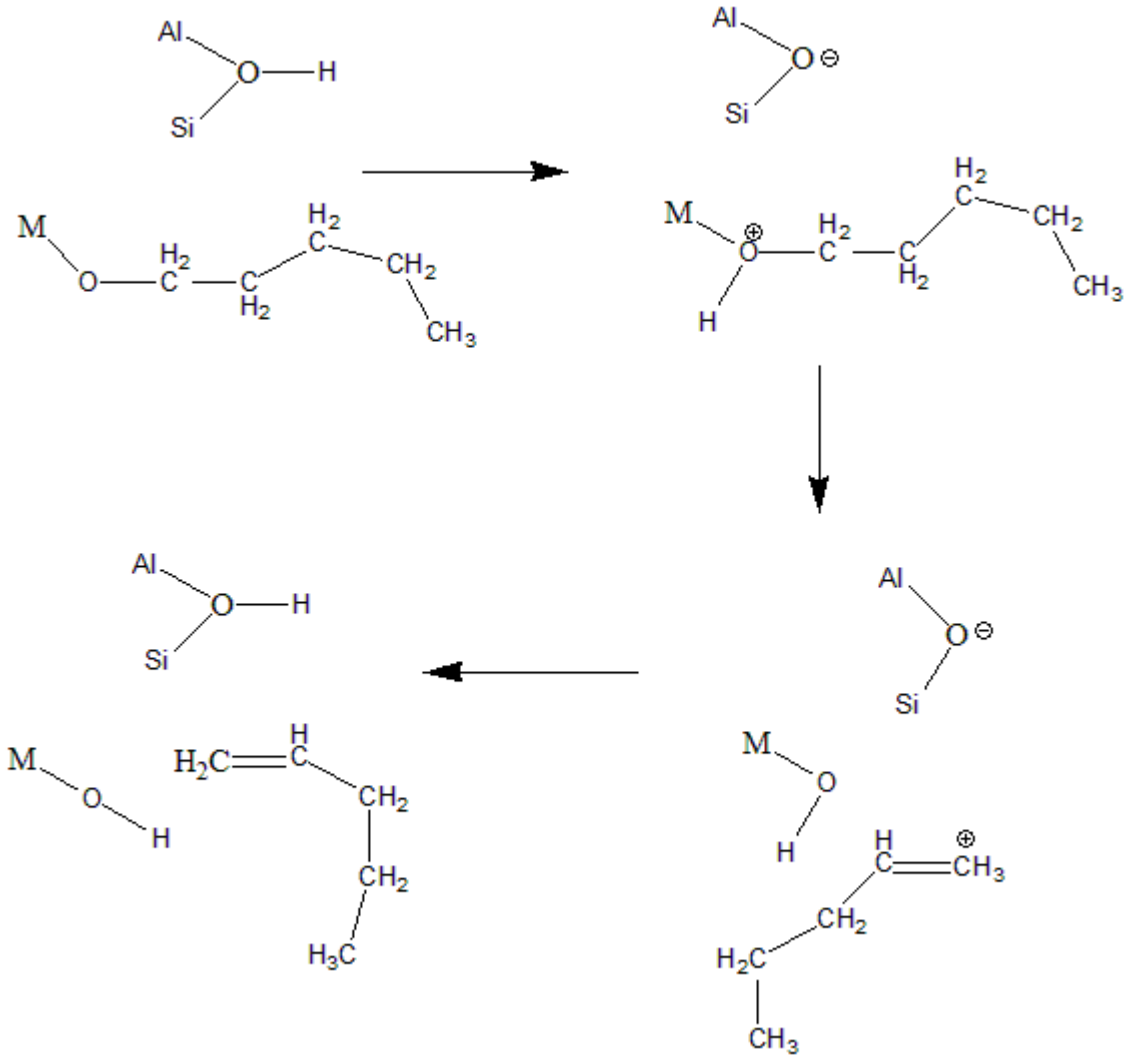

Scheme 1.1. β-Hydrogen abstraction reaction of metal pentoxide to form an alkene (C_5H_{10}) catalysed by a zeolitic acid site [25]

The formation of cation pairs $[C_3H_7\text{-}MH]^+\text{-}H^+$ (where M = Ga, Cr, Fe, etc.) at the Lewis acid sites of a metal-exchanged zeolite catalyst by the reversible, dissociative adsorption of an alkane molecule is the initial step when the paraffin molecule is activated by the monomolecular mechanism. This is followed by dehydrogenation that occurs through β-hydride elimination to produce an alkene and hydrogen gas (**Scheme 1.2**). [26-28]

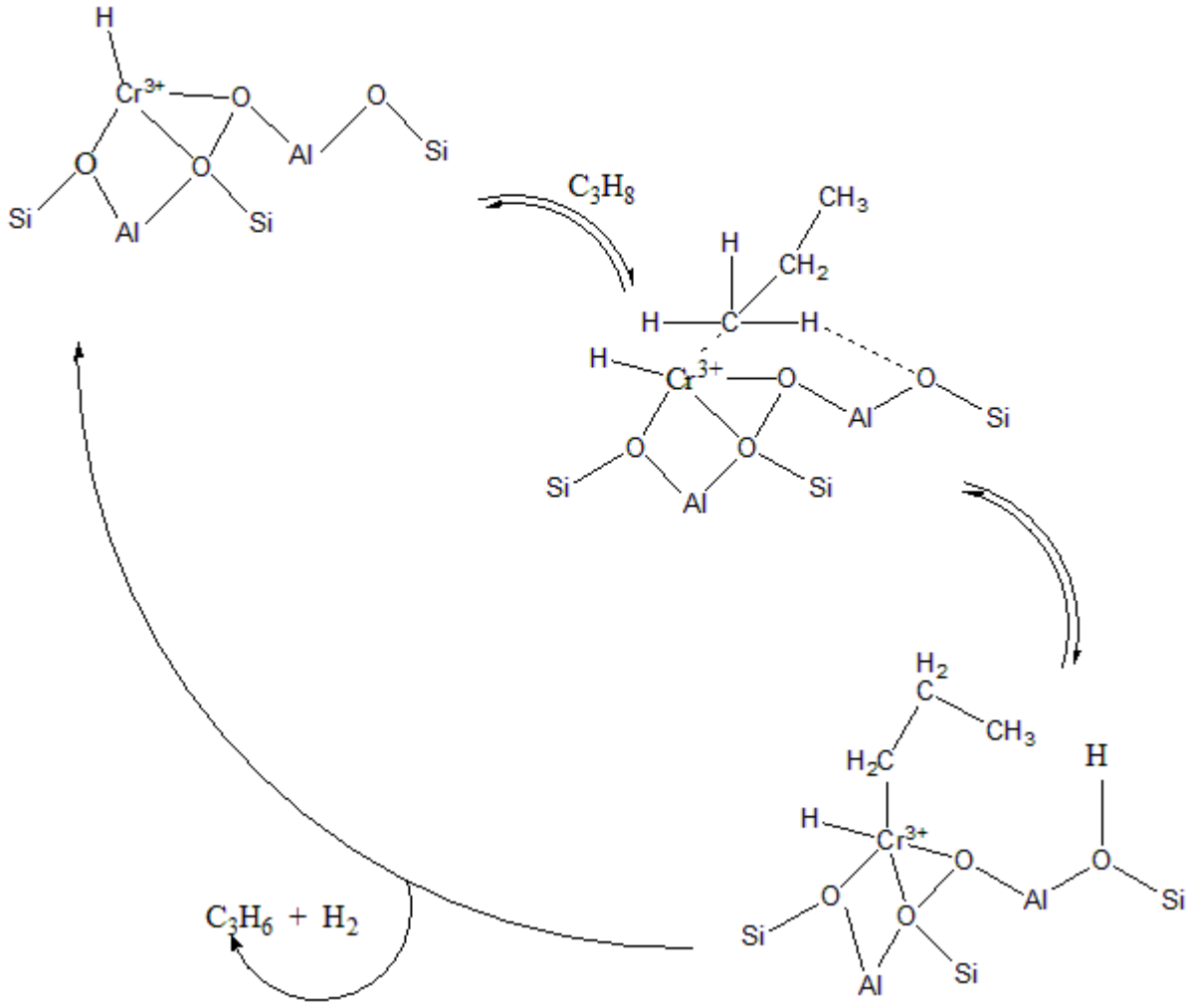

Scheme 1.2. A monomolecular mechanism for the C-H activation using zeolites [27]

In addition to converting the produced H_2 into H_2O, the presence of oxygen during the reaction also causes the carbonaceous species deposits on the catalyst surface to react, creating CO_x. Zeolite materials are of great importance in industry and are often used as absorbents in water treatments, isomerisation, cracking, and also as hydrocarbon synthesis catalysts. [29,30]

The term "zeolite," which derives from the Greek terms zeo and lithos, which indicate "boiling stones," was originally used by a Swedish mineralogist by the name of Cronstedt in 1756 when he discovered that stilbite loses water readily when heated. [30,31] Zeolites are aluminosilicate compounds that are crystalline, and hydrated, with three-dimensional structures that develop from a framework of tetrahedral $[SiO_4]^{4-}$ and $[AlO_4]^{5-}$ units, each of which is connected to another by an oxygen atom. Zeolites' feature of three-dimensional structures is made

up of molecular-sized pores. The framework is normally open and has cavities and channels where cations and water molecules can be found, [31-34] as well as openings that allow for the adsorption of small molecules. The cations can interchange often and to varying degrees with other cations due to their high mobility. [33] Zeolite is different from porous amorphous adsorbents in this way. [35]

Zeolite's general formula is $M_{x/n}$ $[(AlO_2)_x$ $(SiO_2)_y].wH_2O$; where n is the valence of the exchangeable non-framework cation M, $(AlO_2)_x$ $(SiO_2)_y$ are the framework components, wH_2O is adsorbed water, x and y are the total number of tetrahedra per unit cell, w is the number of water molecules per unit cell, and $M_{x/n}$ is the exchangeable non-framework cation. [32-34] Zeolite has a special capacity to adsorb small molecules and ions because it has bonded water in its crystal lattice, which vaporizes when heated. [35]

The zeolite framework structures are often divided into groups based on the individual units that make them up. The individual TO_4 tetrahedral units, where T is either Al or Si as indicated in **Figure 1.2**, are the primary building unit (PBU) of a zeolite structure. [36]

Figure 1.2. Representation of primary tetrahedral units of AlO_4 and SiO_4

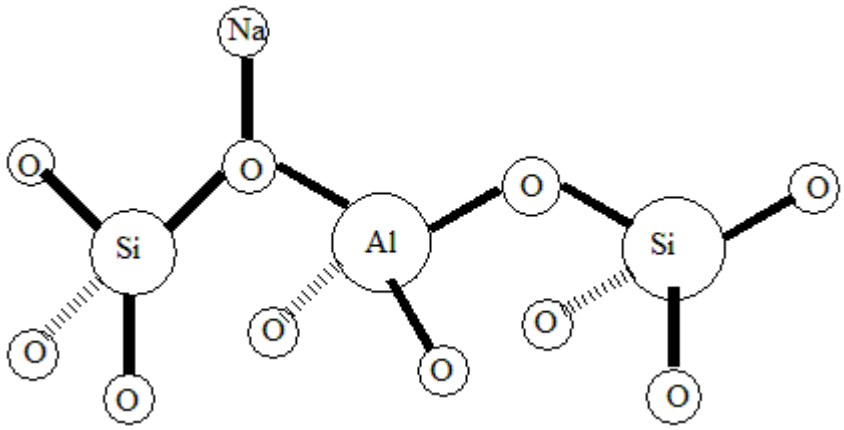

Figure 1.3. Representation of a primary tetrahedral unit of AlO_4 and SiO_4 bonded together to create a three-dimensional structure

As seen in **Figure 1.3**, the primary tetrahedral units of $[AlO_4]^{4-}$ and $[SiO_4]^{5-}$ are joined to each other by sharing oxygen to form secondary building units (SBU). There are therefore sixteen secondary building units that might exist. [37] The arrangement of the secondary building units causes rings with different numbers of Si and Al atoms, sometimes known as "T" atoms, to develop. 4-T to 12-T rings are the most prevalent. [37] Zeolites containing higher T-membered rings have also been synthesized, though to a lesser degree. [38-41] The size of the zeolites' micropores, which range from 4 to 12 Angstroms (Å), is determined by the amount of T atoms in the ring.

Zeolites' physical and chemical characteristics play a significant role in how beneficial they are in various applications. Since zeolites' major physical characteristic is porosity, they are used as molecular sieves. The well-defined three-dimensional networks of pores in zeolites can serve as reaction channels, and the addition of active sites boost their activity and selectivity. Zeolites' channel systems might be mono-, bi-, and tri-directional. [37,42] In general, zeolites are categorized as having 8 rings, 10 rings, or 12 rings as indicated in **Figure 1.3**, depending on how many tetrahedral atoms (TO-atoms) make up the circumference of the pores. A 10-ring could therefore be described as a 20-ring if the oxygen atoms connecting the T-atoms were also taken into account. Small pore zeolites typically have pore sizes between 3.0 Å and 4.5 Å, medium pore zeolites between 4.5 Å and 6.5 Å, and large pore zeolites up to 8.0 Å. [43]

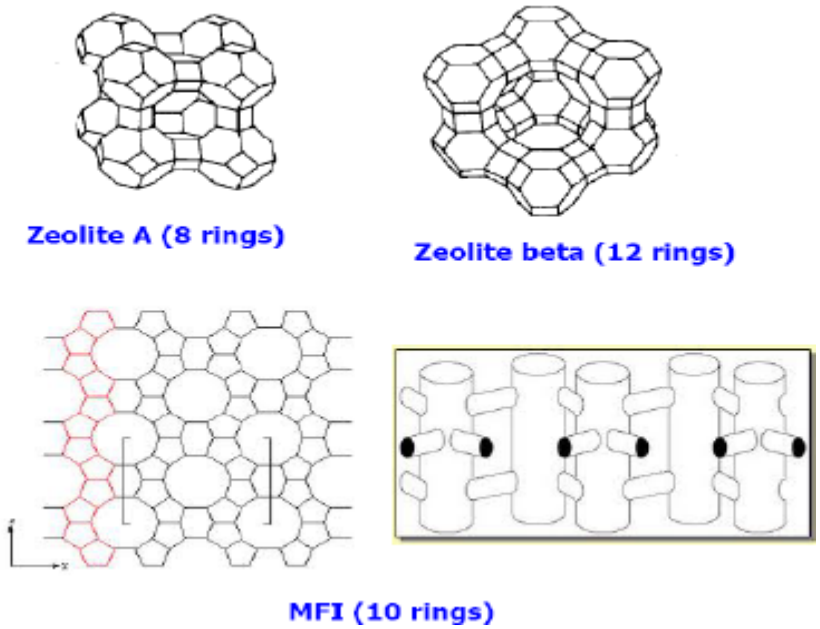

Figure 1.4. Zeolites with interconnected 8-, 10- and 12-ring pores [44]

The quantity of aluminium present in the zeolite's framework has a significant influence on both the chemical and physical characteristics of zeolites. The atomic Si/Al ratio is commonly used to indicate how much aluminium is contained in the zeolites framework. Zeolites having a Si/Al ratio greater than 10 are considered hydrophobic. This is due to the high silica content, which favours covalent Si-O-Si bridges on the inner surface of the zeolite. Zeolites having a Si/Al ratio of about 1 are considered low-silica zeolites and hydrophilic. This is due to its highly negatively charged framework and high concentration of cations or protons. Zeolites with Si/Al ratios between 1.5 and 10 are called intermediate silica zeolites. Additional unique characteristics of zeolitic materials are as follows:

- High surface area,
- High adsorption capacity,
- Molecular dimensions of the pores,
- Partitioning of reactants or products,
- Ability to modify the electronic characteristics of the active sites,
- Ability to pre-activate molecules while they are in the pores due to strong electric fields,
- Molecular confinement. [37,42]

Zeolites are easy to synthesize and modify. This makes zeolitic materials interesting materials. Different methods can be used to synthesize these materials, and this can be done under temperatures ranging from just above 50 ^{o}C to nearly 200 ^{o}C. [45-49] Zeolites are mostly synthesized via the well-known hydrothermal process, which is carried out inside a pressured Teflon reactor vessel. [47,48] Usually this requires a structure directing organic template, however, other researchers have demonstrated that a template free zeolite synthesis is feasible because organic templates are expensive and environmentally harmful. [50,51] In addition to hydrothermal synthesis, the prepared zeolites can be altered utilizing a variety of techniques to produce zeolites with various properties. In place of Si^{4+} or Al^{3+}, the zeolite framework can be modified by substituting alternative tetrahedrally coordinated ions, such as Ga^{3+}, B^{3+}, Ti^{4+}, or Fe^{3+}. The charge-balancing cations found in the adjacent pores balance the negative charge that is dispersed throughout the aluminosilicate structure's framework as a result of the tetrahedral AlO_4 units. This is crucial to the zeolite's ability to serve as a catalyst. The bonding of aluminium and silicon in the zeolite framework is based on Lowenstein's rule, which disallows

the bonding of Al-O-Al in the zeolite framework. Accordingly, there must be four silicate tetrahedrons for every aluminate tetrahedron. [52]

Ionic exchange, chemical vapor deposition (CVD), and impregnation are additional methods for zeolite post-synthesis modification. [53] The metals are coordinated differently in the zeolite for each synthesis method. This then affects the material's chemical properties including its catalytic activity. Therefore, an appropriate synthesis can be chosen to make a zeolite with a particular set of properties depending on the application.

Zeolites can also be modified to further control their acidity and/or shape selectivity. [54] Zeolites are susceptible to three main types of alterations: structural modifications, in which the framework SiO_2 /M_2O_3 (where M is Al or another metal cation like Fe, B, or Ga) is altered, which changes the acidity. Isomorphic substitution is an illustration of this kind of modification; the alteration of the zeolite's surface to further customize the pore opening size. Large organometallic species that cannot adsorb into the pore system might be added, and internal pore alterations that block or change structural acid sites and/or limit internal pore width would also fall under this category. The adsorption and subsequent disintegration of tiny metal hydrides in the zeolite serve as an illustration of this. [54,55]

Other post-synthesis modifications for zeolites include chemical etching and high-temperature calcination. [56,57]

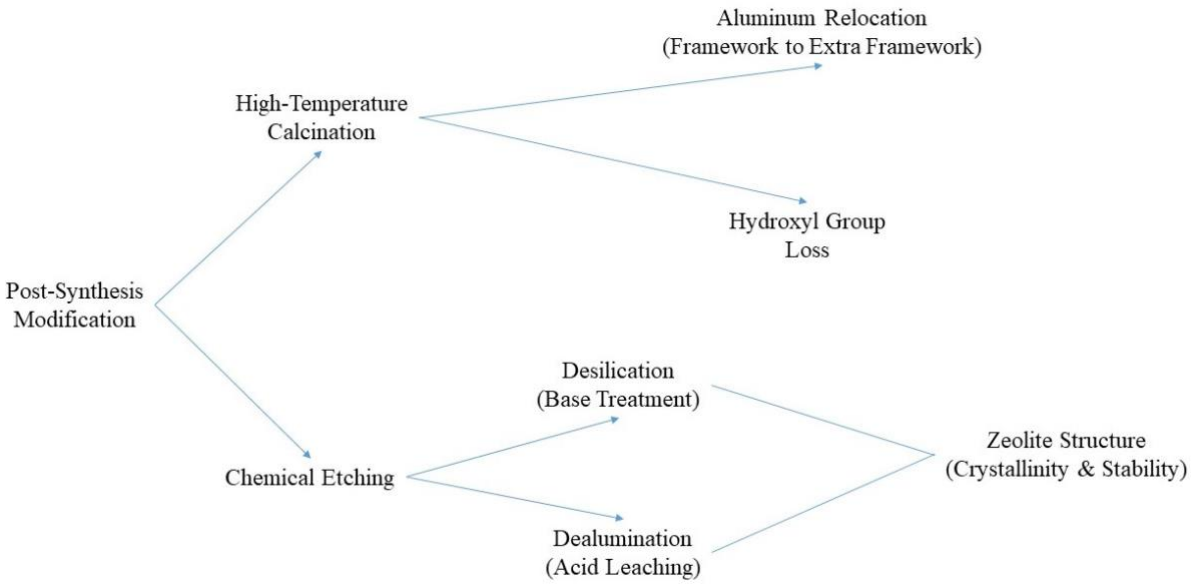

Scheme 1.3. Post-synthesis modifications of zeolites [56-58]

Scheme 1.3 represents the two main post-synthesis modifications for zeolites: chemical etching (dealumination or desilication) and high-temperature calcination. [56-58] Each process leads to specific changes in the zeolite structure, impacting its crystallinity, hydroxyl groups, and aluminum distribution. Careful control of factors such as acid or base concentration and synthesis temperature is crucial for successful modification, ensuring desired outcomes while maintaining the zeolite's integrity and functionality.

Zeolites are amongst the most used catalytic materials in many industrially and ecologically important processes because of the above-discussed qualities. These characteristics include the molecular channels and pores that influence shape selectivity, the Brønsted and/or Lewis acidic sites that are suitable for the coordination of highly dispersed transition metal centers, and the hydrothermal stability that permits the use of zeolites in harsh reaction conditions. The make-up of the "T" atoms in the zeolite framework, the Si/Al ratio, and the charge-balancing cations control the zeolite's acidity (type, strength, and concentration). The quantity of acid sites decreases while the acid sites' strength increases as the Si/Al ratio of the zeolite is raised. The Brønsted acidity of zeolites results from the charge-balancing proton [59,60]. The quantity of aluminium atoms in the framework controls the Si/Al ratio of the zeolite, which also controls the acidity of the zeolite. Proton crowding in the zeolite pores reduces the acid sites' strength. The extra-framework aluminium induces the zeolites' Lewis acidity and the use of alkali metals as charge-balancing cations in zeolites reduces their acid concentration, by inducing basic sites. When present in the zeolite framework as bare cations, these alkali metals also function as strong Lewis acid sites [61].

1.3 Literature Review

Homogeneous and heterogeneous are broad and well-known categories of catalysis and have all been used to study alkane oxidation, since oxidation is among the most significant processes for converting petroleum-based feedstocks into a range of chemicals. [62] So the majority of the literature review in this study is centered on the heterogeneous aspect of catalysis because it is essential to concentrate on the review of the relevant topic for the current investigation.

There is extensive research worldwide on paraffin activation, particularly about oxidative dehydrogenation and oxidation. This is primarily motivated by the requirement for stable, commercially viable catalysts that have good activity and high selectivity toward the desired

products. [62] The work by Lopez-Nieto et al. [63-68], particularly on the oxidation of lower paraffins, has had a considerable impact on the subject of oxidation catalysis. They have demonstrated that the acid-base characteristics and redox nature of a catalyst directly affect the performance of a catalyst for alkane activation using vanadium-based and supported vanadium catalysts.

Thorsteinson et al. [69] studied Mo and V mixed metal oxides in the oxidation of ethane. With a $Mo_{0.73}V_{0.18}Nb_{0.09}O_x$ catalyst, the selective oxidation of ethane to ethene was carried out at 350 ^oC with a conversion of 58 % and a selectivity of 65 %. Lopez Nieto and colleagues [70] also investigated a mixed metal oxide MoVTeNbO catalyst for the oxidation of ethane to ethene. The catalyst was synthesized hydrothermally using heat treatment at 600–700 ^oC under a stream of nitrogen. The resulting catalyst produced a yield of 75 % while the selectivity to ethane was 85 %. Khodakov et al. [71] discovered that the structure of vanadia species supported by zirconia is determined by the vanadium oxides (VO_x) surface density and the temperature of catalyst oxidation pre-treatments because at surface densities of roughly 2-3 VO_x/nm^2, the oxidative dehydrogenation of propane to propene reached constant selectivity values of 80 % at 333 ^oC, whereas at low surface densities and on bulk ZrV_2O_7, the high selectivity to CO_x products seemed to be linked to the exposed unselective Zr-O-Zr and V-O-Zr sites. These studies were done on short-chain alkanes due to the difficulties associated with the regioselectivity of long-chain alkanes.

In another study, by Kaliya et al. [72], the oxidative dehydrogenation of propane and n-butane produced remarkable performance from the novel nitrogen-containing catalyst CoN_X/Al_2O_3. At 600 ^oC, olefin yields of 47.6 % and 37.4 % were achieved for butane and propane conversions of 82 % and 76.7 %, respectively. It is noteworthy that the major products of the oxidative cracking of paraffins at temperatures greater than 400 ^oC were ethene and propene. As a result, efforts have been made to enhance the characteristics of these catalysts. A variety of promoters have been used to increase the catalysts' dehydrogenation efficiency.

Cavani and co-workers [73,74] demonstrated that several factors, including the role of the redox properties of transition metal oxide-based systems, the radical-type contribution, homogeneous and heterogeneously-initiated homogeneous reactions over irreducible metal oxide and noble metal catalysts, the catalysts’ bulk and surface properties, and the control of oxygen supply to the catalyst, affect the selective oxidation of light alkanes to bulk chemicals.

Ntola et al. [75], discovered that vanadium speciation, surface basicity, and oxygen vacancies are substantially more crucial than surface vanadium concentration when it comes to oxidative dehydrogenation of n-octane using glycine, urea, oxalyldihydrazide, citric acid and hydrazine hydrate as fuels for VO_x/MgO catalysts in a solution combustion synthesis to get high selectivity to octenes. The highest conversions they were able to get was for urea and glycine synthesised catalysts, which was 16 % and 15 %, respectively, with the glycine synthesised catalyst having the highest selectivity of 63 % to octenes at 400 ^oC. In another study by Farahani et al. [76], niobium-doped $NiAl_2O_4$ using different concentrations was used as a catalyst in the oxidative dehydrogenation of n-octane at 450 ^oC, 500 ^oC, and 550 ^oC. The results showed that as the amount of niobium used as a dopant increases, the activity of these catalysts appears to also decrease at 450 ^oC and 500 ^oC, and at 550 ^oC the catalysts have the lowest activity due to the high concentration of niobium atoms. As the temperature increases, the selectivity to octenes decreases which indicates that at high temperatures, cracking and combustion of the main products happens sequentially to produce the secondary products (cracked, aromatics, and CO_x).

The benefits of transition metals in oxidative dehydrogenation are that they have a varying number of stable oxidation states, [77] which makes them ideal because they can undergo redox cycling. The common limitations of the above studies were the low surface area of the catalysts, which leads to agglomeration of active metals, limited thermal stability, and complicated synthesis methods that can make reproducibility difficult.

Over the years, zeolitic materials were mostly used in dehydrogenation reactions as paraffins cracking catalysts. [78] However, because of the interesting properties possessed by zeolites, they have been recently used as oxidation catalysts in liquid phase systems. [26,79] Apart from that, few studies have been carried out on the oxidative dehydrogenation of alkanes using zeolitic materials.

Zhou et al. [80] studied the CO_2 assisted oxidative dehydrogenation of propane using Ga-modified zeolites with a low Si/Al ratio at 600 ^oC. It was found that a Ga/Na-ZSM-5(28) catalyst had the highest conversion (≈ 56 %), followed by a Ga/Na-SSZ-39(9) catalyst (≈ 37 %) amongst all the catalysts but when it comes to selectivity, the Ga/Na-SSZ-39(9) catalyst had the highest selectivity ethene and propene. The drawbacks of this study was hydrogenolysis, poor terminal selectivity, and faster deactivation of the catalysts due to CO_x formation. In another study by Daniel et al. [81] the sol-gel method was used to prepare Zr

modified ZSM-5 catalysts with different ratios and oxidative dehydrogenation of propane was carried out. It was found that a Zr/ZSM-5(1:4) catalyst had the best catalytic performance with a conversion of 59.48 % and selectivity of 87.44 % to propene.

A study by Ndlela et al. [82] focussed on the synthesis of both faujasite (FAU) zeolites and silicalites type catalysts with gallium and boron in the framework using a sol-gel technique. The catalysts were tested in the oxidative dehydrogenation of n-octane and BBaY-S (where Y-S = FAU type prepared by sol-gel) with the lowest acidity recorded the highest selectivity (40 %) to octenes and the lowest selectivity (28 %) to CO_x. GaNaY-S without boron in the framework, had the highest acidity and performed oppositely with octenes selectivity of 17 % and CO_x selectivity of 56 %. These catalytic results showed a reliance on the catalysts' acid-base properties and active metal reducibility. The study also revealed that catalysts that are Na-based favored C-2 and C-3 alkenes, whereas Ba-based catalysts favored C-5 and C-6 alkenes more. This difference in regioselectivity between Na and Ba was related to their distinct atomic sizes. These catalysts' gave a positive insight, however the conversion reported was very low.

In another study by Ndlela et al. [26] where different methods of synthesis were studied, they showed that silicalite type catalyst (Ga-BaY) (where Y = FAU type) which is aluminum-free had the lowest total acidity whereas the ionically exchanged faujasite zeolite catalyst (BaGa-NaY) had the highest total acidity since the source of zeolite material's acidity is aluminium. When oxidative dehydrogenation of n-octane was carried out, it was found that the catalysts gave octene selectivities of 33 % and 36 % and CO_x selectivities of 33 % and 35 % for silicalite type and ionically exchanged faujasite zeolite catalysts, respectively. Product distribution is affected by the presence of sodium, the quantity of barium and gallium employed in the catalyst, and the lack of aluminium in the catalyst's framework.

A mechanism probing study was also carried out by Ndlela et al. [83] and it was found that when the catalysts are thermally treated before oxidative dehydrogenation catalytic testing, Lewis acid sites increase and cause n-octane to be activated via a bimolecular mechanism instead of a monomolecular mechanism. Ndlela et al. [84], also showed that different alkaline earth metals influence the acidity of the faujasite zeolite differently and that Ba was the most efficient in decreasing the acidity and inducing the medium-strong basic sites of the Ga-NaY zeolite which were beneficial for oxidative dehydrogenation of n-octane.

With certain benefits and drawbacks, the oxidative dehydrogenation of alkanes is yet to be used in industry as a significant method of producing alkenes. The main drawback of the oxidative

dehydrogenation approach is that because the products are more reactive than the starting material, substantial amounts of CO_x are frequently formed. To produce high yields of oxidative dehydrogenation products and subsequently reduce CO_x production, various catalytic systems have been prepared and tested. It is crucial to note that as the number of carbon atoms increases, the reaction's nature becomes more complex. The objective remains to develop a catalyst system that will convert paraffins to the desired oxidative dehydrogenation products decently while limiting the production of side products (cracks and CO_x).

1.4 Study Rationale

The oxidative dehydrogenation of alkanes to alkenes and aromatics using zeolite-based catalysts has been studied before but with no outcomes that could potentially replace the dehydrogenation catalysts used in industries for the same application. The disadvantages of dehydrogenation reactions are low conversions due to thermodynamic equilibrium constraints, the endothermic nature of the reaction, and the operating conditions which are high temperatures above 450 ^oC, and low yields of alkenes resulting from quick deactivation of the catalyst from coke deposition.

The catalytic effect of zeolites is significantly influenced by acidic and structural properties, and dealuminating the zeolite extracts aluminium atoms from its lattice while enhancing thermal/hydrothermal stabilities. It also creates mesopores for better diffusion of reactants and that can lead to increasing catalytic efficiency and selectivity. Therefore, it is necessary to create a catalyst that is active and selective to the desired products while suppressing further oxidation of the oxidative dehydrogenation products. So the aim is to improve the oxidative dehydrogenation activity of faujasite based zeolite catalysts by using dealumination as a synthesis process, and also by preparing active and stable modified BaGa-NaY catalysts by ionic exchange.

References

1. Bond, G.C. 1987. Heterogeneous Catalysis: Principles and Applications, Oxford University Press, London.

2. Stoffels, M.A., Klauck, F.J.R, Hamadi, T., Glorius, F. and Leker, J. 2020. Technology trends of catalysts in hydrogenation reactions: A patent landscape analysis. Advance Synthesis and Catalysis, 362, 1258-1274.
3. Fung, J. and Wang, I., 1991. Dehydrocyclization of C_6–C_8 n-paraffins to aromatics over TiO_2–ZrO_2 catalysts. Journal of Catalysis, 130, 577–587.
4. Cao, S., Tao, F., Tang, Y. Li, Y. and Yu, J. 2016. Size- and shape-dependent catalytic performances of oxidation and reduction reactions on nanocatalysts. Chemical Society Reviews, 45, 4747-4765.
5. Hagen, J. 2015. Heterogeneously catalysed processes in industry. Industrial Catalysis, 261-298.
6. Chen, G., Tao, J., Liu, C., Yan, B., Li, W. and Li, X. 2017. Steam reforming of acetic acid using Ni/Al_2O_3 catalyst: Influence of crystalline phase of Al_2O_3 support. International Journal of Hydrogen Energy, 43, 20729-20738.
7. De Klerk, A. 2018. Zeolites as catalysts for fuels refining after indirect liquefaction processes. Molecules, 23, 115-131.
8. Ma, S., Huang, S.D. and Liu, Z.P. 2019. Dynamic coordination of cations and catalytic selectivity on zinc-chromium oxide alloys during syngas conversion. Nature Catalysis, 2, 671-677.
9. Kidwai, M., Bansal, V., Saxena, A., Shankar, R. and Mozumdar, S. 2006. Ni-nanoparticles: An efficient green catalyst for chemoselective reduction of aldehydes. Tetrahedron Letters, 47, 4161-4165.
10. Mahmoudi, H., Mahmoudi, M., Doustdar, O., Jahangiri, H., Tsolakis, A., Gu, S. and LechWyszynski, M. 2017. A review of Fischer Tropsch synthesis process, mechanism, surface chemistry and catalyst formulation. Biofuels Engineering, 2, 11-31.
11. Haro, P., Ollero, P., Villanueva Perales, A.L. and Reyes Valle, C. 2012. Technoeconomic assessment of lignocellulosic ethanol production via DME (dimethyl ether) hydrocarbonylation. Energy, 44, 891-901.
12. Singh, S.P. and Singh, D. 2010. Biodiesel production through the use of different sources and characterization of oils and their esters as the substitute of diesel: A review. Renewable and Sustainable Energy Reviews, 14, 200-216.
13. Pillay, B., Mathebula, M.R. and Friedrich, H.B. 2009. The oxidative dehydrogenation of n-hexane over Ni-Mo-O catalysts. Applied Catalysis A: General, 361, 57-64.
14. Viswanathan, B. 2017. Fundamentals of chemical conversion processes and applications. Petroleum: Energy Sources, 1, 29-57.

15. Resasco, D.E. 2000. Dehydrogenation by heterogeneous catalysts. Encyclopaedia of Catalysis, 1-38.
16. Cybulskis, V.J., Bukowski, B.C., Tseng, H.T., Gallagher, J.R., Wu, Z., Wegener, E., Kropf, A.J., Ravel, B., Ribeiro, F.H., Greeley, J. and Miller, J.T. 2017. Zinc promotion of platinum for catalytic light alkane dehydrogenation: Insights into geometric and electronic effects. ACS Catalysis, 7, 4173-4181.
17. Bandaru, H., Mahomed, A.S., Singh, S. and Friedrich, H.B. 2018. The effect of varying the metal ratio in a chromium molybdate catalysts for the oxidative dehydrogenation of *n*-octane. Molecular Catalysis, 460, 74–82.
18. Narayanappa, M., Dasireddy, V.D.B.C. and Friedrich, H.B. 2012. Catalytic oxidation of n-octane over cobalt substituted ceria ($Ce_{0.90}Co_{0.10}O_{2-\delta}$) catalysts. Applied Catalysis A: General, 447, 135–143.
19. Mars, P. and van Krevelen, D.W. 1954. Oxidations carried out by means of vanadium oxide catalysts. Chemical Engineering Science, 3, 41-59.
20. Kaddouri, A., Del Rosso, R., Mazzocchia, C., Gronchi, P., Fumagalli, D. and Therm, J. 2001. Isothermal reduction behaviour of some metal molybdates. Selective light alkane oxydehydrogenation and/or olefins partial oxidation. Journal of Thermal Analysis and Calorimetry, 66, 63-78.
21. Grabowski, R. 2006. Kinetics of oxidative dehydrogenation of $C_2 – C_3$ alkanes on oxide catalysts. Catalysis Reviews, 48, 199-268.
22. Panov, G.I., Uriarte, A.K., Rodkin, M.A. and Sobolev, V.I. 1998. Generation of active oxygen species on solid surfaces. Opportunity for novel oxidation technologies over zeolites. Catalysis Today, 41, 365-385.
23. Finocchio, E., Ramis, G., Busca, G., Lorenzelli, V. and Willey, R.J. 1996. On the mechanisms of light alkane catalytic oxidation and oxy-dehydrogenation: an FT-IR study of the n-butane conversion over $MgCr_2O_4$ and a Mg-vanadate catalyst. Catalysis Today, 28, 381-389.
24. Hodnett, B.K. 2000. Heterogeneous catalysis oxidation: Fundamental and technological aspects of the selective and total oxidation of organic compounds. Wiley-VCH.
25. Lin, X., Hoel, C.A., Sachtler, W.M.H., Poeppelmeier, K.R. and Weitz, E. 2009. Oxidative dehydrogenation (ODH) of ethane with O_2 as oxidant on selected transition metal-loaded zeolites. Journal of Catalysis, 265, 54-62.

26. Ndlela, S.S., Friedrich, H.B. and Cele, M.N. 2021. Oxidative dehydrogenation of *n*-octane using Ba and Ga-modified faujasite type catalysts prepared by different methods. Journal of Porous Materials, 28, 593–603.
27. Phadke, N.M., Mansoor, E., Bondil, M., Head-Gordon, M. and Bell, A.T. 2018. Mechanism and kinetics of propane dehydrogenation and cracking over Ga/H-MFI prepared via vapor-phase exchange of H-MFI $GaCl_3$. Journal of the American Chemical Society, 141, 1614-1627.
28. Pereira, M.S. and Nascimento, M.A.C. 2006. Theoretical study on the dehydrogenation reaction of alkanes catalyzed by zeolites containing nonframework gallium species. Journal of Physical Chemistry, B, 110, 3231-3238.
29. Barthomeuf, D. 1996. Basic zeolites: Characterization and uses in adsorption and catalysis. Catalysis Reviews: Science and Engineering, 38, 521-612.
30. Weckhuysen, B.M. and Yu, J. 2015. Recent advances in zeolite chemistry and catalysis. Chemical Society Reviews, 44, 7022-7024.
31. Dyer, A. 1984. Use of natural zeolites. Chemistry and Industry, 241-245.
32. Szostak, R. 1989. Molecular sieves: Principles of synthesis and identification. Van Nostrand Reinhold: New York, 524.
33. Breck, D.W. 1974. Zeolite molecular sieves. Wiley. New York. 533–534.
34. Farrauto, R.J. 1997. Fundamentals of industrial catalytic processes. London: Blackie Academic. 65.
35. Zhdanov, S.P., khvoshchev, S.S. and Feoktistova, N.N. 1990. Synthetic zeolites. Gordon and Breach Science. 1.
36. Meier, W.M., Olson, D.H. and Baerlocher, C. 1996. Atlas of Zeolite Structure Types. Butterworth-Heinemann, Stoneham, MA, 42-43.
37. Chica, A. 2013. Zeolites: Promised materials for the sustainable production of hydrogen. ISRN Chemical Engineering, 1-19.
38. Freyhardt, C.C., Tsapatsis, M., Lobo, R.F., Balkus Jr. K.J., and Davis, M.E. 1996. A high-silica zeolite with 14-tetrahedra-atom pore opening. Nature, 381, 295-298.
39. Wessels, T., Baerlocher, C., McCusker, L.B. and Creyghton, E.J. 1999. An ordered form of the extra-large-pore zeolite UTD-1: Synthesis and structure analysis from powder diffraction data. Journal of the American Chemical Society, 121, 6242-6247.
40. Strohmaier, K.G. and Vaughan, D.E.W. 2003. Structure of the first silicate molecular sieve with 18-ring pore openings, ECR-34. Journal of the American Chemical Society, 125, 16035-16039.

41. Corma, A., Diaz-Cabañas, M.J., Jorda, J.L., Martinez, C. and Moliner, M. 2006. High-throughput synthesis and catalytic properties of a molecular sieve with 18- and 10-membered rings. Nature, 443, 842-845.
42. Busca, G. 2014. Zeolites and other structurally microporous solids as acid-base materials. Heterogeneous Catalytic Materials, 197-249.
43. Dyer, A. 1988. An Introduction to Zeolite Molecular Sieves. John Wiley & Sons, New York, 1.
44. Daramola, M.O., Asansiola, E. and Ojumu, T.V. 2012. Potential applications of zeolite membranes in reaction coupling separation processes. Materials, 5, 2101-2136.
45. Krisnandi, Y.K., Saragi, I.R., Sihombing, R., Ekananda, R., Sari, I.P., Griffith, B.E. and Hanna, J.V. 2019. Synthesis and characterization of crystalline NaY-zeolite from Belitung kaolin as catalyst for n-hexadecane cracking. Crystals, 9, 404.
46. Sang, S., Liu, Z., Tian, P., Liu, Z., Qu, L. and Zhang, Y. 2006. Synthesis of small crystals zeolite NaY. Materials Letters, 60, 1131- 1133.
47. Widayat, W. and Annisa, A.N. 2017. Synthesis and characterization of ZSM-5 catalyst at different temperatures. Materials Science and Engineering, 214, 012032.
48. Song, Q., Chen, W., Dang, P., Wang, Y. and Li, F. 2018. Synthesis of an excellent MTP catalyst: hierarchical ZSM-5 zeolites with great mesoporosity. Royal Society Open Science, 5, 181691.
49. Santos, B.P.S., Almeida, N.C., Santos, I.S., Marques, M.V. and Fernandes, L.D. 2018. Synthesis and characterization of mesoporous mordenite zeolite using soft templates. Catalysis Letters, 148, 1870-1878.
50. Möller, K., Yilmaz, B., Jacubinas, R.M., Müller, U. and Bein, T. 2011. One-step synthesis of hierarchical zeolite beta via network formation of uniform nanocrystals. Journal of the American Chemical Society, 133, 5284-5295.
51. Chen, L.H., Li, X.Y., Tian, G., Li, Y., Rooke, J.C., Zhu, G.S., Qiu, S.L., Yang, X.Y. and Su, B.L. 2011. Highly stable and reusable multimodal zeolite TS-1 based catalysts with hierarchically interconnected three-level micro-meso-macroporous structure. Engewadte Chemie International Edition, 50, 11156-11161.
52. Lowenstein, W. 1954. The distribution of aluminum in the tetrahedra of silicates and aluminates. American Mineralogist, 39, 92-96.
53. Nagy, J.B., Aiello, R., Giordano, G., Kotavic, A., Testa, F., Kónya, Z. and Kiricsi, I. 2007. Isomorphous substitution in zeolites. Molecular Sieves, 5, 365-478.

54. Wei, A. and Chao, K. 2000. Structural characterization of metal ions incorporated in molecular sieve frameworks. Journal of the Chinese Chemical Society, 47, 33-40.
55. Szostak, R. 1991. Modified zeolites. Studies in Surface Science and Catalysis, 58, 153-199.
56. Triantafillidis, C.S., Vlessidis, A.G., Nalbandian, L. and Evmiridis, N.P. 2001. Effect of the degree and type of the dealumination method on the structural, compositional and acidic characteristics of H-ZSM-5 zeolites. Microporous and Mesoporous Materials, 47, 369-388.
57. FeliTZak-Guzik, A. 2018. Hierarchical zeolites: Synthesis and catalytic properties. Microporous and Mesoporous Materials, 259, 33-45.
58. Silaghi, M.C., Chizallet, C. and Raybaud, P. 2014. Challenges on molecular aspects of dealumination and desilication of zeolites. Microporous and Mesoporous Materials, 191, 82-96.
59. Simon-Masseron, A., Marques, J.P., Lopes, J.M., Ramôa Ribeiro, F., Gener, I. and Guisnet, M. 2007. Influence of Si/Al ratio and crystal size on the acidity and activity of HBEA zeolites. Applied Catalysis A: General, 316, 75-82.
60. Osatiashtiani, A., Puértolas, B., Oliveira, C.C.S., Manayil, J.C., Barbero, B., Isaacs, M., Michailof, C., Heracleous, E, Pérez-Ramírez, J., Lee, A.F. and Wilson, K. 2017. On the influence of Si:Al ratio and hierarchical porosity of FAU zeolites in solid acid catalysed esterification pretreatment of bio-oil. Biomass Conversion and Biorefinery, 7, 331-342.
61. Marakatti, V.S., Rao, P.V.C., Choudary, N.V., Sri Ganesh, G., Shah, G., Maradur, S.P., Halgeri, A.B., Shanbhag, G.V. and Ravishankar, R. 2014. Influence of alkaline earth cation exchanged X-zeolites toward ortho-selectivity in alkylation of aromatics: Hard-soft-acid-base concept. Advanced Porous Materials, 2, 221-229.
62. Punniyamurthy, T., Velusamy, S. and Iqbal, J. 2005. Recent advances in transition metal catalyzed oxidation of organic substrates with molecular oxygen. Chemical Reviews, 105, 2329-2364.
63. Botella, P., Lopez Nieto, J.M., Dejoz, A. and Vazquez, M.I. 2003. Mo-V-Nb mixed oxides as catalysts in the selective oxidation of ethane. Catalysis Today, 78, 507-512.
64. Lopez Nieto, J.M., Botella, P., Concepcion, P., Dejoz, A. and Vazquez, M.I. 2004. Oxidative dehydrogenation of ethane on Te-containing MoVNbO catalysts. Catalysis Today, 91-92, 241-245.
65. Lopez Nieto, J.M., Soler, J., Concepción, P., Herguido, J., Menéndez, M. and Santamaría, J. 1999. Oxidative dehydrogenation of alkanes over V-based catalysts:

Influence of redox properties on catalytic performance. Journal of Catalysis, 185, 324-332.

66. Corma, A., Goberna, C., Lopez Nieto, J.M., Paredes, N. and Perez, M. 1991. Dehydrocyclodimerization of short chain alkanes on Ga/ZSM-5 and Ga/Beta zeolites. Studies in Surface Science and Catalysis, 69, 409-416.
67. Lopez Nieto, J.M., Dejoz, A., Vazquez, M.I., O'Leary, W. and Cunningham, J. 1998. Oxidative dehydrogenation of n-butane on MgO-supported oxide catalysts. Catalysis Today, 40, 215-228.
68. Dejoz, A. López Nieto, J.M., Márquez, F. and Vázquez, M.I. 1999. The role of molybdenum in Mo-doped V-Mg-O catalysts during the oxidative dehydrogenation of n-butane. Applied Catalysis A: General 180, 83-94.
69. Thorsteinson, E.M., Wilson, T.P., Young, F.G. and Kasai, P.H. 1978. The oxidative dehydrogenation of ethane over catalysts containing mixed oxides of molybdenum and vanadium. Journal of Catalysis, 52, 116-132.
70. Lopez Nieto, J.M., Botella, P., Vazquez, M.I. and Dejoz, A. 2002. The selective oxidation dehydrogenation of ethane over hydrothermally synthesised MoVTeNb catalysts. Chemical Communication, 17, 1906-1907.
71. Khodakov, A., Yang, J., Su, S., Iglesia, E. and Bell, A.T. 1998. Structure and properties of vanadium oxide-zirconia catalysts for propane oxidative dehydrogenation. Journal of Catalysis, 177, 343-351.
72. Kaliya, M.L., Kogan, S.B., Froumin, N. and Herskowitz, M. 2002. Novel nitrogen containing heterogeneous catalysts for oxidative dehydrogenation of light paraffins. Catalysis Communications, 3, 327-333.
73. Cavani, F. and Trifiro, F. 1997. The multifunctional properties of heterogeneous catalysts, active and selective in the oxidation of light paraffins. Studies in Surface Science and Catalysis, 110, 19-34.
74. Cavani, F. and Trifiro, F. 1999. Selective oxidation of light alkanes: Interaction between the catalyst and the gas phase on different classes of catalytic materials. Catalysis Today, 51, 561-580.
75. Ntola, P., Friedrich, H.B., Singh, S., Olivier, E.J., Faharani, M. and Mahomed, A.S. 2023. Effect of the fuel on the surface VO_x concentration, speciation and physico-chemical characteristics of solution combustion synthesised VO_x/MgO catalysts for n-octane activation. Catalysis Communications, 174, 106571-106579.

76. Farahani, M.D., Dasireddy, V.D.B.C. and Friedrich, H.B. 2018. Oxidative dehydrogenation of n-octane over niobium-doped $NiAl_2O_4$: An example of beneficial coking in catalysis over spinel. ChemCatChem, 10, 1-12.
77. Gärtner, C.A., van Veen, A.C. and Lercher, J.A. 2013. Oxidation dehydrogenation of ethane: Common principles and mechanistic aspects. ChemCatChem, 5, 3196-3217.
78. Sato, K., Nishimura, Y., Honna, K., Matsubayashi, N. and Shimada, H. 2001. Role of HY zeolite mesopores in hydrocracking of heavy oils. Journal of Catalysis, 200, 288–297.
79. Cele, M.N., Friedrich, H.B. and Bala, M.D. 2014. A study of Fe(III)TPPCl encapsulated in zeolite NaY and Fe(III)NaY in the oxidation of n-octane, cyclohexane, 1-octene and 4-octene. Reaction Kinetics, Mechanisms and Catalysis, 111, 737-750.
80. Zhou, W., Jiang, Y., Sun, Z., Zhou, S., Xing, E., Hai, Y., Chen, G. and Zhao, Y. 2023. Support effect of Ga-based catalysts in the CO_2 assisted oxidative dehydrogenation of propane. Catalysts, 13, 896-707.
81. Daniel, S., Monguen, C.K.F., Kasmi, A.E., Arshad, M.F. and Tian, ZY. 2022. Oxidative dehydrogenation of propane to olefins promoted by Zr modified ZSM-5. Catalysis Letters, 153, 285-299.
82. Ndlela, S.S., Friedrich, H.B. and Cele, M.N. 2021. Faujasite silicalites for oxidative dehydrogenation of n-octane: Influence of alkali metals, gallium, and boron on catalyst activity. Molecular Catalysis, 502, 111393-111399.
83. Ndlela, S.S., Friedrich, H.B. and Cele, M.N. 2020. Effects of framework disruption of Ga and Ba containing zeolitic materials by thermal treatment. Catalysts, 10, 975-987.
84. Ndlela, S.S., Friedrich, H.B. and Cele, M.N. 2020. Effects of modifying acidity and reducibility on the activity of NaY zeolite in the oxidative dehydrogenation of n-octane. Catalysts, 10, 363-375.

Chapter 2

The effect of dealumination on the physicochemical properties of sodium-Y (NaY) zeolite

Abstract

Unmodified NaY zeolite has been shown to be inactive when it comes to the oxidative dehydrogenation (ODH) of medium chain paraffins. This is because of their moderate to low acid sites strength, which is unable to activate the saturated hydrocarbon. Through different modifications, NaY zeolite's properties can be altered to induce ODH activity. This work focussed on the modification of NaY zeolite's acidity by dealumination using different acid treatments, made of citric acid and ethylenediaminetetraacetic acid disodium (EDTA-2Na). Three catalysts were prepared, one was prepared by using citric acid, the other was prepared by mixing both citric acid and EDTA-2Na, and the last catalyst was modified using only EDTA-2Na. As expected, the Si/Al ratio of the modified catalysts increased compared to the parent NaY, with the citric acid modified zeolite recording the highest increase with 28 % dealumination. The acid strength for the modified catalysts increased inducing activity when the catalysts were tested in the ODH reaction. Citric acid modified catalysts gave the lowest conversion (~ 4 %), followed by the EDTA-2Na modified (~ 6 %), and the highest conversion was recorded by the complex modified catalysts (~ 10 %). The selectivity for all the catalysts was mostly towards carbon oxides (CO_x) (~ 92 %) due to the overoxidation from the acidity of the zeolite and the absence of the ODH active metal.

2.1 Introduction

Zeolites are crystalline, microporous minerals made of aluminate and silicate tetrahedra. Since they are used as adsorbents for industrial separation and purification, they have attracted a lot of attention, largely because of their intrinsic and post-synthetic properties. [1,2] Zeolites are currently suitable materials for industrial reactions such as fluid catalytic cracking, hydrocracking, isomerization, and alkylation of various hydrocarbon molecules due to their

strong acidity resulting from Lewis and Brønsted acid sites, coupled with their thermal robustness and easily controllable pore sizes. [2]

Post-synthetic modification of zeolites includes various techniques, which further controls the acid activity and/or shape selectivity of specific zeolite structures. Isomorphic substitution, calcination at high temperatures, chemical etching, impregnation, ionic exchange, and chemical vapor deposition (CVD) are the most commonly used post synthetic modification procedures. [3-7] Each post synthetic modification yields a different material, therefore depending on the application, the zeolite can be altered to be best suited for the application of interest. This study will be focussing on strengthening the acid properties of the commercial NaY zeolite for the application in oxidative dehydrogenation of n-octane reaction. Therefore etching is the suitable procedure that can potentially yield a suitable catalysts for this application. Etching of the zeolite can be carried out by a desilication or dealumination method and that controls the Si/Al framework ratio. Zeolites' atomistic Si/Al framework ratio has a significant impact on their properties. Thermal and hydrothermal stability, concentration and strength of the Brønsted and Lewis acid site, and the nature of the pores are all examples of properties that are affected by the Si/Al ratio of the zeolite. These then consequently affects the catalytic activity and selectivity of the resulting zeolitic material. [8-11]

Etching by desilication can be done by using an alkaline solution. This procedure is carried out to introduce mesoporosity within zeolites, [12] while etching by dealumination is done by acid treatments, and is carried out to increase the strength of the acid sites while decreasing the concentration of acid sites of the zeolite. More aluminium atoms in the zeolite's framework decreases the Si/Al ratio, while increasing the zeolite's acidity. Proton crowding in the zeolite pores however, reduces the acidic sites' strength, which is the key property to the zeolite's activity. [13]

Even though zeolites are a hot topic currently in research [14-17], there is very little that has been done in the oxidative dehydrogenation (ODH) of paraffins using zeolites. This is because, the high acidity of these materials leads to unwanted products such as cracks and carbon oxides (CO_x). However, recent work has shown that the Faujasite-type Y zeolite have a potential of being used as a suitable catalyst for the oxidative dehydrogenation reaction. [3,4,18,19] However, because of the low conversions obtained from these studies, this material still holds a room for improvements.

NaY zeolites have a high Si/Al ratio which renders them as low acidic zeolites. In this study we aim at improving the conversion of oxidative dehydrogenation of n-octane by modifying the acid sites of NaY zeolite by dealumination using different acid treatments (citric acid, EDTA-2Na, and the combination of EDTA-2Na and citric acid). This will result in the strengthening of the acid sites, which will lead to improved zeolite activity.

2.2 Materials and Experimental Methods

2.2.1 Reagents

- Citric acid for acid leaching (AL) treatment,
- Ethylenediaminetetraacetic acid disodium (EDTA-2Na) for chelating agent treatment (CAT),
- Citric acid + Ethylenediaminetetraacetic acid disodium for complex treatment (CT).

2.2.2 Catalysts Preparation

Dealumination was carried out by treating 20 g of commercial parent NaY zeolite with a 100 mL aqueous solution containing the acid treatment modifiers. This treatment was conducted at 80 °C for 4 hours under stirring. Three different solutions were used to modify NaY: citric acid solution (0.2 mol/L), EDTA-2Na solution (0.2 mol/L), and a complex solution of EDTA-2Na (0.1 mol/L) and citric acid (0.1 mol/L). After treatment, each sample suspension underwent filtration and washing with double distilled water, followed by drying overnight at 110 °C. The resulting samples were labeled as NaY[AL], NaY[CAT], and NaY[CT]. Before characterization and catalytic testing, all samples underwent calcination under air at 550°C for 6 hours.

2.2.3 Catalysts Characterisation

X-ray fluorescence (XRF) analysis using the X-Supreme8000 was used to evaluate the chemical composition of the material in order to calculate the silica/alumina ratio. Powder X-ray diffraction patterns for structure and phase identification were performed using a Bruker D8 advance diffractometer equipped with a graphite monochromatic filter operated at 40 kV and 40 mA, (Billerica, USA). The radiation source was CuKα with a wavelength of 1.5406 nm.

Data acquisition was carried out at a step and scanning speed of 0.02° and 0.2 s^{-1}, respectively, and at a 2-theta range of 5° to 90°. N_2 physisorption (also known as Brunauer, Emmett, and Teller (BET)**)** analysis was performed using an Anton Paar Kaomi for Nova, operated at –195.8 °C. Finely ground samples were degassed under vacuum for 1 hour at 90 °C, then 150 °C for another hour and then at 400 °C for 12 hours under flow of N_2 before analysis. Infrared spectra were recorded at room temperature using a Perkin Elmer Spectrum 100 FT-IR Spectrometer equipped with a Universal ATR Sampling Accessory. Pyridine IR spectra were recorded using the same equipment. For pyridine IR, 0.25 g samples were treated with 0.5 mL of liquid pyridine and left to dry for the whole night before recording the spectra in the region of 1400–1700 cm^{-1} to determine the acidic sites' type. For morphology and surface structure, SEM images were obtained using a Zeiss Ultra Plus field emission gun scanning electron microscope (FEG-SEM) with Smart SEM Software (Oberkhochen, Germany). Before analysis, samples were coated with gold using a Q150R series high vacuum Quorum sputter coater. TGA thermal analysis was used to measure the thermal stability of the material from 25–800 °C. The analysis was carried out using the METTLER TOLEDO TGA/DSC1, ISF Model 1346 with STAR^e software version 9.20 instrument in flowing air at a heating rate of 300°C/h.

2.2.4 Catalysts Testing

Catalyst testing was carried out at a temperature of 450 °C in a laboratory-scale continuous-flow fixed-bed, gas phase reactor. The reactor tube was made of stainless steel with an inner diameter of 10 mm. The reactions were carried out with *n*-octane (Merk, assay > 98 %) and a concentration in a gas mixture (v/v) above the upper flammability limit of n-octane. In all reactions, the concentration of *n*-octane was maintained at 6 %. A calibrated Lab Alliance Series II HPLC Pump was used to feed *n*-octane into the system and the feed mass was weighed using an electronic balance. The *n*-octane fed in was kept at 130 °C through the heated supply lines using heating tape. The temperature was controlled with a CB-100 RK temperature controller with internal playback and monitored with K-type thermocouples. All reactions were carried out using 1.0 mL of a pelletized catalyst (pellet sizes was between 600 μm and 1000 μm) between two thin layers of glass wool positioned in the hottest zone of the calibrated reactor block. The spaces in the reactor tube were filled with 24 grit carborundum and sealed at both ends with glass-wool. Total gas flow was measured using a Ritter drum type wet gas flow meter. All liquid products and unreacted feed were collected in a cylindrical stainless-

steel vessel, cooled to ≈ 3.0 ºC. A Perkin Elmer Clarus 400 GC equipped with a 30 m × 530 µm Supelco Carboxen 106 PLOT column and a thermal conductivity detector was used to analyze COx products. Liquid and gaseous products were analyzed using a Shimadzu GC-2025, equipped with a 50 m ×200 µm PONA capillary column and flame ionization detector. All the data points were obtained in triplicate with carbon balances ranging from 97 % to 100 % and an error of ± 3 %.

2.3 Results and Discussion

2.3.1 Catalysts Characterization

2.3.1.1 XRF

X-ray Fluorescence analysis results shown in **Table 2.1** confirmed the successful partial removal of aluminium from the NaY framework using different acid treatments. The extent of dealumination was determined by comparing Si/Al the ratios of parent NaY and the acid treated NaY zeolites (refer to **Table A1**). The maximum dealumination (28 %) was achieved using the acid leaching method, followed by complex treatment, where both citric acid and EDTA-2Na used with 14 %. EDTA-2Na on its own removed about 9 % of framework aluminium. EDTA-2Na low dealumination activity is attributed to the limited ability of this salt to remove the framework aluminium. EDTA is known to be efficient in removing non-framework aluminium. [20] Acetic acid on the other hand achieved more dealumination, as it can also remove the framework aluminium. This is in line with the crystallinity from the XRD results, in which NaY[CT] has the highest % crystallinity as a result of non-framework aluminium removal. [20]

Table 2.1. XRF percentage dealuminated of NaY using different acid treatments

Catalysts	Acid Treatment	Concentration (mol/L)	Dealumination (%)
NaY[AL]	Citric Acid	0.2	28
NaY[CAT]	EDTA-2Na	0.2	9
NaY[CT]	Citric Acid + EDTA-2Na	0.1	14

2.3.1.2 Powder XRD

The X-ray powder diffraction (XRD) diffractograms **(Figure 2.1)** of all the samples showed the faujasite Y phase. This shows that the dealumination of the parent NaY did not negatively affect the structure of the faujasite zeolite. The modification did not also change the intensities of the characteristic peaks of the parent NaY greatly. However, the crystallinity calculations (refer to **Appendix**) showed that the NaY[AL] (67.6 %) and NaY[CT] (69 %) had a slight decrease in crystallinity compared to the parent NaY (71 %). NaY[CAT] (83 %) had the highest crystallinity compared to all the samples, which could be attributed to the removal of non-framework aluminium. [20]

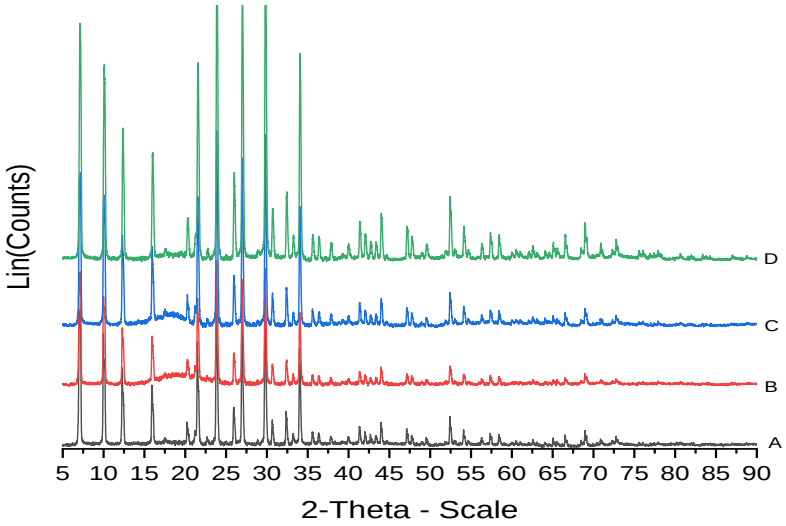

Figure 2.1. XRD diffractograms of (**A**) NaY, (**B**) NaY[AL], (**C**) NaY[CT], (**D**) NaY[CAT]

2.3.1.3 FT-IR

Figure 2.2 shows the FT-IR spectra of the parent and dealuminated NaY zeolites. All the samples showed similar bands, implying a negligible change in the structure of the zeolite between the modified samples. The bands at about 460 cm^{-1} are due to the T-O bending vibration of the internal tetrahedral in the zeolite, where T can either be Si or Al. [21] Bands around 553 cm^{-1} and 668 cm^{-1} are attributed to the double-ring vibration and symmetric stretching band, respectively, associated with FUA characteristic bands. [21,22] These results agree with XRD results which showed that the faujasite framework is still intact after the dealumination procedure. Si-O bending/internal tetrahedral asymmetric stretching is responsible for the strong band at about 980 cm^{-1}, and the H-O-H symmetric stretching band can be seen at around 1654 cm^{-1}. [19,23] Bands corresponding to O-Si-H bending absorption and Si-H stretching are identified at 2000-2300 cm^{-1}. [24,25]

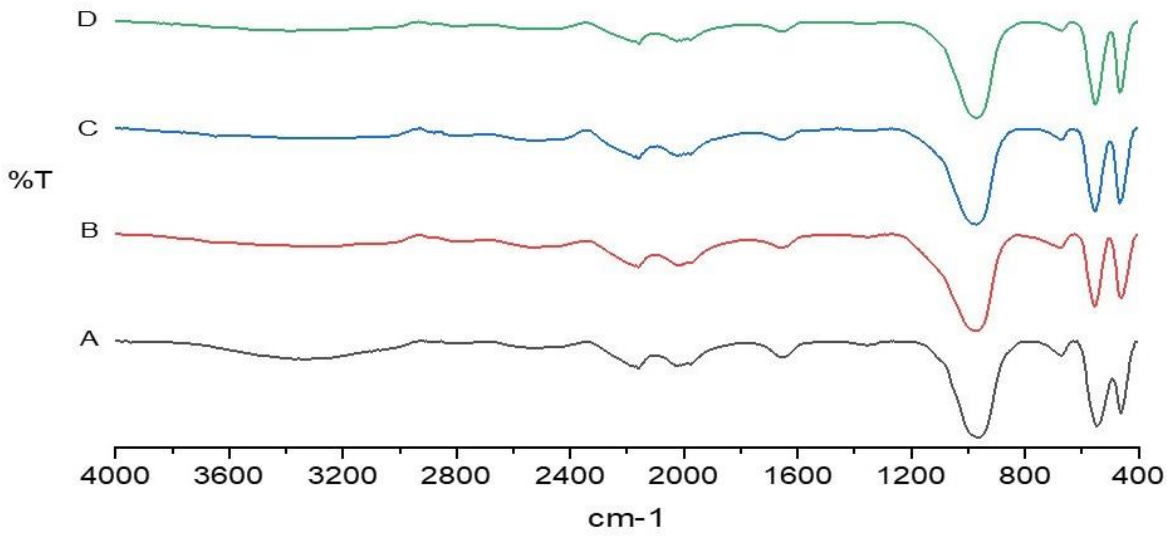

Figure 2.2. FT-IR Spectra of (**A**) NaY, (**B**) NaY[AL], (**C**) NaY[CT], (**D**) NaY[CAT]

2.3.1.4 Scanning Electron Microscopy

The difference in the morphological make-up of the prepared catalysts is shown in **Figure 2.3**. The conventional cubic shape of the faujasite type zeolites was evident for all the modified samples, with NaY[AL] showing a certain amount of cubic distortion, which may be related to the high amount and the type of aluminium (framework) that was removed from the structure

of the zeolite. NaY[CAT) showed the least distortion relating to the least amount of aluminium removed and the fact that this aluminium was the non-framework aluminium. [18,20]

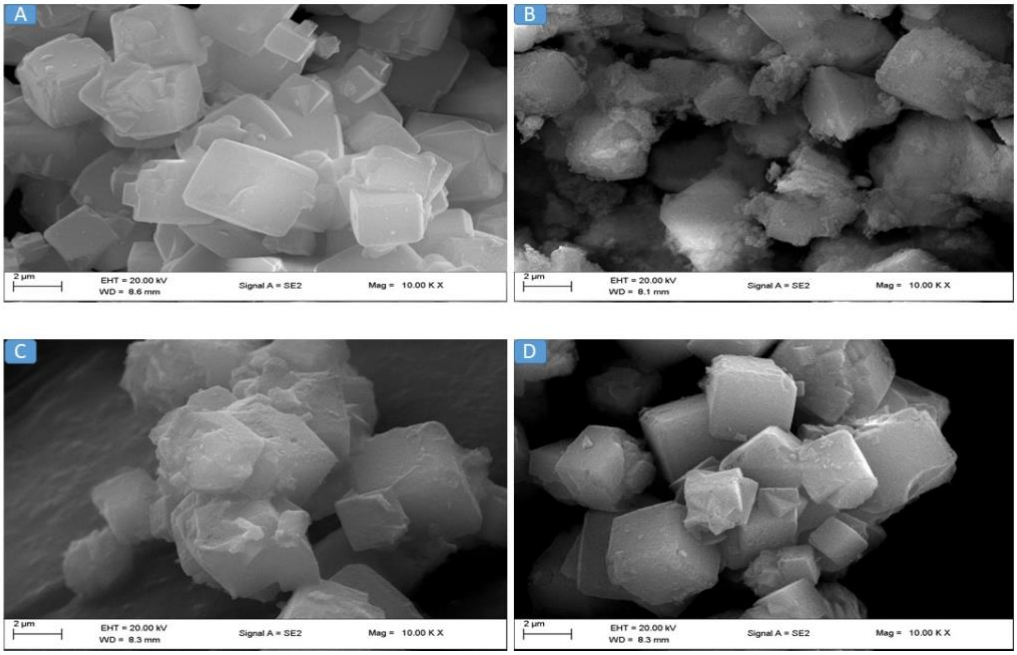

Figure 2.3. SEM Micrographs of (**A**) NaY, (**B**) NaY[AL], (**C**) NaY[CT], (**D**) NaY[CAT]

2.3.1.5 Brunauer, Emmett, and Teller (BET) Studies

Figure 2.4 shows that the N_2 adsorption-desorption of all the prepared samples fit under the IUPAC classification's definition of a type IV adsorption isotherm which is associated with mesoporous materials. The dealuminated samples fall under the IUPAC classification of hysteresis loop of H3 type curves, exhibiting a hysteresis loop around p/p_o = ~0.38, suggesting the presence of micropores as well as mesopores. [26,27] By using the Debye-Scherrer equation to adjust the crystallite sizes of the samples, it was possible to establish that the NaY particle size was less than 80 nm as shown in **Figure 2.5**. It can also be seen that in the mesoporous area, where the principal pore width is 4 nm, the samples displayed a wide pore size distribution. However, it is known that catalysts exhibit a tight and uniform pore size distribution at the sharpness of the initial step (at p/p_o = 0.05-0.30). [27,28]

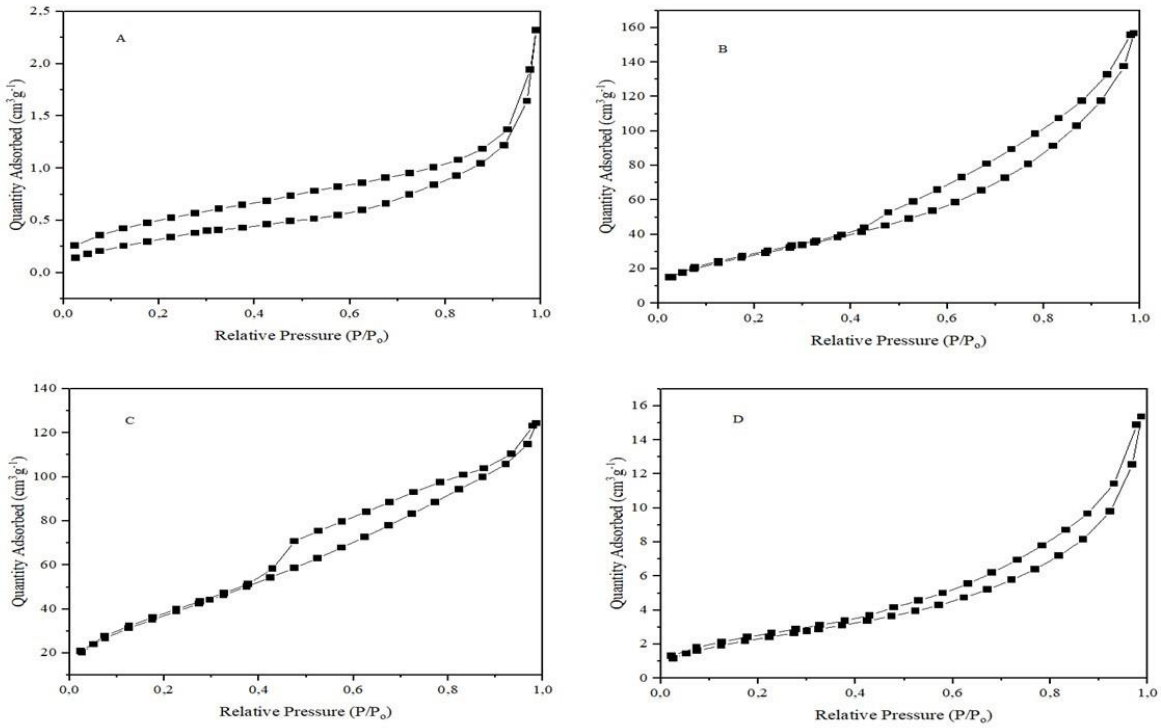

Figure 2.4. N_2 Adsorption/Desorption Isotherms of (**A**) NaY, (**B**) NaY[AL], (**C**) NaY[CT], (**D**) NaY[CAT]

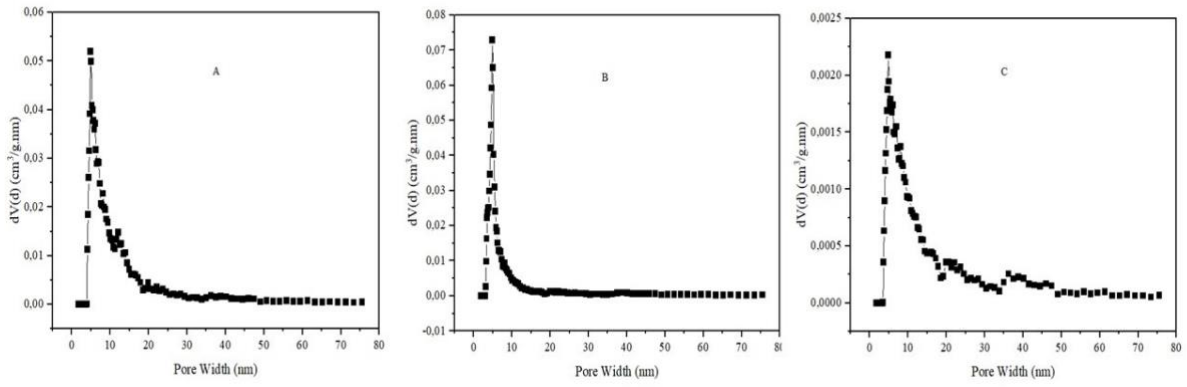

Figure 2.5. Pore Size Distribution of (**A**) NaY[AL], (**B**) NaY[CT], (**C**) NaY[CAT]

2.3.1.6 Pyridine FT-IR

Pyridine was adsorbed and desorbed at room temperature to qualitatively analyse the type and nature of acid sites in both the parent and the modified NaY zeolites. **Figure 2.6** shows the FT-IR spectra of the analysed samples at the pyridine vibration range of 1400-1700 cm^{-1}. Physically adsorbed pyridine exhibits absorption bands at 1574 cm^{-1} and 1590 cm^{-1} due to

hydrogen bonding with surface hydroxyl groups. The band at 1485 cm^{-1} is assigned to the interaction of Lewis and Brønsted acid sites. [4,19] Two bands at 1442 cm^{-1} and 1624 cm^{-1} are related to Lewis-bonded pyridine, with the latter associated with the strong Lewis acids sites. [29,30] All the samples prepared did not show any bands associated with pyridinium ions (PyH^+), which suggests that the samples lack the presence of medium to strong Brønsted acid sites.

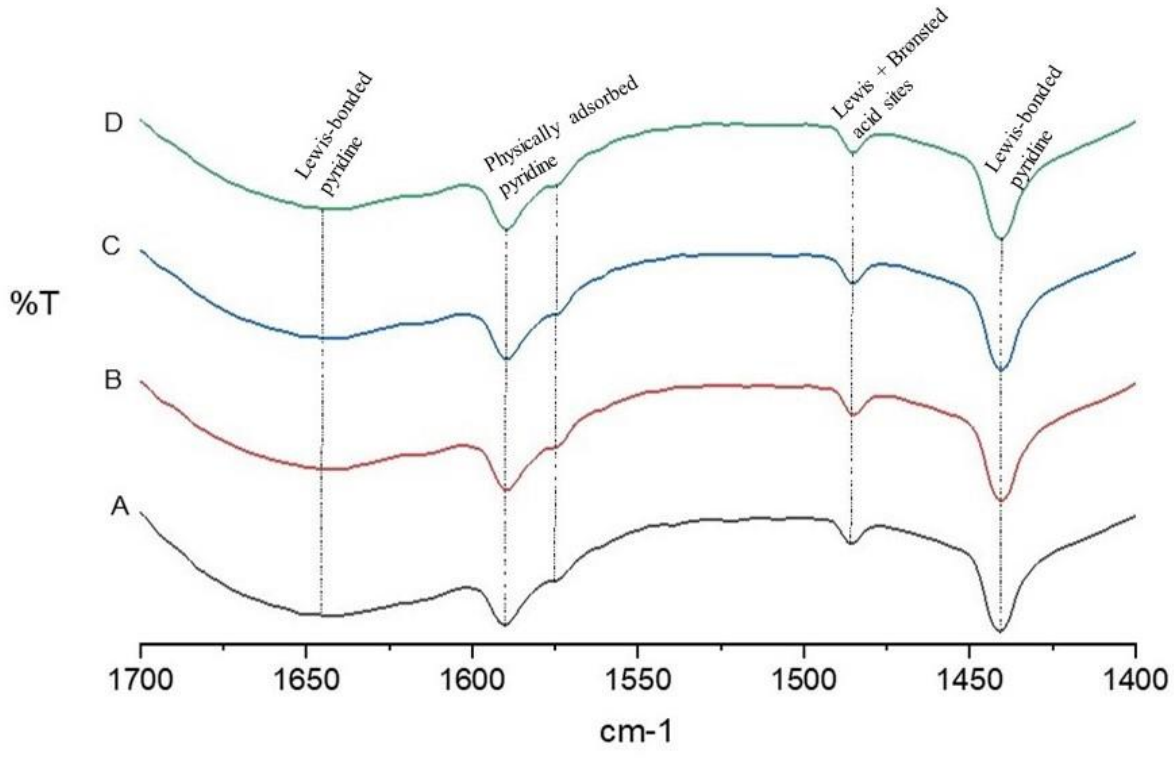

Figure 2.6. Pyridine FT-IR Spectra of (**A**) NaY, (**B**) NaY[AL], (**C**) NaY[CT], (**D**) NaY[CAT] carried out at T = 25 ^oC

2.3.1.7 Thermogravimetric Analysis

The TGA analysis (**Figure 2.7**) showed three distinctive events at temperatures 25–200 ^oC, 200–400 ^oC, and 400–1000 ^oC. For all the prepared catalysts, the total weight loss was less than 20 %. This loss was found in the low temperature range (~ 15 % loss) and was attributed to the loss of water and hydroxyl groups weakly bound to the non-framework aluminium. The medium temperature loss (~ 5 % loss) was due to dehydroxylation within the framework of the zeolitic material. [4] These results suggest that all the prepared catalysts are stable up to at least 1000 ^oC, despite experiencing gradual weight loss between 400 ^oC and 1000 ^oC.

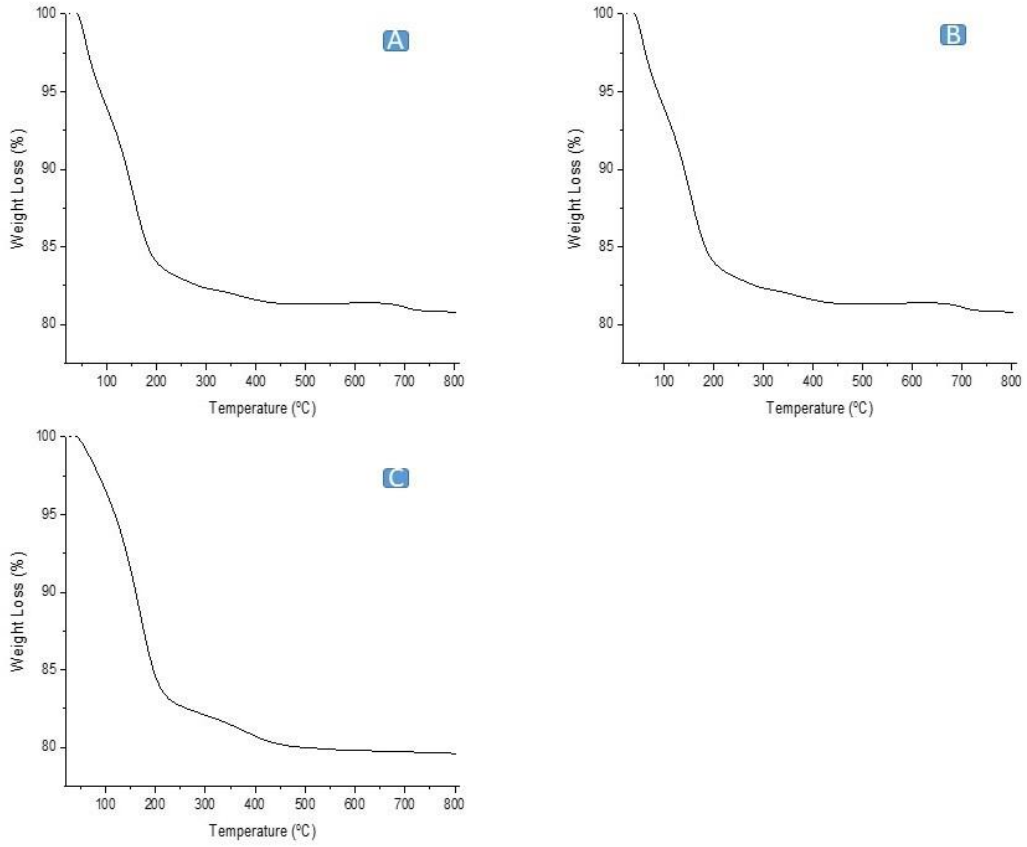

Figure 2.7. Thermogravimetric Analysis Curves of (**A**) NaY[AL], (**B**) NaY[CT], (**C**) NaY[CAT]

2.3.2 Catalysts Testing

The following conditions were used to evaluate the modified catalysts for the activation of n-octane in order to determine the impact of dealumination on the physicochemical properties of a NaY zeolite: T = 450 °C, Gas hourly space velocity (GHSV) = 8000 h^{-1}, C:O = 8:1 and catalyst = 1 mL. The results obtained (**Figure 2.8**) showed that all the prepared catalysts were active, recording conversions higher than 4 % with a carbon balance above 97 %. NaY[CT] had the highest conversion (10.2 %). The higher conversion could be attributed to the removal of both the non- and framework aluminium, which leads to improved pore volumes and surface area. When two of the modifiers are combined, they tend to be very effective in altering the microporous structure and inducing mesopores. [20] The overall activity from all the catalysts can be attributed to the presence of the strong Lewis acid sides as it was shown in **Section 2.3.1.6**. All the prepared modified zeolites were very selective towards CO_x (~ 92 %). This was attributed to the absence of an ODH-promoting metal. The only controlling factor was acidity,

which led to the over oxidation. NaY[AL] with the highest % dealumination showed the highest selectivity to cracked products, which was as per expectations since the removal of framework aluminium strengthens the acid sites that are responsible for the cracking mechanism. All the catalysts gave low selectivity towards octenes, due to the acid nature of the catalysts which facilitated the production of CO_x. The tested catalysts were active and showed no signs of coking.

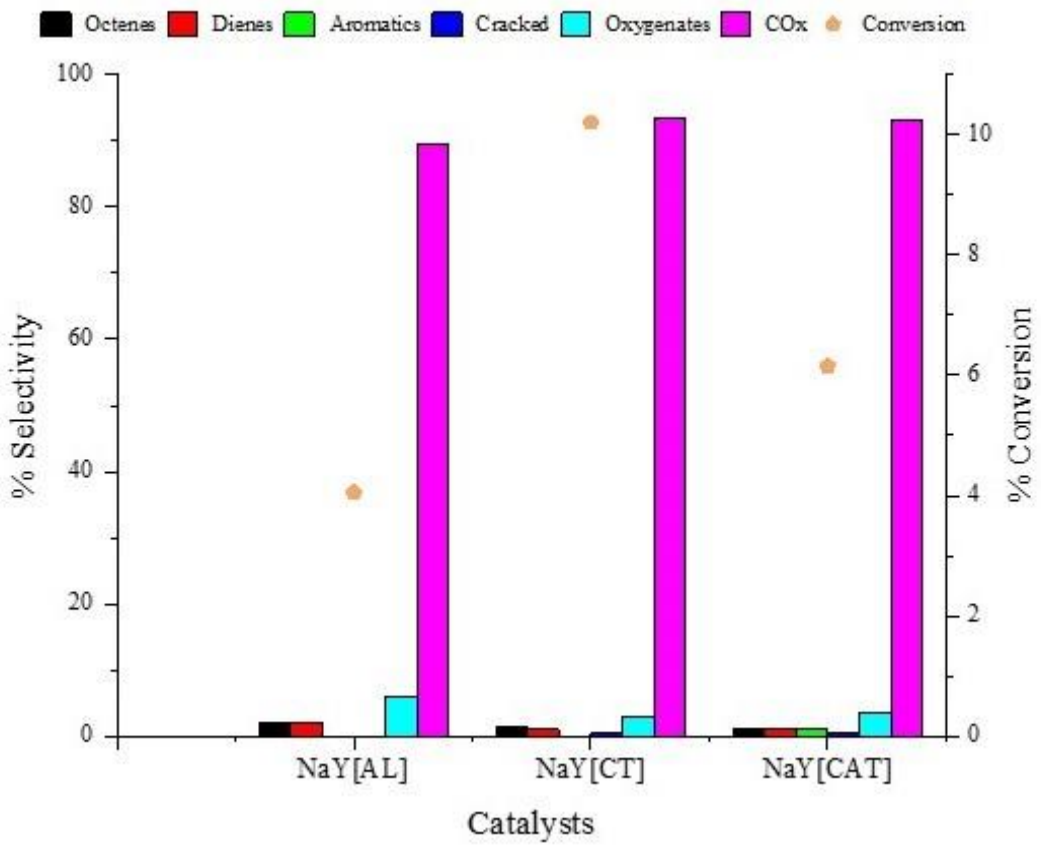

Figure 2.8. Effect of dealumination on the conversion of n-octane and product selectivity towards octenes isomers, dienes, aromatics, cracked products, oxygenates, and carbon oxides at a fixed temperature of 450 ^{o}C, GHSV = 8000 h^{-1}, C:O = 8:1

2.4 Conclusions

This study showed that different acid treatment modifications of the NaY can be successfully done without changing the framework structure of the faujasite zeolite. Stronger acid sites shown by the citric acid treatment suggest that this modification is more effective in the removal of framework aluminium, whereas a mixture of citric acid and EDTA-2Na was

effective in the removal of both the framework and non-framework aluminium, which affects the surface area and overall porous nature of the zeolite. P-XRD analysis showed that the crystallinity of the NaY zeolite is affected by the type of acid treatment used, with EDTA-2Na leading to a highly crystalline catalyst. All the prepared catalysts showed the presence of more Lewis acid sites, compared to Brønsted acid sites, this was confirmed by the low cracked product selectivities. All the prepared catalysts were active with conversions above 4 %. The complex treatment modified catalyst showed the highest conversion (~ 10 %) owing to the strengthened acid sites, improved pore volumes, and surface areas.

References

1. Wu, Z. and Zhao, D. 2011. Ordered mesoporous materials as adsorbents. Chemical Communications, 47, 3332-3338.
2. Vermeiren, W. and Gilson, J.P. 2009. Impact of zeolites on the petroleum and petrochemical industry. Topic in Catalysis, 52, 1131-1161.
3. Ndlela, S.S., Friedrich, H.B. and Cele, M.N. 2021. Oxidative dehydrogenation of n-octane using Ba and Ga-modified faujasite type catalysts prepared by different methods. Journal of Porous Materials, 28, 593-603.
4. Ndlela, S.S., Friedrich, H.B. and Cele, M.N. 2020. Effects of framework disruption of Ga and Ba containing zeolitic materials by thermal treatment. Catalysts, 10, 975-987.
5. Silaghi, M.C., Chizallet, C. and Raybaud, P. 2014. Challenges on molecular aspects of dealumination and desilication of zeolites. Microporous and Mesoporous Materials, 191, 82-96.
6. Alamdari, A. and Karimzadeh, K. 2018. Oxidative dehydrogenation of liquefied petroleum gas on copper, zinc and iron oxide impregnated on MFI zeolite assisted by electric power. Catalysts, 8, 270-295.
7. Hu, S., Liu, J., Chen, J., Meng, J., Ye, G. and Zhou, X. 2022. Reducing external surface diffusion barriers by chemical vapor deposition for improved zeolite catalysis. Industrial and Engineering Chemistry Research, 17, 5747-5756.
8. Pliekhov, O., Pliekhova, O., Arcon, I., Bondino, F., Magnano, E., Mali, G. and Logar, N.Z. 2020. Study of water adsorption on EDTA dealuminated zeolite Y. Microporous and Mesoporous Materials, 302, 110208-110214.

9. Feng, A., Yu, Y., Mi, L., Cao, Y., Yu, Y. and Song, L. 2019. Synthesis and characterization of hierarchical Y zeolites using NH_4HF_2 as dealuminating agent. Microporous and Mesoporous Materials, 280, 211-218.
10. Yurtaeva, A.S., Sorokina, T.P., Plekhova, K.S., Potapenko, O.V., Gulyaeva, T.I., Talsi, V.P. and Doronin, V.P. 2021. Effect of modification conditions on the physicochemical characteristics of Y zeolite as a component of a petrochemical cracking catalyst. Petroleum Chemistry, 61, 352-331.
11. Yan, Z., Ma, D., Zhuang, J., Liu, X., Liu, X., Han, X., Bao, X., Chang, F., Xu, L. and Liu, Z. 2003. On the acid-dealumination of USY zeolite: A solid state NMR investigation. Journal of Molecular Catalysis A: Chemical, 194, 153–167.
12. Gackowski, M., Tarach, K., Kuterasinski, L., Podobinski, J., Sulikowski, B. and Datka, J. 2019. Spectroscopic IR and NMR studies hierarchical zeolites obtained by desilication of zeolite Y: Optimization of the desilication route. Microporous and Mesoporous Materials, 281, 134-141.
13. Zang, J., Yu, H., Liu, G, Hong, M., Liu, J. and Chen, T. 2023. Research progress on modification of zeolite Y for improved catalytic properties. Inorganics, 11, 22-41.
14. Qiu, B., Lu, W.-D., Gao, X.-Q., Sheng, J., Ji, M., Wang, D. and Lu, A.-H. 2023. Boosting of propylene selectivity over embryonic borosilicate zeolite catalyst for oxidative dehydrogenation of propane. Journal of Catalysis, 417, 14-21.
15. Liu, P., Zhang, L., Wang, X., Du, M., Hao, Y., Li, L., Chen, X., Sun, N. and Wei, W. 2023. Preparation, structured-performance relationship, and reaction network of ZnZSM-5 for oxidative dehydrogenation of ethane with CO_2. Chemistry-A European Journal, 29, 1-10.
16. Bikbaeva, V., Nesterenko, N., Konnov, S., Nguyen, T.-S., Gilson, J.-P. and Valtchev, V. 2023. A low carbon route to ethylene: Ethane oxidative dehydrogenation with CO_2 on embryonic zeolite supported Mo-carbide catalyst. Applied Catalysis B: Environmental, 320, 122011-122020.
17. Gambo, Y., Lucky, R.A., Ba-Shammakh, M.S. and Hossain, M.M. 2023. Integrating dehydrogenation of alkanes with selective hydrogen combustion - A sustainable route for olefin production using tandem catalysis. Molecular Catalysis, 551, 113554-113568.

18. Ndlela, S.S., Friedrich, H.B. and Cele, M.N. 2021. Faujasite silicalites for oxidative dehydrogenation of n-octane: Influence of alkali metals, gallium, and boron on catalyst activity. Molecular Catalysis, 502, 111393-111399.
19. Ndlela, S.S., Friedrich, H.B. and Cele, M.N. 2020. Effects of modifying acidity and reducibility on the activity of NaY zeolite in the oxidative dehydrogenation of n-octane. Catalysts, 10, 363-375.
20. Qiao, K., Wei, L., Feng, R., Yan, Z., Zhang, Z. and Gao, X. 2015. Preparation and characterization of hierarchical USY by post-treatment. Applied Petrochemical Research, 5, 313-319.
21. Zhao, J., Yin, Y., Li, Y., Chen, W. and Liu, B. 2016. Synthesis and characterization of mesoporous zeolite Y by using block copolymers as templates. Chemical Engineering Journal, 284, 405-411.
22. Huang, Y., Wang, K., Dong, D., Li, D., Hill, M.R., Hill, A.J. and Wang, H. 2010. Synthesis of hierarchical porous zeolite NaY particles with controllable particle sizes. Microporous and Mesoporous Materials, 127, 167-175.
23. Shariatinia, Z. and Bagherpour, A. 2018. Synthesis of zeolite NaY and its nanocomposites with chitosan as adsorbents for lead(ii) removal from aqueous solution. Powder Technology, 338, 744-763.
24. He, L.-N., Wang, D.-M. and Hasegawa, S. 2000. A study of plasma-deposited amorphous SiO_x:H ($0 \leq x \leq 2.0$) films using infared spectroscopy. Journal of Non-Crystalline Solids, 261, 67-71.
25. Young, T.F. and Chen, C.P. 2000. Study on the Si-Si vibration states of the near surface region of porous silicon. Journal of Porous Materials, 7, 339-343.
26. Sotomayor, F., Cychosz, K.A. and Thommes, M. 2018. Characterization of micro/mesoporous materials by physisorption: Concepts and case studies. Accounts of Materials and Surface Research, 3, 34-50.
27. Sing, K.S.W., Everett, D.H., Haul, R.A.W., Moscou, L., Pierotti, R.A., Rouquerol, J. and Siemieniewska, T. 1985. Reporting physisorption data for gas/solid systems with special reference to the determination of surface area and porosity. Pure and Applied Chemistry, 57, 603-619.
28. Jawad, A. and Ahmed, S. 2023. Analysis and process evaluation of metal dopant (Zr, Cr)-promoted Ga-modified ZSM-5 for the oxidative dehydrogenation of propane in the presence and absence of CO_2. Royal Society of Chemistry Advances, 13, 11081-11095.

29. Parker, L.M., Bibby, D.M. and Burns, G.R. 1991. Fourier-transform infrared study of pyridine sorbed on zeolite HY. Journal of the Chemical Society, Faraday Transactions, 87, 3319-3323.
30. Akçay, M. 2005. The surface acidity and characterization of Fe-montmorillonite probed by in situ FT-IR spectroscopy of adsorbed pyridine. Applied Catalysis A: General, 294, 156-160.

Chapter 3

Oxidative dehydrogenation of n-octane using gallium containing dealuminated sodium-Y (NaY) zeolites

Abstract

The activation of n-octane using gallium (Ga) containing dealuminated NaY catalysts was studied using the oxidative dehydrogenation reaction. All the previously dealuminated catalysts were modified by 2 %wt of gallium using an ionic exchange procedure. The incorporation of Ga was to facilitate the oxidative dehydrogenation properties of the dealuminated zeolites. Successful incorporation of Ga into the extra framework of the zeolites was confirmed by SEM-EDX, whereas the p-XRD, FT-IR, and SEM all confirmed that all the modified catalysts kept the faujasite structure. Acidity characterisation using Pyridine FT-IR showed no change in the distribution of the acid sites before and after the addition of gallium into the dealuminated NaY zeolites. TPR analysis of the Ga-modified zeolites showed different reduction profiles which was attributed to the different dealumination techniques which resulted in different positions of Ga in the pores of the zeolites. Catalytic data showed that the conversion over all the catalysts increased with the introduction of Ga. This was consistent with previous studies. The conversion increase for all the catalysts was ~ 2 % for all three catalysts. Ga-NaY[AL] showed no decrease in the carbon oxides (CO_x) selectivity, while the two other catalysts Ga-NaY[CT] and Ga-NaY[CAT] showed a decrease in the CO_x selectivity from ~ 94 % and 93 % to ~ 88 % and 90 % respectively.

3.1 Introduction

In contrast to the currently commercialized dehydrogenation reaction, the oxidative dehydrogenation (ODH) reaction is exothermic and operates under lower temperatures and at standard pressure. This in itself makes oxidative dehydrogenation desirable and a potential choice for use in industry. This method is attractive since it avoids the extra regeneration step in an industrial application and the catalyst employed is less prone to coking. [1] Oxidative dehydrogenation may have the ability to get over the primary technical issues associated with

dehydrogenation and it has been explored as a viable substitute technique for producing olefins from paraffins. [2-4]

Olefins' high reactivity and susceptibility to further oxidation in the presence of oxygen gas through adsorption onto the catalyst surface provide the primary drawback in oxidative dehydrogenation reactions. Thus, basic catalysts are necessary to maintain high alkene yields under oxidative conditions. [5,6] In general, adding promoters to a catalyst can change its characteristics and increase its catalytic activity. [7] Oxidative dehydrogenation reactions have previously been explored using transition metal oxide-based catalysts supported by hydrotalcite, SBA-15, rare earth metals, MgO, SiO_2, Al_2O_3, ZrO_2, and TiO_2. [5,6,8-13] These systems work on the basis of the acid-base characteristics of the catalyst and the reducibility of the active metals.

Zeolites provide several ways to adjust their properties, including dealumination, isomorphic substitution, ionic exchange, and desilication. They are employed in industry as isomerization and cracking catalysts, as well as adsorbents. [14] Their interesting characteristics which include large surface area, thermal stability, and well-defined pores together with their simplicity in synthesis and modification, have drawn the use of these materials in a variety of catalytic applications. [15]

Cheng et al. [16] showed that ethane dehydrogenation in the presence of CO_2 at 650 ^oC can have a selectivity of 92 % and a conversion of 25 % when Ga supported on Na-ZMS-5 is used as a catalyst. It was determined that the dispersion of GaOx species by the silanols on the surface played a huge role in the catalytic behavior.

Ndlela et al. [17] studied oxidative dehydrogenation of n-octane using catalysts synthesized via the sol-gel technique. It was reported that the silicalites type catalyst (BBaY-S), which had the lowest acidity, recorded the highest selectivity of 40 % to octenes and the lowest selectivity of 28 % to carbon oxides (CO_x), whilst the faujasite zeolite (GaNaY-S), which had the highest acidity, performed oppositely with octenes selectivity of 17 % and CO_x selectivity of 56 %. The catalytic findings demonstrated that the acid-base characteristics and active metal reducibility of the catalysts were important.

In this work, we studied the effect of modifying the previously dealuminated NaY zeolites (**Section 2**) by the introduction of the oxidative dehydrogenation active gallium metal using an ionic exchange procedure. Results from **Section 2** demonstrated the effect of dealumination on the strength of the acid sites which was very influential in improving the oxidative

dehydrogenation conversion but led to high selectivities of CO_x. Therefore, to decrease the CO_x selectivity while improving the oxidative dehydrogenation products, the catalysts were modified by gallium which is an active metal.

3.2 Materials and Experimental Methods

3.2.1 Catalysts Preparation

Preparation of Ga-NaY zeolites was carried out as follows: A solution of 0.56 g $Ga(NO_3)_3$ in 45 mL of double distilled water was mixed with 15 g of the dealuminated NaY samples, (NaY[AL], NaY[CAT, and NaY[CT]) in a 150 mL round bottom flask. The samples were then stirred at 80 ^oC for four hours. Thereafter, the contents were cooled to room temperature, filtered under vacuum, and washed thoroughly with double distilled water before drying at 110 ^oC overnight. The ionic exchange procedure was carried out twice to ensure sufficient loading of gallium on the zeolites. [19] The catalysts were then denoted as Ga-NaY[AL], Ga-NaY[CAT], and Ga-NaY[CT]. Additionally, all the samples were calcined under air for 6 hours at 550 ^oC before characterisation.

3.2.2 Catalysts Characterisation

Powder X-ray diffraction patterns was performed for structure and phase identification using a Bruker D8 advance diffractometer equipped with a graphite monochromatic filter operated at 40 kV and 40 mA, (Billerica, USA). The radiation source was CuKα with a wavelength of 1.5406 nm. Data acquisition was performed at a step and scan rate of 0.02^o and 0.2 s^{-1}, respectively, and at a 2-theta range of 5^o to 90^o. Infrared spectra was recorded at room temperature using a Perkin Elmer Spectrum 100 FT-IR Spectrometer equipped with a Universal ATR Sampling Accessory at a Gauge pressure of 124. IR spectra of pyridine was also recorded using the same instrument. For pyridine IR, 0.25 g of sample was treated with 0.5 mL of liquid pyridine. Then, the samples were allowed to dry overnight before the spectra in 1400–1700 cm^{-1} region were recorded for acidic sites' determination. Using a Zeiss Ultra Plus field emission gun scanning electron microscope (FEG-SEM) with Smart SEM Software (Oberkhochen, Germany), SEM-EDX images were acquired for morphology and surface structure. The samples were coated with gold using a Q150R series high vacuum Quorum sputter coater prior analysis. TGA thermal analysis was performed to determine the material's

thermal stability. The METTLER TOLEDO TGA/DSC1, ISF Model 1346 with STAR^e software version 9.20 instrument was used for analysis, with a heating rate of 300 $^oC/h$ in flowing air. Temperature programmed experiments were carried out using a Micromeritics 2900 AutoChem II Chemisorption Analyzer but first the catalysts were degassed at 400 ^oC overnight. For temperature programmed reduction (TPR), the catalyst was prepared by heating it under an argon stream (30 mL/min) at 400 ^oC for 30 min and then cooled to 80 ^oC. After that, a reducing agent of 5 % hydrogen in argon was added at a flow rate of 30 mL/min. Samples were analysed under static air from room temperature to 950 ^oC at a ramp rate of 20 ^oC/min. [20]

3.2.3 Catalysts Testing

Testing of the catalysts was done in a laboratory-scale, fixed-bed, continuous-flow gas phase reactor at 450 ^oC. The reactor tube had an inner diameter of 10 mm and was constructed of stainless steel. n-Octane (Merk, assay > 98 %) at a concentration in a gas mixture (v/v) above the maximum flammability limit of n-octane was used in the reactions. The n-octane content was maintained at 6 % in each reaction. The system was supplied with n-octane using a calibrated Lab Alliance Series II HPLC Pump, and the feed mass was measured with an electronic balance. Using heating tape, the n-octane fed in was maintained at 130 ^oC via the heated supply lines. K-type thermocouples were used to monitor the temperature and a CB-100 RK temperature controller with internal playback was used to control it. A 1.0 mL pelletized catalyst (with pellet sizes ranging from 600 μm to 1000 μm) was used for every reaction, sandwiched between two thin layers of glass wool that were placed in the reactor block's hottest zone after calibration. Glass wool was used to seal the ends of the reactor tube after 24 grit carborundum had been poured into the gaps. A Ritter drum type wet gas flow meter was used to measure the total gas flow. A cylindrical stainless-steel jar was used to collect all liquid products and unreacted feed, and it was cooled to around 3.0 ^oC. COx products were analyzed using a Perkin Elmer Clarus 400 GC fitted with a 30 m × 530 μm Supelco Carboxen 106 PLOT column and a thermal conductivity detector. A Shimadzu GC-2025, fitted with a 50 m ×200 μm PONA capillary column and flame ionization detector, was utilized to analyze liquid and gaseous products.

3.3 Results and Discussion

3.3.1 Catalysts Characterization

3.3.1.1 Powder XRD

The introduction of Ga by ionic exchange on the dealuminated NaY zeolites did not alter the framework structure of the faujasite zeolite as seen in F**igure 3.1**. All the samples showed the typical diffraction peaks of the faujasite (FAU) structure. Due to the small amount of gallium employed and a good dispersion achieved (**Figure 3.4**), the modified zeolites solely displayed the NaY phase and also did not exhibit any gallium oxide peaks [19,21]. The three Ga-modified catalysts showed similar p-XRD diffraction peaks (but shorter in height indicating the gradual decrease in crystallinity) as the NaY catalysts before the modification described in **Section 2.3**.

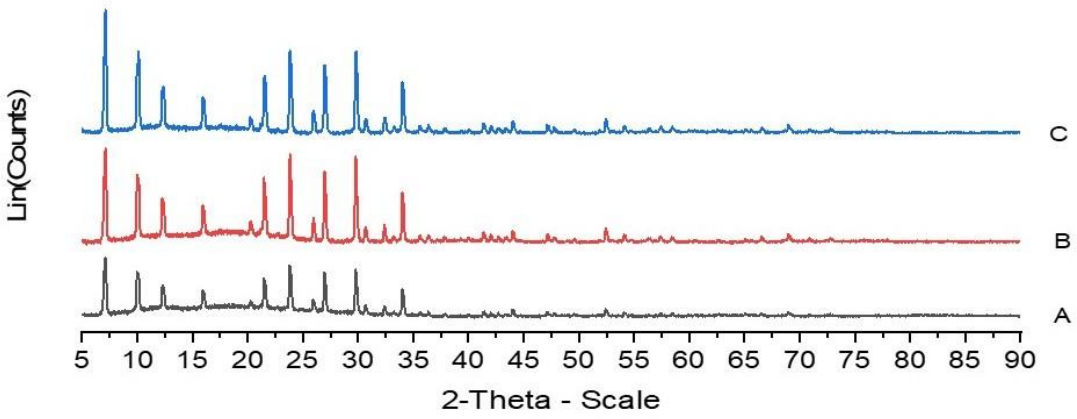

Figure 3.1. XRD diffractograms of (A) Ga-NaY[AL], (B) Ga-NaY[CT], (C) Ga-NaY[CAT]

3.3.1.2 FT-IR

Figure 3.2 shows the FT-IR spectra of the Ga exchanged samples. The results are consistent with those shown in **Section 3.3.1.1**, which showed similar results as those in **Section 2.3**. This further suggests no change in structure upon the introduction of Ga into the extra framework of the dealuminated NaY zeolites. The band at about 460 cm^{-1} is assigned to T-O (where T is either Si or Al), due to bending vibrations of the internal tetrahedra within the zeolite. [22] The bands around 550 cm^{-1} and 666 cm^{-1} are assigned to double-ring vibrations and symmetric stretching bands, respectively, and are associated with the FUA characteristic bands. [22,23]

The strong band at approximately 970 cm^{-1} is caused by Si-O bending/internal tetrahedra asymmetric stretching, while the H-O-H symmetric stretching band is visible at approximately 1654 cm^{-1}. [19,24] Bands around 2000-2300 cm^{-1} are assigned to Si-H stretching and O-Si-H bending absorptions. [25,26] The broad band in the range of 2900-3600 cm^{-1} can be attributed to stretching vibrations of hydroxyl groups of water molecules. [27,28]

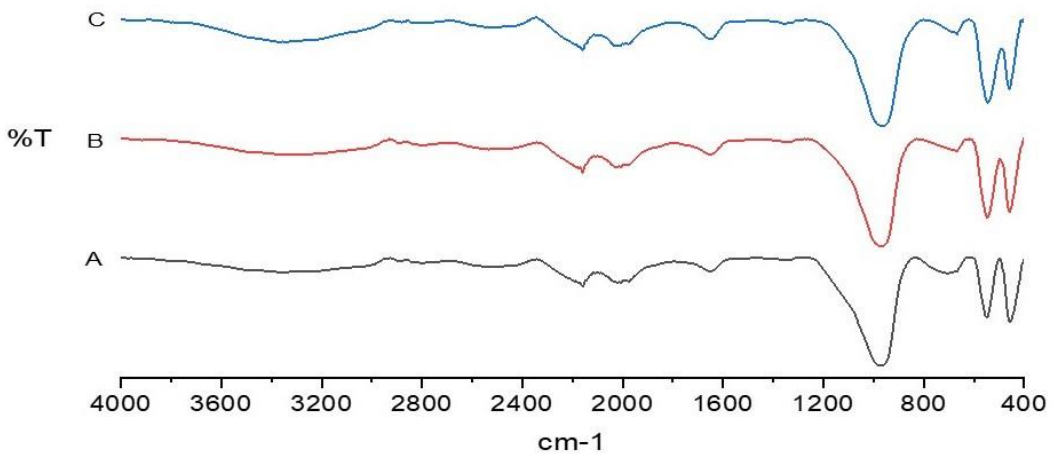

Figure 3.2. FT-IR Spectra of (**A**) Ga-NaY[AL], (**B**) Ga-NaY[CT], (**C**) Ga-NaY[CAT]

3.3.1.3 Scanning Electron Microscopy

SEM analyses showed the surface morphology of the modified NaY zeolites (**Figure 3.3**) as the typical cubic shape of a faujasite type zeolite. [18] The cubic distortion observed from all the catalysts was due to the dealumination procedure as shown in **Section 2.3**. The introduction of gallium did not further distort the cubic shape of all the prepared catalysts. SEM-EDX (**Figure 3.4**) showed the even distribution of the metal present in the prepared NaY catalysts. The results obtained also indicate the successful introduction of gallium in dealuminated NaY zeolites. The notable roughness of the surface on the micrographs is due to the repeated twinning of the NaY crystallite slabs during the ionic exchange procedure. [29]

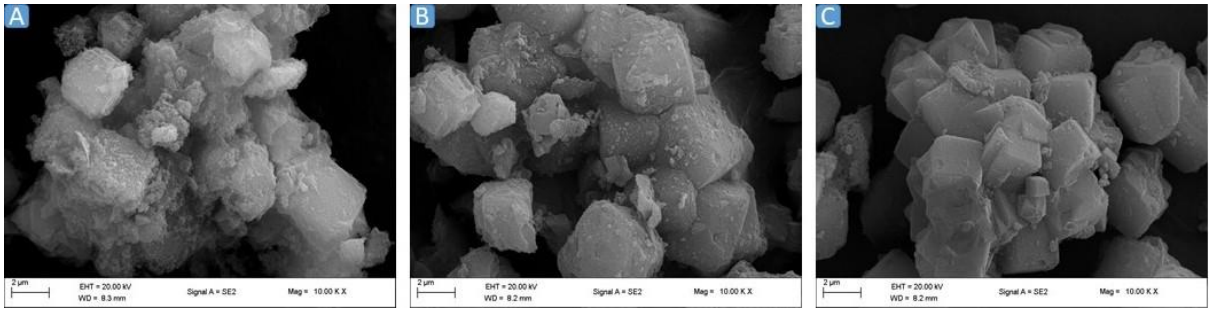

Figure 3.3. SEM Micrographs of (**A**) Ga-NaY[AL], (**B**) Ga-NaY[CT], (**C**) Ga-NaY[CAT]

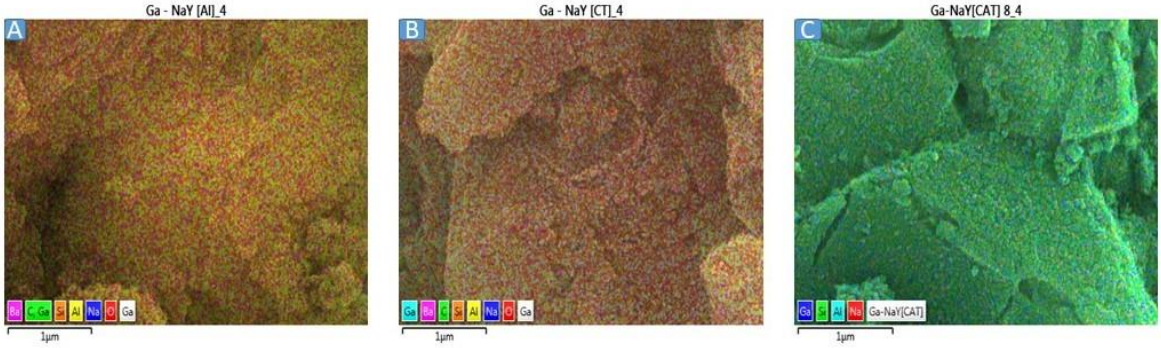

Figure 3.4. SEM-EDX Micrographs of (**A**) Ga-NaY[AL], (**B**) Ga-NaY[CT], (**C**) Ga-NaY[CAT]

3.3.1.4 Pyridine FT-IR

Pyridine FT-IR was carried out by the adsorption and desorption of pyridine at room temperature to qualitatively analyze the type and nature of acid sites in the Ga-modified NaY zeolites. The FT-IR spectra of the Ga-exchanged catalysts in the pyridine vibration range of 1400-1700 cm^{-1} are shown in **Figure 3.5**. The spectra obtained are similar to those shown in **Section 2.3**, which suggests the same type and distribution of the acid sites before and after gallium modification. Physically adsorbed pyridine has absorption bands at 1575 cm^{-1} and 1590 cm^{-1} because of surface hydroxyl groups and hydrogen bonding. The band at 1441 cm^{-1} demonstrates the pyridine adsorption on Lewis acidic sites. The Lewis and Brønsted acid sites interact to form the band at 1485 cm^{-1}. [30,31] The introduction of gallium did not induce any medium to strong Brønsted acid sites, which is evident by the absence of bands associated with pyridinium ions (PyH^{+}).

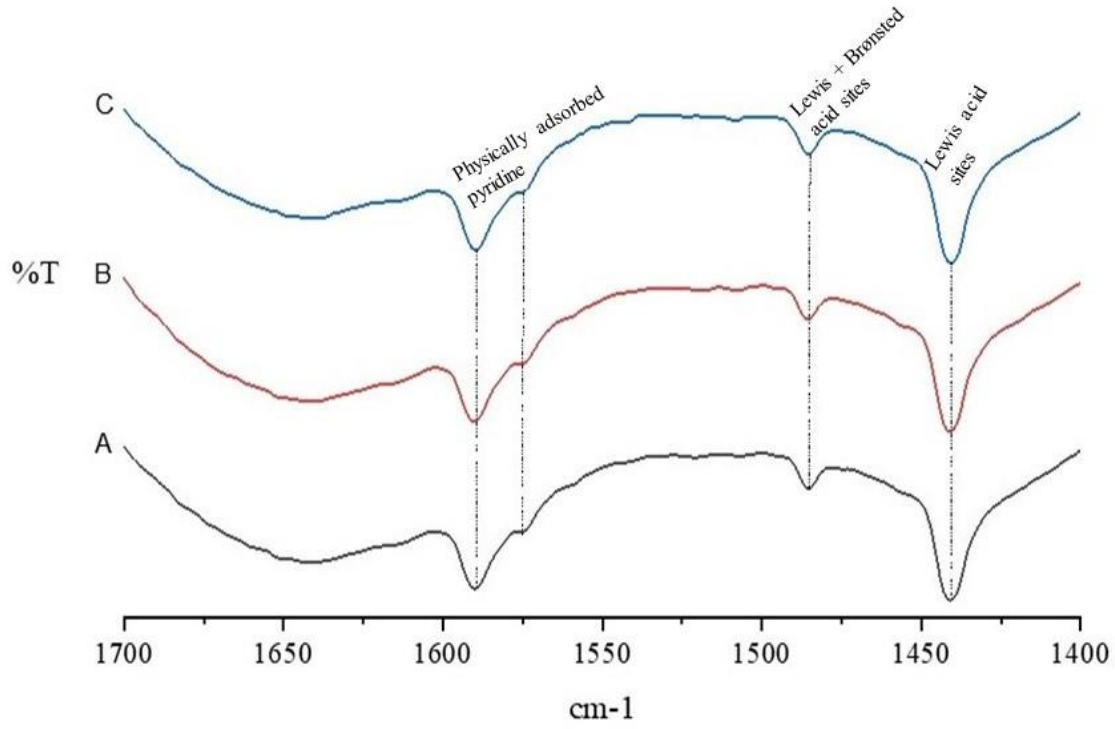

Figure 3.5. Pyridine FT-IR Spectra of (**A**) Ga-NaY[AL], (**B**) Ga-NaY[CT], (**C**) Ga-NaY[CAT] carried out at T = 25 ^{o}C

3.3.1.5 Temperature Programmed Reduction (TPR)

The temperature-programmed reduction profiles of the prepared catalysts are shown in **Figure 3.6**. Understanding the reducibility of gallium in the zeolite material is important because the activation of paraffin in oxidative dehydrogenation is dependent on the redox properties of the active metal. The TPR profiles for all the prepared catalysts showed reduction at three different temperature regions, the low temperature region (100-300 ^{o}C), medium temperature region (300-500 ^{o}C), and high temperature region (500-800 ^{o}C). Reduction peaks at low temperatures are caused by the chemisorption of hydrogen to Ga^{1+} species. [32] Reduction peaks that appeared from 500 ^{o}C to 800 ^{o}C are due to the extra framework Ga species. [33] Well-dispersed Ga species are responsible for the reduction peak, which occurs at temperatures between 460 ^{o}C and 690 ^{o}C. [34,35] A zeolite and a highly dispersed Ga species can interact strongly to form Ga^{3+} species, which can then be reduced to Ga^{1+}. [35] This means that peaks appearing above 650 ^{o}C are associated with a reduction of Ga^{3+} to Ga^{1+}. All the prepared catalysts showed peaks in all the defined regions, but with different hydrogen consumption quantities, which is

due to both non- and framework dealumination. [18] This then suggests that the Ga species are dispersed outside the framework and some inside the framework.

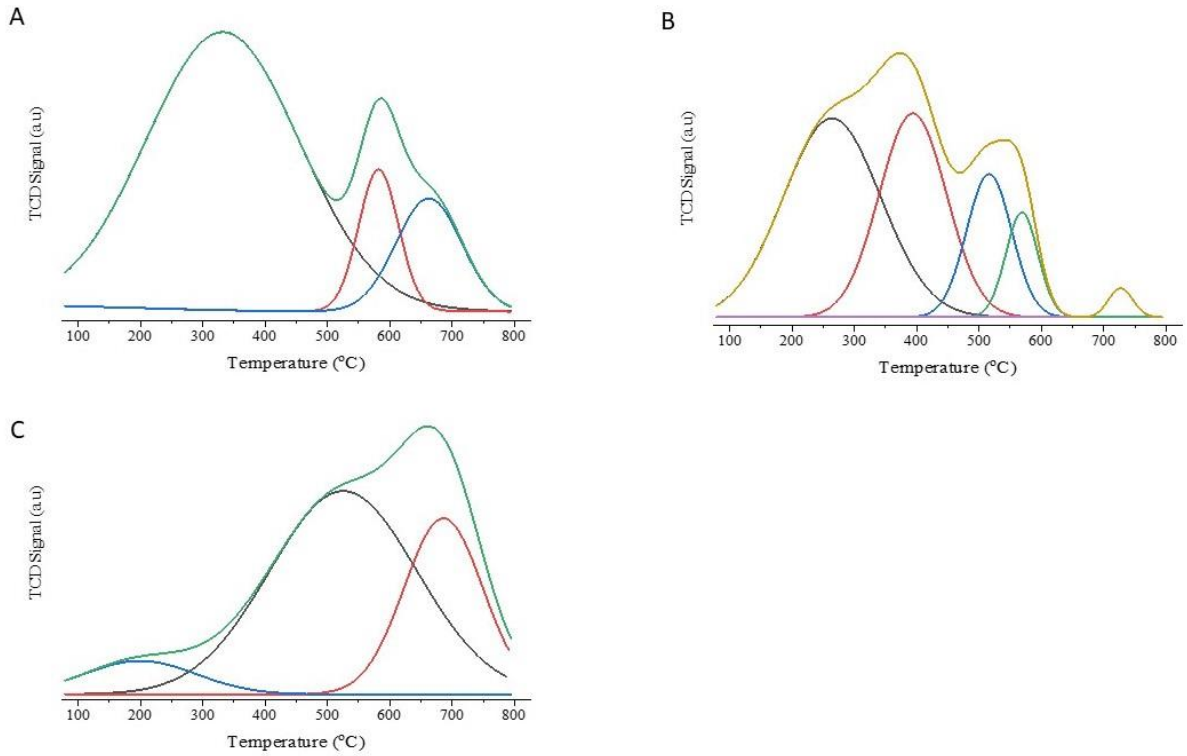

Figure 3.6. TPR Profiles of (**A**) Ga-NaY[AL], (**B**) Ga-NaY[CT], (**C**) Ga-NaY[CAT]

3.3.1.6 Thermogravimetric Analysis (TGA)

Three separate occurrences were seen in the thermogravimetric analysis curves of the gallium exchanged catalysts (**Figure 3.7**), at temperatures between 25 ^{o}C and 200 ^{o}C, 200 ^{o}C and 450 ^{o}C, and 450 ^{o}C and 850 ^{o}C. The loss of water and hydroxyl groups that were loosely linked to the extra framework cations at low temperatures contributed most of the 14 %, 18 %, and 16 % weight loss for Ga-NaY[AL], Ga-naY[CT], and Ga-NaY[CAT], respectively. The slight weight lost at medium temperatures was due to dehydroxylation inside the zeolitic material's structure. [36] These TGA results suggest that these catalysts are thermally stable up to at least 1000 ^{o}C.

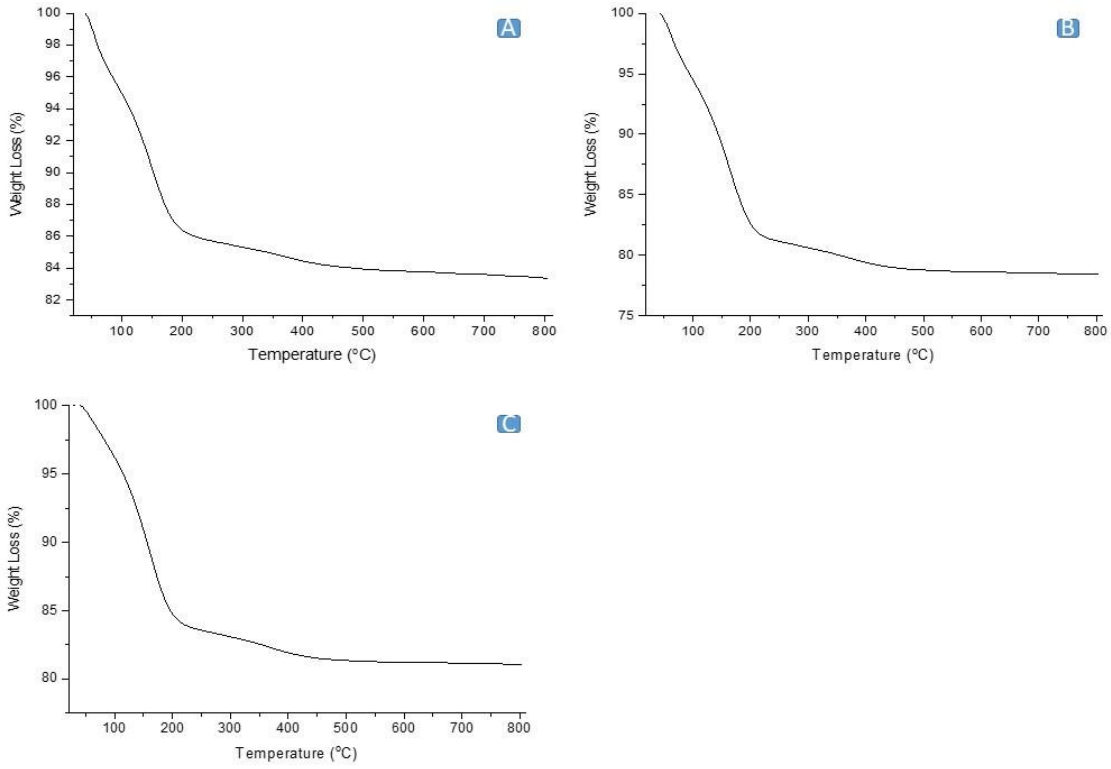

Figure 3.7. Thermogravimetric Analysis Curves of (**A**) Ga-NaY[AL], (**B**) Ga-NaY[CT], (**C**) Ga-NaY[CAT]

3.3.2 Catalysts Testing

Ga exchanged dealuminated NaY catalysts was subjected to oxidative dehydrogenation of n-octane under the following conditions: Temperature of 450 ^{o}C, gas hourly space velocity (GHSV) of 8000 h^{-1}, C:O: 8:1 and 1 mL of catalyst, to study the effectiveness of the active metal on the dealuminated NaY catalysts. The conversion of n-octane and selectivities are shown in **Figure 3.8**. Comparing the results with those obtained in **Section 2.3.2** it can be seen that the introduction of Ga has enhanced the conversion for all the catalysts, in the following order Ga-NaY[AL] < Ga-NaY[CAT] < Ga-NaY[CT]. The magnitude of conversion increased with gallium modification by about ~ 2 % for each catalyst, besides Ga-NaY[CT] which was just below 1 %. These increases in conversion are attributed to Ga acting as Lewis acid sites on the extra framework of the zeolite. [18,33] All the catalysts had a conversion above 6 %. Upon the introduction of Ga in high Si/Al ratio NaY catalyst (NaY[AL]), there was a decrease in side reactions such as cracking and cyclization. This might be the result of fewer acid sites with medium to strong strengths. [16] Having the oxidative dehydrogenation-promoting metal

led to a decrease in selectivity towards CO_x over both Ga-NaY[CT] and Ga-NaY[CAT]. The decrease in CO_x production was ~ 4 % for both catalysts. There were no observable changes for the Ga-NaY[AL] catalyst due to its high acidity which facilitated the overoxidation. The results, as expected, showed the influence of Ga as the ODH-promoting metal, however, still the acidity outweighed that effect as overoxidation led to high selectivity towards CO_x. The Ga-NaY[CT] catalyst having the lowest selectivity towards CO_x gave the highest selectivity to octenes (2 %). Also, the decrease in CO_x selectivity of Ga-NaY[CT] and Ga-NaY[CAT] led to an increase in selectivity of dienes, 1.5 % and 5 %, respectively. For Ga-NaY[AL] it remained the same. Lastly, all of the catalysts showed no signs of coking.

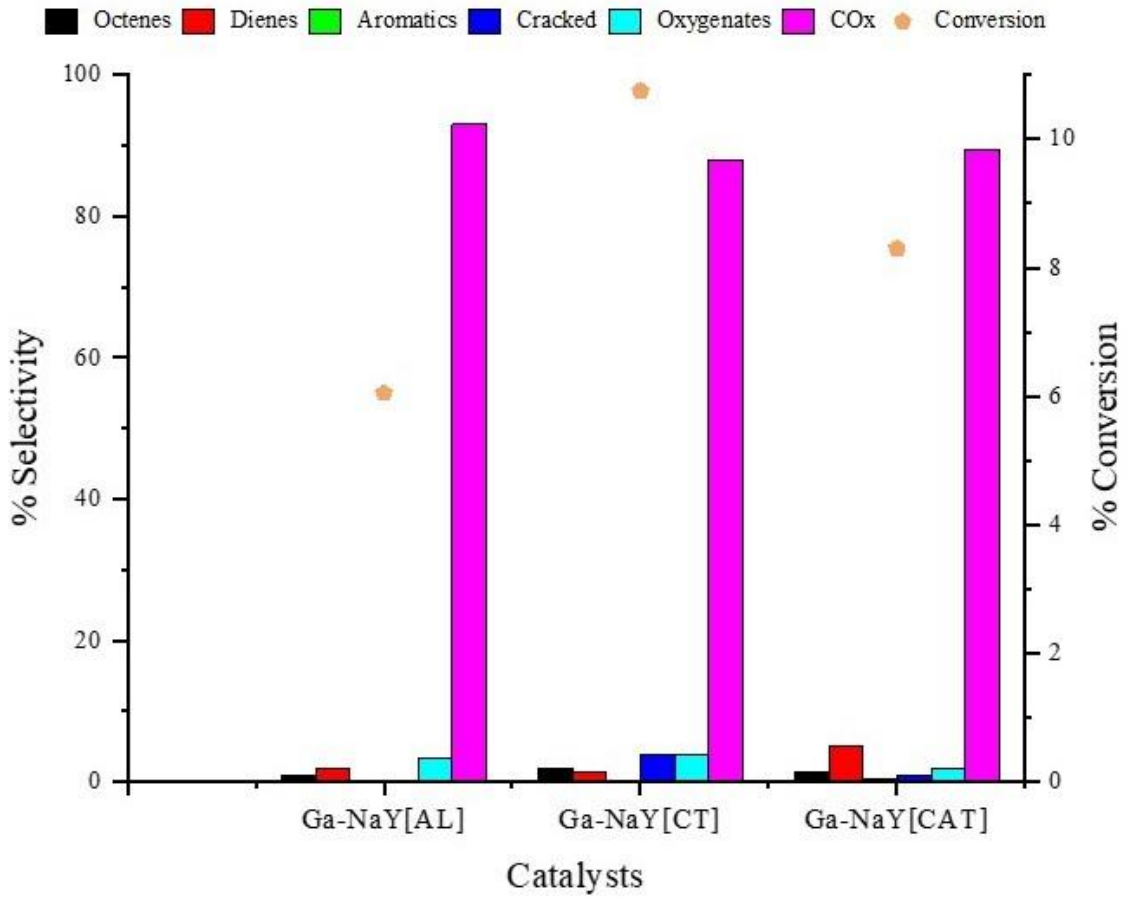

Figure 3.8. Effect of Ga containing dealuminated catalysts on the oxidative dehydrogenation of n-octane (6 ± 1 %) and products selectivity towards octenes isomers, dienes, aromatics, cracked products, oxygenates, and carbon oxides at a fixed temperature of 450 ^{o}C, GHSV of 8000 h^{-1}, C:O : 8:1

3.4 Conclusion

This study showed that the incorporation of gallium by ionic exchange changes the physical makeup of the NaY zeolites. The distribution and the type of acid sites before and after the addition of gallium were constant when pyridine FT-IR was carried out. The TPR analysis showed that the gallium introduced in NaY zeolites dealuminated by different methods leads to different hydrogen uptake which in turn leads to different TPR reduction profiles. As expected, the introduction of gallium facilitated the ODH reaction leading to an increase in both the conversion and olefin products. This was not the case for Ga-NaY[AL] which had the highest acidity and led to the highest overoxidation product selectivities. Ga-NaY[CT] and Ga-NaY[CAT] showed decreased selectivities towards CO_x. All the prepared catalysts were more selective towards the undesired CO_x products than the olefins as a result of the acidity that was introduced by dealumination.

References

1. Elkhalifa, E.A. and Friedrich, H.B. 2010. Oxidative dehydrogenation of n-octane using vanadium-magnesium oxide catalysts with different vanadium loadings. Applied Catalysis A: General, 373, 122-131.
2. Narayanappa, M, Dasireddy, V.D.B.C. and Friedrich, H.B. 2012. Catalytic oxidation of n-octane over cobalt substituted ceria ($Ce_{0.90}Co_{0.10}O_{2-\delta}$) catalysts. Applied Catalysis A: Ceneral, 447-448, 135-143.
3. Al-Ghamdi, S.A. and de Lasa, H.I. 2014. Propylene production via propane oxidation dehydrogenation over VO_x/γ-Al_2O_3 catalyst. Fuel, 128, 120-140.
4. Krasnobaeva, O.N., Belomestnykh, I.P., Nosova, T.A., Kondakov, D.F. and Danilov, V.P. 2018. Ytterbium-containing oxide catalysts for oxidative dehydrogenation of hydrocarbons. Russian Journal of Inorganic Chemistry, 63, 1394-1399.
5. Qiu, B., Jiang, F., Lu, W.-D., Yan, B., Li, W.-C., Zhao, Z.-C. and Lu, A.-H. 2020. Oxidative dehydrogenation of propane using layered borosilicate zeolite as an active and selective catalyst. Journal of Catalysis, 385, 176-182.
6. Gounden, N., Friedrich, H.B., Mahadevaiah, N. and Fadlalla, M.I. 2014. Octenes and aromatics from the oxidative dehydrogenation of n-octane over Co/TiO_2 catalysts. Catalysis Letters, 144, 2043–2051.

7. Elkhalifa, E.A. and Friedrich, H.B. 2015. Effects of boron and barium dopants on VMgO catalysts employed in the oxidative dehydrogenation of n-octane. Kinetics and Catalysis, 56, 212-221.
8. Elkhalifa, E.A. and Friedrich, H.B. 2014. Oxidative dehydrogenation and aromatization of n-octane over VMgO catalysts obtained by using different MgO precursors and different precursor treatments. Journal Molecular Catalysis A: Chemical, 392, 22–30.
9. Vedrine, J.C. 2016. Heterogeneous catalytic partial oxidation of lower alkanes (C_1–C_6) on mixed metal Oxides. Journal of Energy Chemistry, 25, 936–946.
10. Dasireddy, V.D.B.C., Singh, S. and Friedrich, H.B. 2012. Oxidative dehydrogenation of n-octane using vanadium pentoxide-supported hydroxyapatite catalysts. Applied Catalysis A: General, 421, 58– 69.
11. Yun, Y.S., Lee, M., Sung, J., Yun, D., Kim, T.Y., Park, H., Lee, K.R., Song, C.K., Kim, Y., Lee, J., Seo, Y.-J., Song, I.K. and Yi, J. 2018. Promoting effect of cerium on MoVTeNb mixed oxide catalyst for oxidative dehydrogenation of ethane to ethylene. Applied Catalysis B: Environmental, 237, 554–562.
12. Khodakov, A., Yang, J., Su, S., Iglesia, E. and Bell, A.T. 1998. Structure and properties of vanadium oxide-zirconia catalysts for propane oxidative dehydrogenation. Journal of Catalysis, 177, 343-351.
13. Kaliya, M.L., Kogan, S.B., Froumin, N. and Herskowitz, M. 2002. Novel nitrogen containing heterogeneous catalysts for oxidative dehydrogenation of light paraffins. Catalysis Communications, 3, 327-333.
14. Boronat, M. and Corma, A. 2015. Factors controlling the acidity of zeolites. Catalysis Letter, 145, 162–172.
15. Corma, A. 2003. State of the art and future challenges of zeolites as catalysts. Journal of Catalysis, 216, 298–312.
16. Cheng, Y., Lei, T., Miao, C., Hua, W., Yue, Y. and Gao, Z. 2018. Ga_2O_3/NaZSM-5 for C_2H_6 dehydrogenation in the presence of CO_2: Conjugated effect of silanol. Microporous and Mesoporous Materials, 268, 235–242.
17. Ndlela, S.S., Friedrich, H.B. and Cele, M.N. 2021. Faujasite silicalites for oxidative dehydrogenation of n-octane: Influence of alkali metals, gallium, and boron on catalyst activity. Molecular Catalysis, 502, 111393-111399.
18. Qiao, K., Wei, L., Feng, R., Yan, Z., Zhang, Z. and Gao, X. 2015. Preparation and characterization of hierarchical USY by post-treatment. Applied Petrochemical Research, 5, 313-319.

19. Ndlela, S.S., Friedrich, H.B. and Cele, M.N. 2020. Effects of modifying acidity and reducibility on the activity of NaY zeolite in the oxidative dehydrogenation of n-octane. Catalysts, 10, 363-375.
20. Bandaru, H., Mahomed, A.S., Singh, S. and Friedrich, H.B. 2018. The effect of varying the metal ratio in a chromium molybdate catalysts for the oxidative dehydrogenation of *n*-octane. Molecular Catalysis, 460, 74–82.
21. Chanthaanont, P. and Sirivat, A. 2013. Effect of transition metal ion-exchanged into the zeolite Y on electrical conductivity and response of PEDOT-PSS/MY composites toward CO_2. Advances in Polymer Technology, 32, 21367-21372.
22. Zhao, J., Yin, Y., Li, Y., Chen, W. and Liu, B. 2016. Synthesis and characterization of mesoporous zeolite Y by using block copolymers as templates. Chemical Engineering Journal, 284, 405-411.
23. Huang, Y., Wang, K., Dong, D., Li, D., Hill, M.R., Hill, A.J. and Wang, H. 2010. Synthesis of hierarchical porous zeolite NaY particles with controllable particle sizes. Microporous and Mesoporous Materials, 127, 167-175.
24. Shariatinia, Z. and Bagherpour, A. 2018. Synthesis of zeolite NaY and its nanocomposites with chitosan as adsorbents for lead(ii) removal from aqueous solution. Powder Technology, 338, 744-763.
25. He, L.-N., Wang, D.-M. and Hasegawa, S. 2000. A study of plasma-deposited amorphous SiO_x:H ($0 \leq x \leq 2.0$) films using infared spectroscopy. Journal of Non-Crystalline Solids, 261, 67-71.
26. Young, T.F. and Chen, C.P. 2000. Study on the Si-Si vibration states of the near surface region of porous silicon. Journal of Porous Materials, 7, 339-343.
27. Pal, N., Pramanik, M., Bhaumik, A. and Ali, M. 2014. Highly selective and direct oxidation of cyclohexane to cyclohexanone over vanadium exchanged NaY at room temperature under solvent-free conditions. Journal of Molecular Catalysis A: Chemical, 392, 299-307.
28. Król, M., Mozgawa, W., Jastrzębski, W. and Barczyk, K. 2012. Application of IR spectra in the studies of zeolites from D4R and D6R structural groups. Microporous Mesoporous Material, 156, 181-188.
29. Kim, W.-G., So, J., Won Choi, S., Liu, Y., Dixit, R.S., Sievers, C., Sholl, D.S., Nair, S. and Jones, C.W. 2017. Hierarchical Ga-MFI catalysts for propane dehydrogenation. Chemistry of Materials, ACS Publications, 1-36.

30. Penkova, A., Bobadilla, L.F., Romero-Sarria, F., Centeno, M.A. and Odriozola, J.A. 2014. Pyridine adsorption on NiSn/MgO-Al_2O_3: An FTIR spectroscopic study of surface acidity. Applied Surface Science, 317, 241-251.
31. Parker, L.M., Bibby, D.M. and Burns, G.R. 1991. Fourier-transform infrared study of pyridine sorbed on zeolite HY. Journal of the Chemical Society, Faraday Transactions, 87, 3319-3323.
32. Ndlela, S.S., Friedrich, H.B. and Cele, M.N. 2021. Faujasite silicalites for oxidative dehydrogenation of n-octane: Influence of alkali metals, gallium, and boron on catalyst activity. Molecular Catalysis, 502, 111393-111399.
33. Xin, M., Xing, E., Gao, X., Wang, Y., Ouyang, Y., Xu, G., Luo, Y. and Shu, X. 2019. Ga substituted during modification of ZSM-5 and its influences on catalytic aromatization performance. Industrial and Engineering Chemistry Research, 58, 6970-6981.
34. Shao, C.-T., Lang, W.-Z., Yan, X. and Guo, Y.-J. 2017. Catalytic performance of gallium oxide based-catalysts for the propane dehydrogenation reaction: Effects of support and loading amount. Royal Society of Chemistry, 7, 4710-4723.
35. Jawad, A. and Ahmed, S. 2023. Analysis and process evaluation of metal dopant (Zr,Cr)-promoted Ga-modified ZSM-5 for the oxidative dehydrogenation of propane in the presence and absence of CO_2. Royal Society of Chemistry, 13, 11081-11095.
36. Ndlela, S.S., Friedrich, H.B. and Cele, M.N. 2020. Effects of framework disruption of Ga and Ba containing zeolitic materials by thermal treatment. Catalysts, 10, 975-987.

Chapter 4

Influence of Ba on the ODH activity in dealuminated gallium-sodium-Y (Ga-NaY) zeolites

Abstract

Post-synthetic modification of a series of dealuminated Ga-NaY zeolites by the introduction of barium was carried out using a modified ionic exchange procedure. The introduction of 1.5 %wt of barium was to induce basic sites on the surface of the Ga-NaY zeolites in order to facilitate the quick desorption of oxidative dehydrogenation (ODH) products. This in turn further limits the overoxidation of primary products to carbon oxides (CO_x). P-XRD and the SEM analysis showed that the introduction of Ba into the Ga-NaY zeolites changed the framework structure of the zeolite, which was evident by the disappearance of some characteristic peaks between the 20^o-30^o 2-theta scale region. The typical cubic shape for the morphology of the faujasite-type zeolite was distorted for all the prepared catalysts. The framework disruption of the prepared catalysts may be due to the subsequent ionic exchange procedures carried out during the introduction of gallium and then the barium ions. Pyridine IR showed a similar distribution of the acid sites with the Ga-NaY zeolites, and ammonia temperature programmed desorption (NH_3-TPD) showed that all the catalysts contained strong acid sites, with BaGa-NaY[AL] having the most acidity as expected. Due to the high acidity of the catalysts, the effect of Ba was only slightly noticed in the results, with a 4 % decrease in CO_x selectivity and an increase in cracked products and oxygenates, especially for BaGa-NaY[CT].

4.1 Introduction

Byproducts of coal- and gas-to-liquids processes are medium- and long-chain linear paraffins. The supply of these low-value compounds is predicted to expand quickly because of the growing number of these plants worldwide, and it is necessary to transform them into value-added products. [1] Researchers have employed oxidative dehydrogenation involving medium- to long-chain paraffins as an alternative method of producing high-value-added products due

to the fact that the introduction of oxygen leads to reduced carbon deposition on the surface of a catalyst and reduced thermodynamic limitations. [2-5] By doing so, they have avoided using zeolites because of their propensity to induce deep oxidation and rapid deactivation caused by coke deposition. Zeolites are widely employed in the oxidative dehydrogenation of short-chain alkanes. [6] Consequently, a modification technique that eliminates zeolites' unwanted characteristics without compromising their stability in the oxidative dehydrogenation of medium-to-long-chain paraffins remains to be discovered.

Due to their high acidity, zeolites are not the best catalysts for the oxidative dehydrogenation of alkanes. Because zeolites are acidic, they generally cause excessive CO_x generation, catalyst deactivation from coke deposition, and undesirable side reactions that are selective to cracked products. [7] It has been demonstrated that adding multivalent metals to a zeolite's structure reduces the acidity of the material. [8] Therefore, the simplicity of synthesizing and modifying zeolites has attracted the use of these materials in different catalytic applications. [9] Zeolite material have a high thermal stability and a large surface area facilitating dispersion, which raises catalytic activity even at low concentrations of an active metal. Apart from these characteristics, zeolites also provide the opportunity to add the active metal to the material's external or internal structure, resulting in a material with a distinct catalytic activity. [7-11]

Prior research has demonstrated that oxidative dehydrogenation catalysts containing basic oxides are more selective. Higher selectivities are obtained from the quick desorption of the generated olefins from the catalytic surface, which is facilitated by the presence of basic centers. Basic promoters like alkali and alkaline earth metals have been employed to accomplish this. Such promoters are used because of their great stability as well as their catalytic capabilities, basicity, and structure. [12-14] Promoter basicity and concentration also have an impact on catalytic performance. The catalytic surface contact between promoters and the catalyst has been linked to the effects. It has previously been proposed that oxidative dehydrogenation requires a significant role from the acid-base nature of the catalyst surface. [14]

Recent studies have shown that zeolites can be modified and used in oxidative dehydrogenation reactions, however, the activity of the catalysts was very low (about 10 %) with good selectivity. [11,13] Therefore, this study will focus on further modifying the faujasite zeolite by the dealumination method which will strengthen the acidic sites responsible for the activity of the catalyst. This will then improve the conversion while maintaining the selectivity to

octenes and aromatics. The dealuminated zeolites will then be exchanged by gallium which is an oxidative dehydrogenation active metal and barium to induce basic sites for desorption of the products.

4.2 Materials and Experimental Methods

4.2.1 Catalysts Preparation

The three catalysts prepared as described in **Section 3.2** were further modified by the introduction of barium using the ionic exchange procedure as follows; BaGa-NaY[AL], BaGa-NaY[CAT], and BaGa-NaY[CT] catalysts were prepared by exchanging a 0.04 mol solution of $Ba(NO_3)_2$ with 8 g of Ga-NaY[AL], Ga-NaY[CAT], and Ga-NaY[CT] at 80 ^oC for four hours. The resulting catalysts were filtered, washed and dried the same way as Ga-NaY[AL], Ga-NaY[CAT], and Ga-NaY[CT]. The prepared catalysts were calcined under flowing air at 550 ^oC for six hours before characterization and testing. [13]

4.2.2 Catalysts Characterisation

X-ray diffraction (powder) was performed for the purpose of identifying structure and phase using a Bruker D8 advance diffractometer equipped with a graphite monochromatic filter operated at 40 kV and 40 mA, (Billerica, USA). The radiation source was CuKα with 1.5406 nm wavelength. The data was acquired at a step and scan rate of 0.02^o and 0.2 s^{-1}, respectively, and at a 2-theta range of 5^o to 90^o. Infrared spectra were recorded at room temperature using a Perkin Elmer Spectrum 100 FT-IR Spectrometer equipped with a Universal ATR Sampling Accessory at a Gauge pressure of 124. The same device was also used to record the pyridine's IR spectra. 0.5 mL of liquid pyridine was applied to 0.25 g of material for pyridine infrared analysis. After that, the samples were allowed to dry overnight and the spectra in the 1400–1700 cm^{-1} region were recorded to determine acidic sites' type. SEM-EDX images were obtained for morphology and surface structure using a Zeiss Ultra Plus field emission gun scanning electron microscope (FEG-SEM) with Smart SEM Software (Oberkhochen, Germany). Before examination, the samples were coated with gold using a high vacuum Quorum sputter coater from the Q150R series. The thermal stability of the material was assessed using TGA thermal analysis. The METTLER TOLEDO TGA/DSC1, ISF Model 1346 with STAR^e software version 9.20 instrument was used for analysis, with a heating rate of 300

°C/h in flowing air. Temperature-programmed desorption (TPD) and temperature-programmed reduction (TPR) experiments were performed using a Micromeritics 2900 AutoChem II Chemisorption Analyzer. For ammonia temperature programmed desorption (NH_3-TPD), the catalyst (≈ 0.06 g) was flushed for 30 minutes at 350 °C with a helium flow rate of 20 mL/min. After that, the temperature was reduced to 80 °C. For 30 minutes, the catalyst was exposed to a 4.1 % ammonia-helium gas mixture at a rate of 20 mL/min. The excess ammonia was removed by flushing the system with helium at a flow rate of 30 mL/min for 30 minutes. [15] The same helium flow (30 mL/min) was then used to remove the adsorbed ammonia. The TPD tests were carried out by heating the sample to 900 °C in a constant helium flow at 10 °C/min. For TPR, the catalyst was prepared by heating it under an argon stream (30 mL/min) at 400 °C for 30 min and then cooled to 80 °C. Then, a 5 % hydrogen-reducing agent in argon was added at a flow rate of 30 mL/min. Samples were analyzed in still air, from room temperature to 950 °C, at a ramp rate of 20 °C/min. [2]

4.2.3 Catalysts Testing

The catalysts were tested at 450 °C in a laboratory-scale, fixed-bed, continuous-flow gas phase reactor. The reactor tube was made of stainless steel and had an inner diameter of 10 mm. n-Octane (Merk, assay > 98 %) at a concentration in a gas mixture (v/v) above the maximum flammability limit of n-octane was employed in the reactions. In every reaction, the n-octane content was maintained at 6 %. An electronic balance was used to monitor the feed mass and a calibrated Lab Alliance Series II HPLC Pump was used to supply the system with n-octane. Heated supply lines were used to maintain the supplied n-octane at 130 °C using heating tape. The temperature was controlled by a CB-100 RK temperature controller with internal playback and monitored by K-type thermocouples. After calibration, the hottest zone of the reactor block was positioned with two thin layers of glass wool surrounding a 1.0 mL pelletized catalyst (pellet sizes varied from 600 μm to 1000 μm). The reactor tube was filled with 40-grit carborundum and sealed at the ends with glass wool. The total gas flow was measured using a Ritter drum-type wet gas flow meter. All liquid products and unreacted feed were collected in a cylindrical stainless-steel jar that was chilled to around 3.0 °C. A Perkin Elmer Clarus 400 GC equipped with a 30 m × 530 μm Supelco Carboxen 106 PLOT column and a thermal conductivity detector was used to examine CO_x products. Liquid and gaseous products were

analyzed using a Shimadzu GC-2025 equipped with a 50 m ×200 µm PONA capillary column and flame ionization detector.

4.3 Results and Discussion

4.3.1 Catalysts Characterization

4.3.1.1 Powder XRD

The incorporation of barium on the dealuminated Ga-NaY zeolites using ionic exchange resulted in the collapse/ disruption of the faujasite framework, which is evident by the decrease in the intensity of the p-XRD peaks, and disappearance of some characteristic peaks between 20°-25° 2-theta range (**Figure 4.1**). The change in the structure was dominant for BaGa-NaY[AL], with the highest dealumination ratio. The cause for the framework disruption may be due to the subsequent ionic exchange procedure done on the zeolite for the introduction of Ga and Ba. [13] The disruption may also be caused by the dealumination effect, where Ba can occupy the framework position where aluminium was removed (this is the case for BaGa-NaY[CT], where both framework and extra framework aluminium were removed). [16] For BaGa-NaY[CT] and BaGa-NaY[CAT], the disruption is less as most dealumination was for the extra framework aluminium.

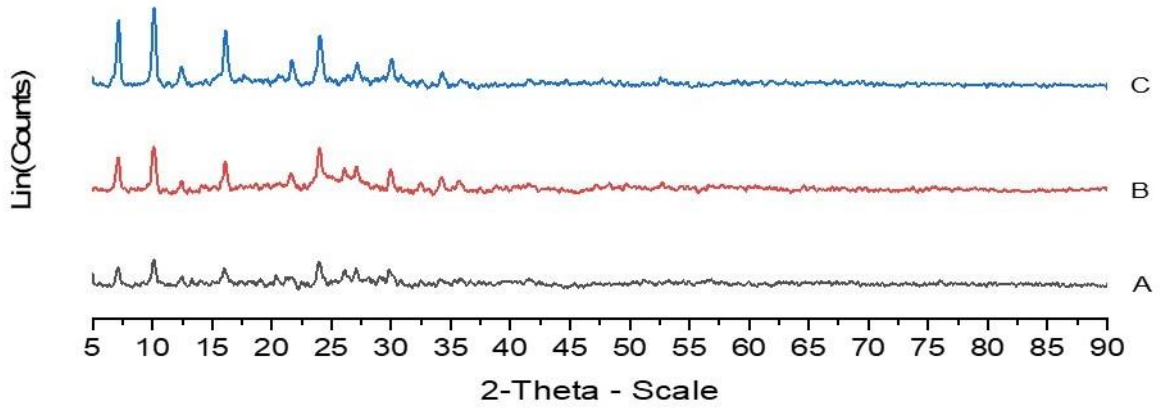

Figure 4.1. XRD diffractograms of (**A**) BaGa-NaY[AL], (**B**) BaGa-NaY[CT], (**C**) BaGa-NaY[CAT]

4.3.1.2 FT-IR

Figure 4.2 shows the FT-IR spectra of the Ba exchanged samples. Upon the introduction of the alkali earth metal to the Ga-NaY zeolites, the band intensities were weakened. This further supports the framework disruption argument in **Section 4.3.1.1**. The faujasite typical IR bands are still present, which suggests that the catalysts are still a faujasite type, however with defects. [13] The bands around 450 cm^{-1} and 560 cm^{-1} are attributed to T-O, where T can either be Si or Al, bending vibrations of internal and external tetrahedra in the zeolite, respectively. [17,18] The band around 695 cm^{-1} is assigned to a symmetric stretching band and is associated with the faujasite characteristic bands [17]. Si-O bending/internal tetrahedral asymmetric stretching is responsible for the strong band at about 970 cm^{-1}, while H-O-H symmetric stretching is visible at about 1660 cm^{-1}. [13,19] The bands corresponding to Si-H stretching and O-Si-H bending absorption are located between 2000 cm^{-1} and 2300 cm^{-1}. [20,21] The broad band around 2450 cm^{-1} is associated with the symmetric and antisymmetric H_3O^+ vibrations involving the two additional OH groups bonded to the $AlOSi^-$ bridging oxygen. [22]

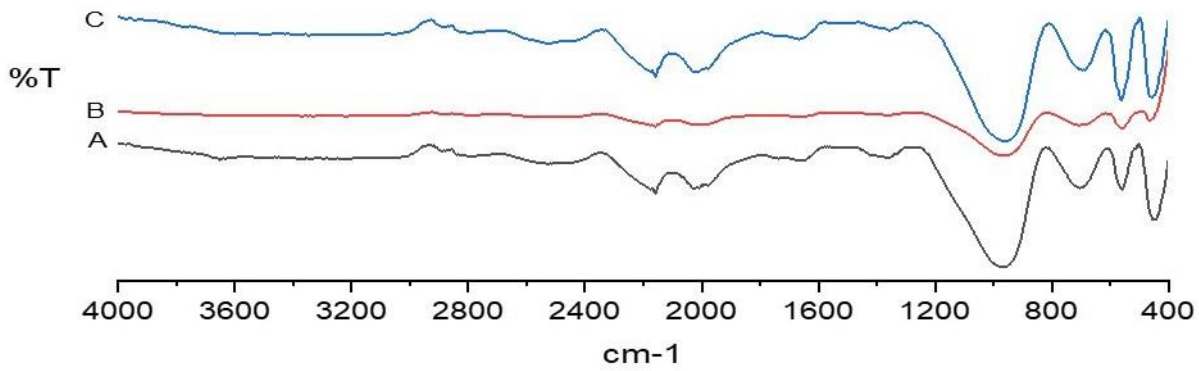

Figure 4.2. FT-IR Spectra of (**A**) BaGa-NaY[AL], (**B**) BaGa-NaY[CT], (**C**) BaGa-NaY[CAT]

4.3.1.3 Scanning Electron Microscopy

The surface morphology of the Ba containing Ga-NaY zeolites (**Figure 4.3**) did not show the typical cubic shape of a faujasite-type zeolites. [19] The cubic distortion observed from all the catalysts further supports results obtained from p-XRD. SEM-EDX (**Figure 4.4**) showed the even distribution of the metals present in the prepared NaY catalysts. The results obtained also indicate the successful introduction of barium in dealuminated Ga-NaY zeolites.

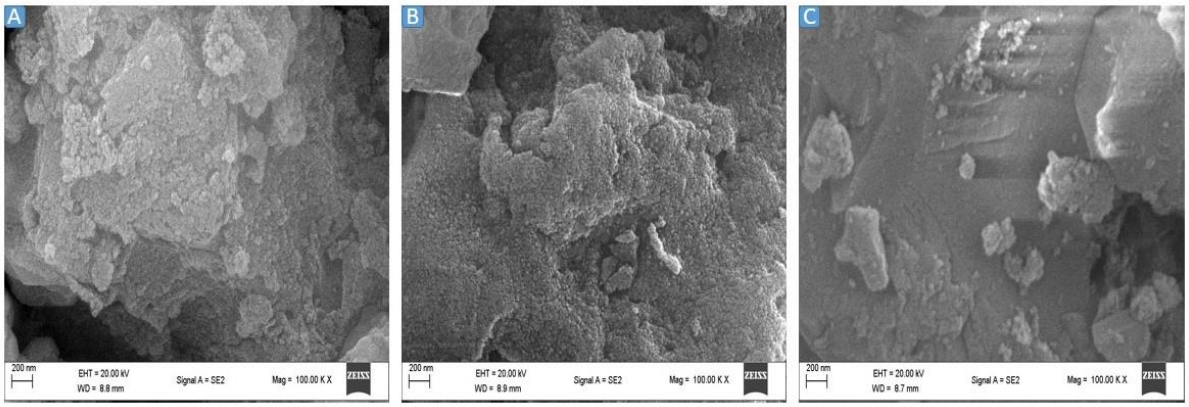

Figure 4.3. SEM Micrographs of (**A**) BaGa-NaY[AL], (**B**) BaGa-NaY[CT], (**C**) BaGa-NaY[CAT]

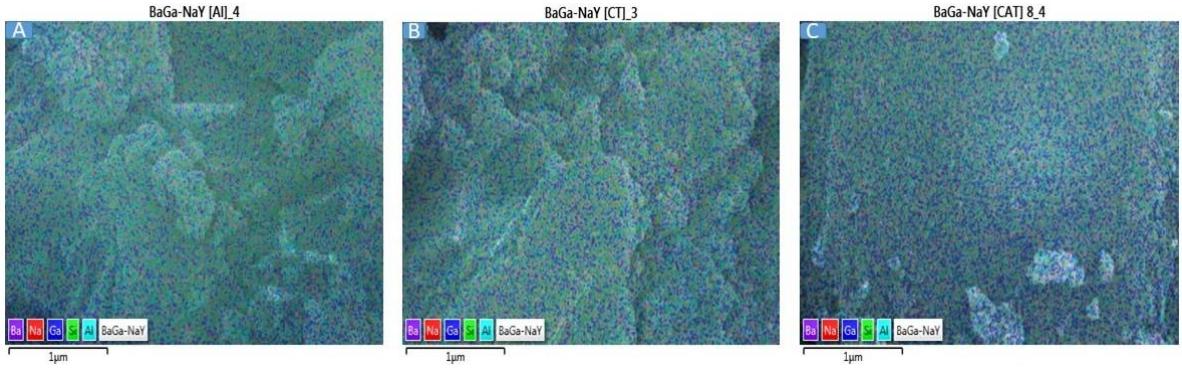

Figure 4.4. SEM-EDX Micrographs of (**A**) BaGa-NaY[AL], (**B**) BaGa-NaY[CT], (**C**) BaGa-NaY[CAT]

4.3.1.4 Pyridine FT-IR

To qualitatively analyze the type of acid sites, pyridine was adsorbed and desorbed at 25 ºC. The catalysts' FT-IR spectra in the 1400-1700 cm^{-1} pyridine vibration region are displayed in **Figure 4.5**. The spectra obtained are similar to those obtained in **Section 2.3** and **3.3**, which indicates the similarity in the type and distribution of the acid sites before and after barium and gallium introduction. Hydrogen bonds and surface hydroxyl groups physically adsorbed on pyridine exhibit absorption bands at 1575 cm^{-1} and 1590 cm^{-1}. Adsorption of pyridine on Lewis acidic sites is seen by the band at 1441 cm^{-1}. At 1486 cm^{-1}, the band is formed by the interaction between the Lewis and Brønsted acid sites. [23] Bands that are associated with pyridine adsorption on Brønsted acid sites were not evident for all the samples.

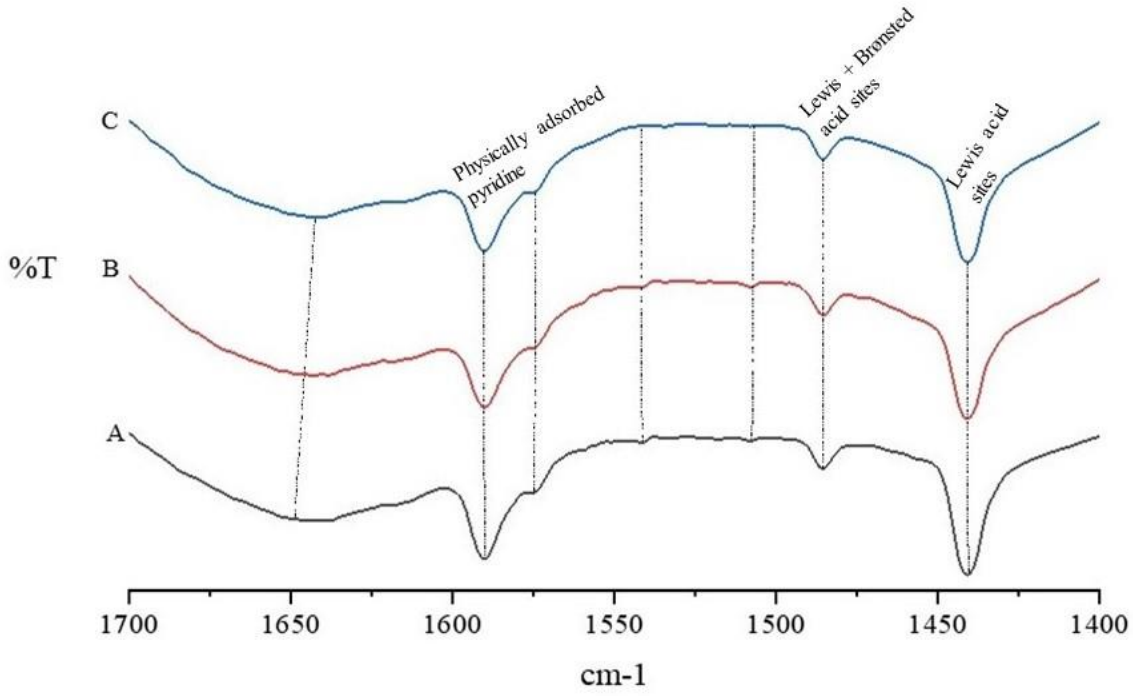

Figure 4.5. Pyridine FT-IR Spectra of (**A**) BaGa-NaY[AL], (**B**) BaGa-NaY[CT], (**C**) BaGa-NaY[CAT] carried out at room temperature

4.3.1.5 Ammonia-Temperature Programmed Desorption (NH_3-TPD)

Ammonia TPD was carried out to quantitatively study the acidity of the prepared catalysts. All the prepared catalysts possessed strong acid sites (refer to **Figure A1**), as ammonia desorption was only at high temperatures (≥400 ^oC). NaY zeolites are well-known for having weak acid sites, because of their low Si/Al ratio and high density of acid centers. [24] Dealumination of the NaY catalysts decreased the acid density while enhancing the acidic strength. Also, the ionic exchange of Ga and calcination at high temperatures may have resulted in the migration of some framework aluminium to the extra framework, causing an increase in acidic strength. [13,24,25] Quantitatively, BaGa-NaY[AL] had the highest acidity as expected, from the high % dealumination (104.3 µmol g^{-1}). BaGa-NaY[CT] was the second highest (33.3 µmol g^{-1}), and 11.8 µmol g^{-1} was recorded by BaGa-NaY[CAT]. BaGa-NaY[CT]'s acidity was higher than that of BaGa-NaY[CAT] because aluminium removal for the former was mostly from the framework and the latter, more extra framework, which is not as effective in increasing the acidity of the zeolite. [16]

4.3.1.6 Temperature Programmed Reduction (TPR)

Temperature programmed reduction profiles for the prepared catalysts are shown in **Figure 4.6.** The chemisorption of hydrogen to Ga^{+} species is the cause of the reduction peaks at lower temperatures. [10] Extra framework Ga species are responsible for reduction peaks starting from 400 ^{o}C to 700 ^{o}C. [26] The reduction peak at temperatures ranging from 420 ^{o}C to 700 ^{o}C is linked to the reduction of extra framework Ga^{3+} to Ga^{2+} and Ga^{+}, resulting from highly dispersed Ga and a zeolite interaction. [6,13,27,] Reduction peaks at high temperatures suggest that reduction was difficult for BaGa-NaY[AL] and BaGa-NaY[CT] compared to the BaGa-NaY[CAT] catalyst. This is because gallium in the former two catalysts may have occupied the framework positions where aluminium was removed, whereas, in the BaGa-NaY[AL], gallium only occupies the easily accessible extra framework positions. The reduction peak for BaGa-NaY[AL] centered at 655 ^{o}C is linked to the interaction of highly dispersed Ga species with dealuminated NaY, which results in the reduction of Ga^{3+} to Ga^{+}. [28]

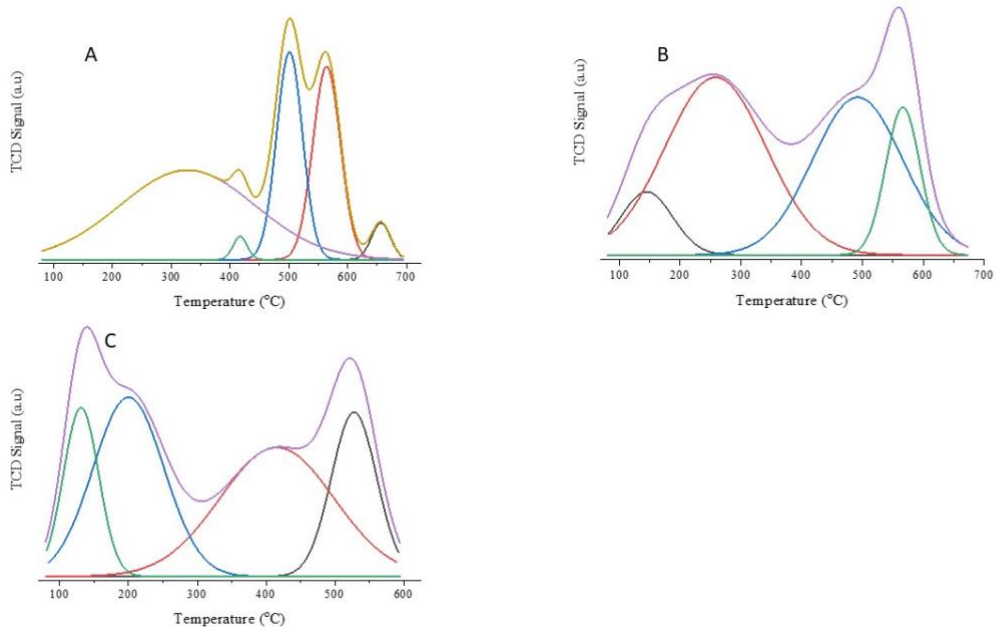

Figure 4.6. TPR Profiles of (**A**) BaGa-NaY[AL], (**B**) BaGa-NaY[CT], (**C**) BaGa-NaY[CAT]

4.3.1.7 Thermogravimetric Analysis (TGA)

Thermogravimetric analysis curves of the prepared catalysts (**Figure 4.7**) showed three different events at temperatures ranging from 25–200 ^{o}C, 200-550 ^{o}C, and 550-800 ^{o}C. BaGa-NaY[CAT] had the least total weight loss of about 0.5 %, followed by BaGa-NaY[CT] having

about 3.5 % weight loss, then BaGa-NaY[AL] having about 6 % weight loss. The loss of water and hydroxyl groups that were only weakly attached to the extra framework cations led to weight loss in the low temperature range. The zeolitic material's internal dehydroxylation caused weight loss in intermediate temperature ranges. [29] These results suggest that the introduction of barium stabilizes the zeolite catalysts, as the weight loss was much less than when the catalysts had Ga only.

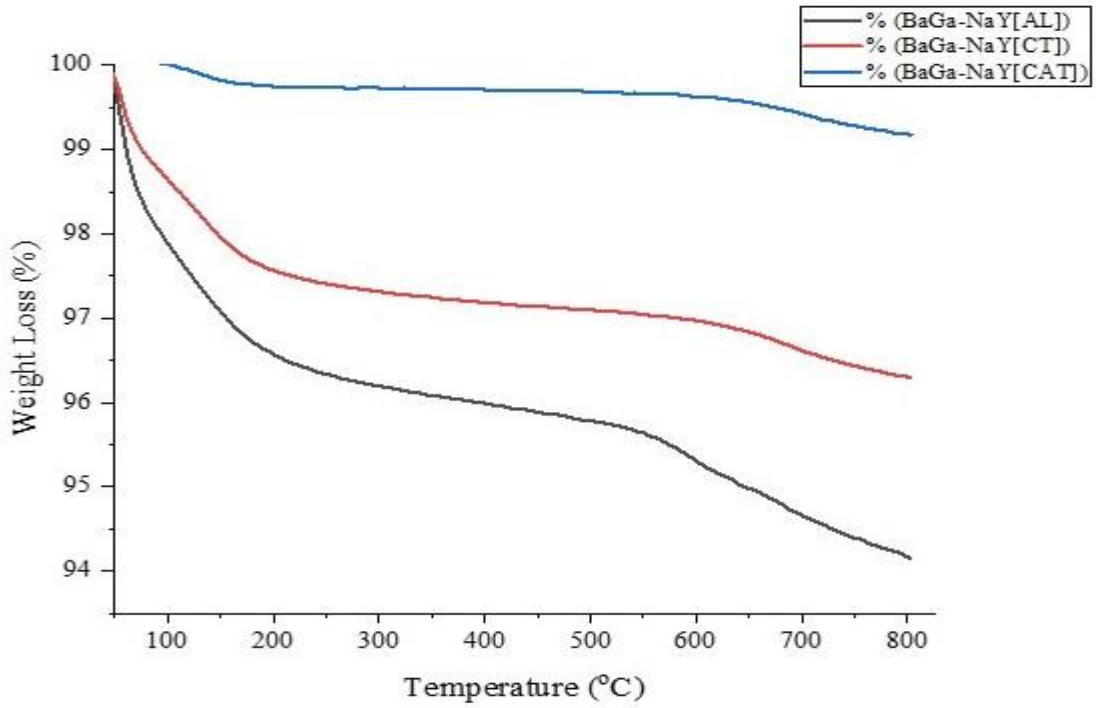

Figure 4.7. Thermogravimetric Analysis Curves of BaGa-NaY catalysts

4.3.2 Catalysts Testing

All the prepared catalysts were tested under the following conditions: T = 450 °C, GHSV = 8000 h^{-1}, C:O = 8:1, and catalyst = 1 mL; for the activation of n-octane using oxidative dehydrogenation reaction in order to determine the impact of Ba introduced by ionic exchange on the dealuminated Ga-NaY. **Figure 4.8** showed that BaGa-NaY[AL], with the highest acidity, gave the highest conversion (~ 7.6 %), and the highest selectivity to CO_x. The introduction of Ba did not show any effects on the product selectivity for this catalyst. BaGa-NaY[CT] and BaGa-NaY[CAT] showed a decrease in conversion, with the former recording ~ 7.7 % and the latter recording just above 1.5 % conversion. The introduction of barium for both these catalysts led to a slight decrease in the CO_x production and an increase in the cracked

and oxygenated products. This suggests that the desorption of products was improved, however, the acid sites still dominated as the increase in the desorbed products was mostly cracked products. [11,29,30]. All the prepared catalysts showed no sign of coking with a carbon balance of +/- 98 %.

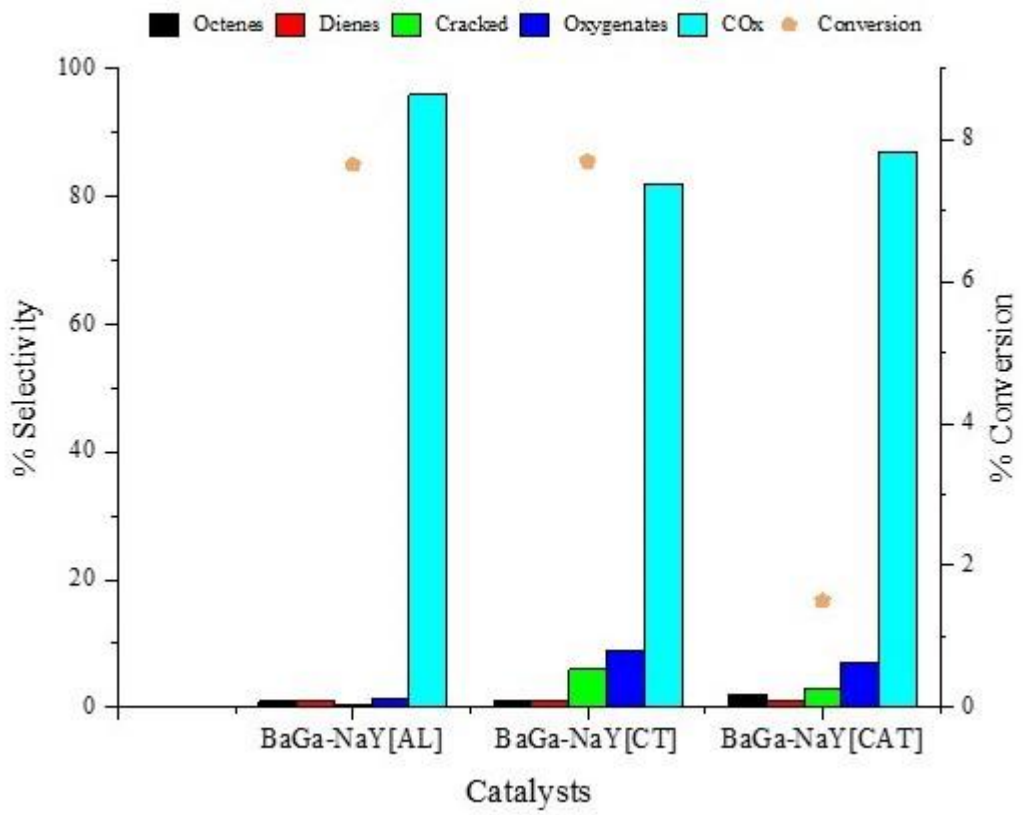

Figure 4.8. Effect of ionic exchange of Ga and Ba on the dealuminated catalysts on the oxidative dehydrogenation of n-octane and products selectivity towards octenes isomers, dienes, aromatics, cracked products, oxygenates, and carbon oxides at a fixed temperature of 450 ^{o}C, GHSV = 8000 h^{-1}, C:O = 8:1

4.4 Conclusion

The study has shown that the introduction of Ba in the dealuminated Ga-NaY zeolites led to the collapse of the faujasite framework, as shown by p-XRD and SEM analysis. Acidity data from NH_3-TPD showed that all the prepared catalysts had strong acid sites, which influenced the activity toward the ODH reaction. The introduction of Ba in Ga-NaY[AL] did not affect the activity of the catalysts, this catalyst showed the highest acidity, conversion, and selectivity

towards CO_x. The introduction of Ba in both Ga-NaY[CT] and Ga-NaY[CAT] led to a decrease in CO_x production, but the production of cracked products increased. This suggests that the cracked products in barium modified catalysts were able to be desorbed from the catalysts' surface before they were further oxidized to CO_x.

References

1. Elkhalifa, E.A. and Friedrich, H.B. 2010. Oxidative dehydrogenation of n-octane using vanadium-magnesium oxide catalysts with different vanadium loadings. Applied Catalysis A: General, 373, 122-131.
2. Bandaru, H., Mahomed, A.S., Singh, S. and Friedrich, H.B. 2018. The effect of varying the metal ratio in a chromium molybdate catalysts for the oxidative dehydrogenation of *n*-octane. Molecular Catalysis, 460, 74–82.
3. Narayanappa, M., Dasireddy, V.D.B.C. and Friedrich, H.B. 2012. Catalytic oxidation of n-octane over cobalt substituted ceria ($Ce_{0.90}Co_{0.10}O_{2-\delta}$) catalysts. Applied Catalysis A: General, 447, 135–143.
4. Song, X., Zhou, F., Ma, H., Liu, Y. and Wu, G. 2023. Comparative study of the oxidative dehydrogenation of cyclohexane over vanadium isomorphic-substituted hydroxyapatite and hydroxyapatite-supported vanadium oxide. Molecular Catalysis, 542, 113105-113114.
5. Dasireddy, V.D.B.C., Khan, F.B., Bharuth-Ram, K., Singh, S. and Friedrich, H.B. 2020. Non oxidative and oxidative dehydrogenation of n-octane using $FePO_4$: Effect of different $FePO_4$ phases on the product selectivity. Catalysis Science and Technology, 10, 7591-7600.
6. Jawad, A. and Ahmed, S. 2023. Analysis and process evaluation of metal dopant (Zr,Cr)-promoted Ga-modified ZSM-5 for the oxidative dehydrogenation of propane in the presence and absence of CO_2. Royal Society of Chemistry, 13, 11081-11095.
7. Aliev, A.M., Shabanova, Z.A., Nadzhaf-Kuliev, U.M. and Medzhidova, S.M. 2016. Oxidative dehydrogenation of cyclohexane over modified zeolite catalysts. Petroleum Chemistry, 56, 639–645.
8. Shamzhy, M., Opanasenko, M., Concepción, P. and Martínez, A. 2019. New trends in tailoring active sites in zeolite-based catalysts. Chemical Society Reviews, 48, 1095-1149.

9. Corma, A. 2003. State of the art and future challenges of zeolites as catalysts. Journal of Catalysis, 216, 298–312.
10. Ndlela, S.S., Friedrich, H.B. and Cele, M.N. 2021. Faujasite silicalites for oxidative dehydrogenation of n-octane: Influence of alkali metals, gallium, and boron on catalyst activity. Molecular Catalysis, 502, 111393-111399.
11. Ndlela, S.S., Friedrich, H.B. and Cele, M.N. 2021. Oxidative dehydrogenation of n-octane using Ba and Ga-modified faujasite type catalysts prepared by different methods. Journal of Porous Materials, 28, 593-603.
12. Li, G., Zhang, Y., Zhang, G., Sun, Y. and Liu, J. 2023. Effect of promoters on the catalytic performance of Ni-based catalysts for dry reforming of methane. Chemical Engineering and Technology, 46, 918-926.
13. Ndlela, S.S., Friedrich, H.B. and Cele, M.N. 2020. Effects of modifying acidity and reducibility on the activity of NaY zeolite in the oxidative dehydrogenation of n-octane. Catalysts, 10, 363-375.
14. Madeira, L.M., Martìn-Aranda, R.M., Maldonado-Hódar, F.J., Fierro, J.L.G. and Portela, M.F. 1997. Oxidative dehydrogenation of n-butane over alkali and alkaline earth-promoted α-$NiMoO_4$ catalysts. Journal of Catalysis, 169, 469–479.
15. Elkhalifa, E.A. and Friedrich, H.B. 2015. Effects of boron and barium dopants on VMgO catalysts employed in the oxidative dehydrogenation of n-octane. Kinetics and Catalysis, 56, 212-221.
16. Qiao, K., Wei, L., Feng, R., Yan, Z., Zhang, Z. and Gao, X. 2015. Preparation and characterization of hierarchical USY by post-treatment. Applied Petrochemical Research, 5, 313-319.
17. Huang, Y., Wang, K., Dong, D., Li, D., Hill, M.R., Hill, A.J. and Wang, H. 2010. Synthesis of hierarchical porous zeolite NaY particles with controllable particle sizes. Microporous and Mesoporous Materials, 127, 167-175.
18. Zhao, J., Yin, Y., Li, Y., Chen, W. and Liu, B. 2016. Synthesis and characterization of mesoporous zeolite Y by using block copolymers as templates. Chemical Engineering Journal, 284, 405-411.
19. Shariatinia, Z. and Bagherpour, A. 2018. Synthesis of zeolite NaY and its nanocomposites with chitosan as adsorbents for lead(ii) removal from aqueous solution. Powder Technology, 338, 744-763.

20. He, L.-N., Wang, D.-M. and Hasegawa, S. 2000. A study of plasma-deposited amorphous SiO_x:H ($0 \leq x \leq 2.0$) films using infared spectroscopy. Journal of Non-Crystalline Solids, 261, 67-71.
21. Young, T.F. and Chen, C.P. 2000. Study on the Si-Si vibration states of the near surface region of porous silicon. Journal of Porous Materials, 7, 339-343.
22. Pelmenschikov, A.G. and van Santen, R.A. 1993. Water-adsorption on zeolites: ab-initio interpretation of IR data. Journal of Physical Chemistry, 97, 10678-10680.
23. Penkova, A., Bobadilla, L.F., Romero-Sarria, F., Centeno, M.A. and Odriozola, J.A. 2014. Pyridine adsorption on NiSn/MgO-Al_2O_3: An FTIR spectroscopic study of surface acidity. Applied Surface Science, 317, 241-251.
24. Zang, J., Yu, H., Liu, G., Hong, M., Liu, J. and Chen, T. 2023. Research progress on modification of zeolite Y for improved catalytic properties. Inorganics, 11, 22-41.
25. Almutairi, S.M.T., Mezari, B., Filonenko, G.A., Magusin, P.C.M.M., Rigutto, M.S., Pidko, E.A. and Hensen, E.J.M. 2013. Influence of extraframework aluminum on the brønsted acidity and catalytic reactivity of faujasite zeolite. ChemCatChem, 5, 452–466.
26. Xin, M., Xing, E., Gao, X., Wang, Y., Ouyang, Y., Xu, G., Luo, Y. and Shu, X. 2019. Ga substituted during modification of ZSM-5 and its influences on catalytic aromatization performance. Industrial and Engineering Chemistry Research, 58, 6970-6981.
27. Shao, C.-T., Lang, W.-Z., Yan, X. and Guo, Y.-J. 2017. Catalytic performance of gallium oxide based-catalysts for the propane dehydrogenation reaction: Effects of support and loading amount. Royal Society of Chemistry, 7, 4710-4723.
28. Xiao, H., Zhang, J., Wang, X., Zhang, Q., Xie, H., Han, Y. and Tan, Y. 2015. A highly efficient Ga/ZMS-5 catalyst prepared by formic acid impregnation and in situ treatment for propane aromarization. Catalysis Science and Technology, 5, 4081-4090.
29. Ndlela, S.S., Friedrich, H.B. and Cele, M.N. 2020. Effects of framework disruption of Ga and Ba containing zeolitic materials by thermal treatment. Catalysts, 10, 975-987.
30. Abbot, J. 1989. Role of brønsted and lewis acid sites during cracking reactions of alkanes. Applied Catalysis, 47, 33–44

Chapter 5

Summary and Conclusions

Alkanes, especially linear alkanes, are common hydrocarbons mainly produced in the petrochemical industry by Fischer–Tropsch processes. In the past, the building blocks of the chemical industry have been aromatics and alkenes; however, alkanes can provide a less expensive alternative feedstock. Therefore, there is a global need to convert and benefit from these low-value, underutilized resources to produce products that have increased value. [1] A lot of work has been done on the oxidative conversion of alkanes utilizing various catalytic material classes or catalytic system designs. [2-4] The potential to develop affordable and ecologically acceptable methods for synthesizing partly oxidized organic molecules and olefins has motivated these studies. Moreover, the need to transform medium-to-long-chain alkanes into valuable products has grown along with the global production of these compounds. Oxidative dehydrogenation (ODH) is an attractive method due to its reduced thermodynamic limitations, exothermicity, and low catalyst deactivation. However, the commonly used catalysts for oxidative dehydrogenation are the metal oxide catalysts, which tend to suffer from quick deactivation due to coke deposition. Therefore, zeolites with interesting properties such as high surface area, thermal stability, well-defined pores, high crystallinity, and ease of modification make them interesting potential materials for oxidative dehydrogenation. [5-7]

This study focussed on the advancement of the use of faujasite zeolites in the oxidative dehydrogenation of n-octane by studying the influence of different dealumination processes on the acidity, structure, and activity of the catalyst. The dealuminated zeolites were further modified by the ionic exchange of gallium and barium for the facilitation of ODH and desorption of the ODH products. The faujasite zeolite of interest was NaY which is characterised by a low Si/Al ratio and high surface area. The prepared catalysts were characterized using X-ray fluorescence (XRF) for elemental composition. Power X-ray (XRD), FT-IR, Brunauer Emmett and Teller (BET), and Scanning Electron Microscopy (SEM) were used for structure, morphology, and phase identification. Ammonia temperature programmed desorption (NH_3-TPD) and pyridine-IR were used to study the acidic nature of the zeolitic catalysts. Temperature-programmed reduction (TPR) was used to study the reducibility of

gallium. Thermogravimetric analysis was used to study the thermal stability of the catalysts. The catalysts were tested in the oxidative dehydrogenation of n-octane under the same reaction conditions to study the activity of the catalysts.

The first part of this study was to strengthen the acid sites of a commercially obtained NaY zeolite by dealumination using different solutions of citric acid, EDTA-2Na, and both EDTA-2Na and citric acid of specific concentrations. After the modification, the Si/Al ratio of the modified catalysts increased compared to the parent NaY, with the citric acid modified zeolite recording the highest increase of 28 % dealumination. The lowest dealumination was for the EDTA-2Na modified zeolite (9 %). Catalytic data showed that the modified catalysts could activate medium chain paraffin (n-octane), and this was due to the increased acid strength of the modified catalysts. The study showed that the activity of the dealuminated catalysts depends on the type of acid used for the dealumination, as this affects the extent of dealumination and also the type of aluminium getting dealuminated (framework or non-framework). [8] Complex modified catalysts recorded the highest conversion because of the removal of both framework and non-framework aluminium which improved both the surface area and pore volumes of the catalyst. The results obtained also confirmed results from the previous studies that the stronger the acidity of the catalysts, the more selective it will be towards the CO_x and the cracked products under the ODH conditions.

The results obtained showed that one needed to improve the ODH properties of the prepared catalysts. A series of gallium modified catalysts were then prepared from the dealuminated NaY zeolite catalysts. This was carried out using a modified ionic exchange. As expected, the conversion for all the catalysts was enhanced in the following order: Ga-NaY[AL] < Ga-NaY[CAT] < Ga-NaY[CT]. The difference in the conversion increase was due to the removal of either non- or framework aluminium which caused the Ga species to be in different positions in the pores of the zeolites. This was also evident from the different reduction profiles obtained for the catalysts from the TPR analysis. The increase in the conversion was attributed to Ga acting as the Lewis acid site on the extra framework of the zeolite. [8,9] The results, as expected showed the influence of Ga as the oxidative dehydrogenation-promoting metal, however, still the acidity outweighed that effect as overoxidation led to high selectivity towards CO_x.

Lastly, post-synthetic modification of a series of dealuminated Ga-NaY zeolites by the introduction of barium was carried out using an ionic exchange procedure in order to facilitate the quick desorption of the oxidative dehydrogenation products. Due to the high acidity of the

catalysts, the effect of Ba was only slightly noticed in the results, with only a small decrease in CO_x selectivity. A notable increase in the cracked products and oxygenates was recorded. These results showed that the introduction of Ba does introduce basicity, hence the CO_x went down as the products were desorbed more quickly than cracked products and oxygenates. The extent at which this happened may be a question of how much barium was added.

Therefore, the study showed that the dealuminated NaY zeolites can activate a medium-chain paraffin such as n-octane because of the strengthened acid sites. The conversion depends on the type of acid modifier used, as some remove the framework aluminium, some the non-framework and some can remove both. Mixing two modifiers had a positive effect on the activation of n-octane in terms of conversion. The introduction of gallium, as expected from the literature, improved the conversion and selectivity of the catalysts by lowering the CO_x selectivity. Barium on the other hand had minimal influence. However, it also behaved as expected by reducing the CO_x selectivity and increasing cracked products and oxygenates selectivity. The results of the study gave improved conversions, but not good selectivity towards the ODH products (olefins and aromatics), and this could be because of the small concentrations of gallium and barium used for the modification. For future study, different wt% of gallium and barium can be investigated together with the method of introducing the two metals. This may lead to improvement when it comes to using dealuminated NaY zeolites for the ODH reactions.

References

1. Elkhalifa, E.A. and Friedrich, H.B. 2010. Oxidative dehydrogenation of n-octane using vanadium-magnesium oxide catalysts with different vanadium loadings. Applied Catalysis A: General, 373, 122-131.
2. Asinger, F. 2016. Paraffins: Chemistry and Technology, Elsevier Science.
3. Cavani, F. and Trifirò, F. Partial oxidation of C_2 to C_4 paraffins. Basic Principles in Applied Catalysis, 75, 21-84.
4. Vedrine, J.C. 2016. Heterogeneous partial (amm)oxidation and oxidative dehydrogenation catalysis on mixed metal oxides. Catalysts, 6, 22-48.
5. Zang, J., Yu, H., Liu, G, Hong, M., Liu, J. and Chen, T. 2023. Reasearch progress on modification of zeolite Y for improved catalytic properties. Inorganics, 11, 22-41.

6. Wu, Z. and Zhao, D. 2011. Ordered mesoporous materials as adsorbents. Chemical Communications, 47, 3332-3338.
7. Vermeiren, W. and Gilson, J.P. 2009. Impact of zeolites on the petroleum and petrochemical industry. Topics in Catalysis, 52, 1131-1161.
8. Qiao, K., Wei, L., Feng, R., Yan, Z., Zhang, Z. and Gao, X. 2015. Preparation and characterization of hierarchical USY by post-treatment. Applied Petrochemical Research, 5, 313-319.
9. Xin, M., Xing, E., Gao, X., Wang, Y., Ouyang, Y., Xu, G., Luo, Y. and Shu, X. 2019. Ga substituted during modification of ZSM-5 and its influences on catalytic aromatization performance. Industrial and Engineering Chemistry Research, 58, 6970-6981.

Appendix

Degree of crystallinity calculation:

$$\text{Crystallinity} = \frac{Sum\ total\ of\ relative\ intensities\ of\ NaY\ observed}{Sum\ total\ of\ relative\ intensities\ of\ NaY\ standard} \times 100\ \%$$

Where the sum total of relative intensities taken were for the characteristic peaks (2∅, 6.2 º, 15.6 º, and 22.1 º), Commercial NaY was taken as the standard.

Calculation of the conversion, selectivity and carbon balance:

$$\text{Conversion} = \frac{Moles\ of\ reactants\ initially\ added - Moles\ of\ Reactants\ out}{Moles\ of\ reactant\ initially\ \ added} \times 100\ \%$$

$$\text{Selectivity} = \frac{Moles\ of\ Specific\ product\ formed}{Moles\ of\ all\ products\ formed} \times 100\ \%$$

$$\text{Carbon Balance} = \frac{Moles\ of\ carbon\ out}{Moles\ of\ carbon\ in} \times 100\ \%$$

Table A1. XRF results for elemental composition

Catalysts	Concentration (mol/L)	Si content (mass%)	Al content (mass%)
NaY	-	14.8	14.3
NaY[AL]	0.2	16.9	11.7
NaY[CAT]	0.2	13.9	13.2
NaY[CT]	0.1	15.6	13.0

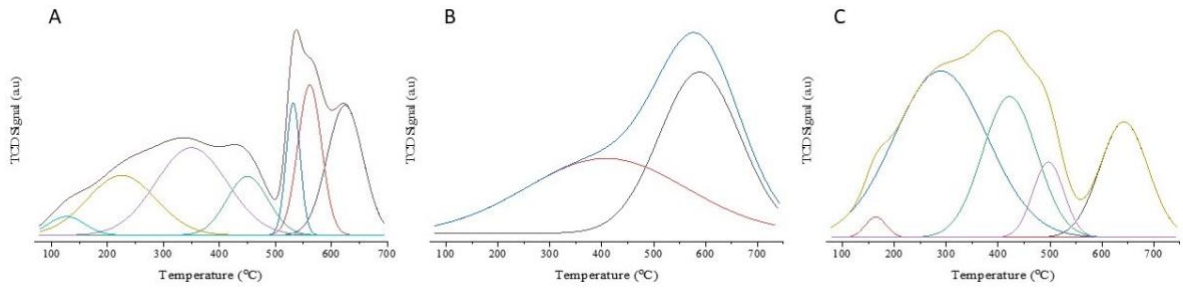

Figure A1. NH_3-TPD Profiles of (**A**) BaGa-NaY[AL], (**B**) BaGa-NaY[CT], (**C**) BaGa-NaY[CAT]

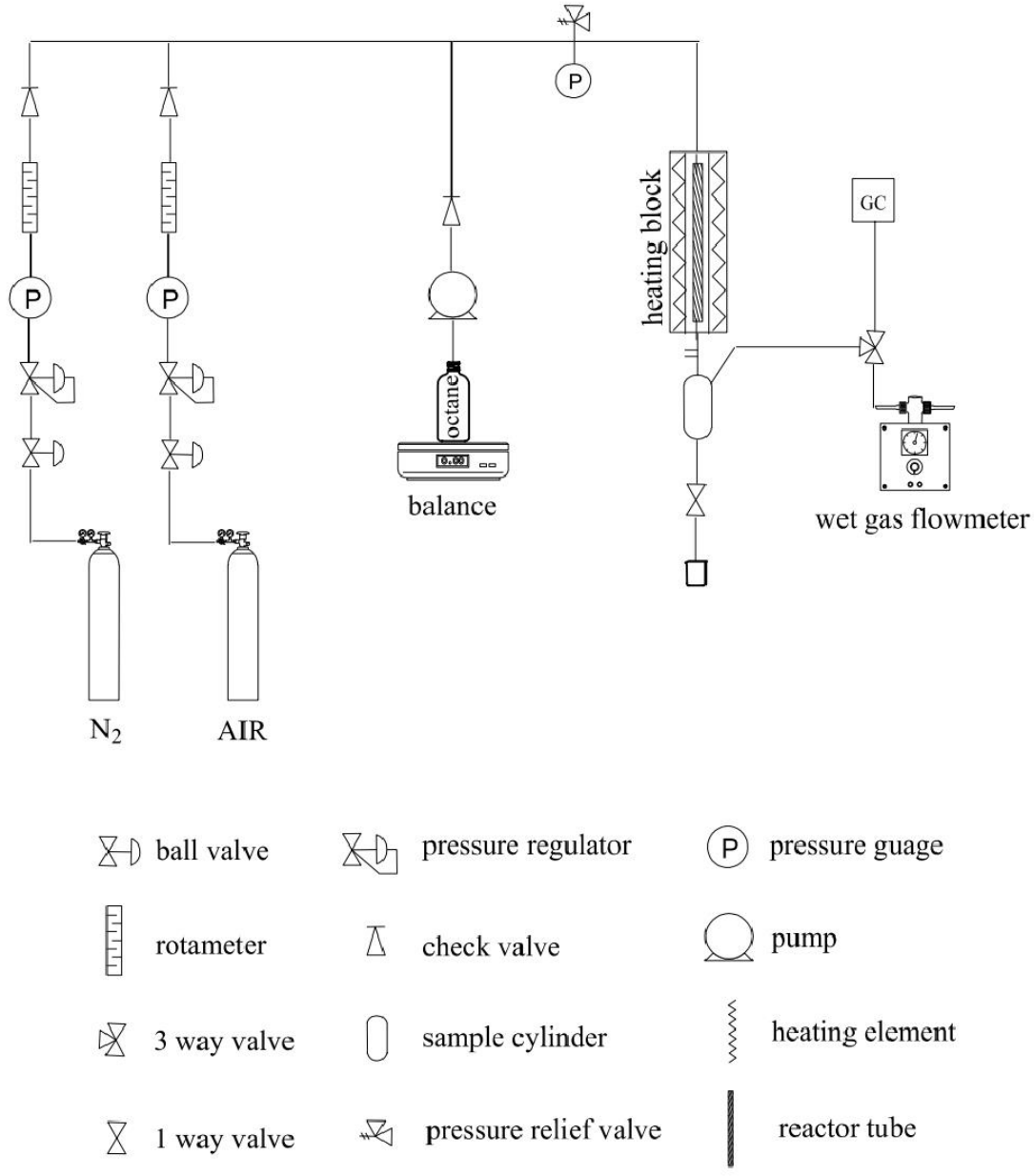

Figure A2. Reactor design (schematic representation) used for experimental work

SHIMADZU
LabSolutions

Majid repot

<Sample Information>

Sample Name	: BaGa-NaY[AL]2		
Sample ID	: BaGa-NaY[AL]2		
Data Filename	: BaGa-NaY[AL]2.gcd		
Method Filename	: Shamla_Mar 2019_Octane.gcm		
Batch Filename	:		
Vial #	: 1	Sample Type	: Unknown
Injection Volume	: 1 uL		
Date Acquired	: 2023/11/17 09:23:46	Acquired by	: System Administrator
Date Processed	: 2023/11/17 09:59:22	Processed by	: System Administrator

<Chromatogram>

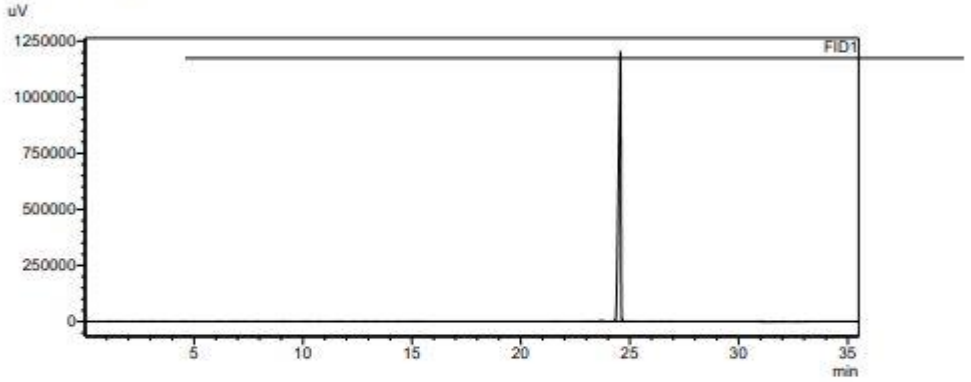

<Peak Table>

FID1

Peak#	Ret. Time	Name	Area	Area%
1	0.107		283	0.003
2	1.061		141	0.002
3	1.405		849	0.009
4	1.593		151	0.002
5	2.209		577	0.006
6	2.560		373	0.004
7	2.617		147	0.002
8	2.811	Propene	235	0.003
9	3.013	Butene	412	0.005
10	3.174		230	0.003
11	3.488		815	0.009
12	3.626	Pentene	574	0.006
13	4.407		122	0.001
14	4.455		287	0.003
15	4.532		455	0.005
16	4.960		374	0.004
17	6.056		295	0.003
18	6.149		192	0.002
19	6.274		145	0.002

Figure A3. GC chromatogram processed results for BaGa-NaY[AL] (liquid)

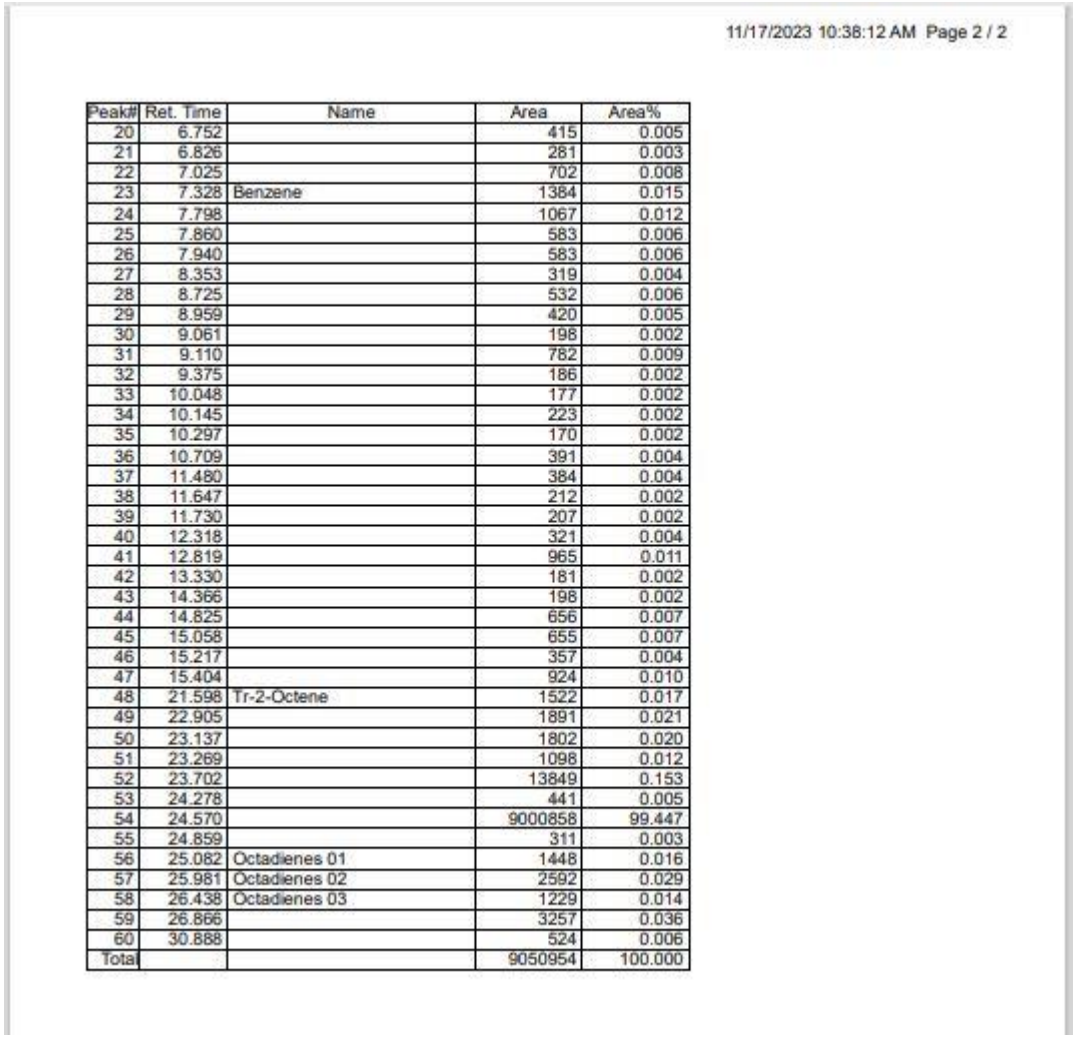

11/17/2023 10:38:12 AM Page 2 / 2

Peak#	Ret. Time	Name	Area	Area%
20	6.752		415	0.005
21	6.826		281	0.003
22	7.025		702	0.008
23	7.328	Benzene	1384	0.015
24	7.798		1067	0.012
25	7.860		583	0.006
26	7.940		583	0.006
27	8.353		319	0.004
28	8.725		532	0.006
29	8.959		420	0.005
30	9.061		198	0.002
31	9.110		782	0.009
32	9.375		186	0.002
33	10.048		177	0.002
34	10.145		223	0.002
35	10.297		170	0.002
36	10.709		391	0.004
37	11.480		384	0.004
38	11.647		212	0.002
39	11.730		207	0.002
40	12.318		321	0.004
41	12.819		965	0.011
42	13.330		181	0.002
43	14.366		198	0.002
44	14.825		656	0.007
45	15.058		655	0.007
46	15.217		357	0.004
47	15.404		924	0.010
48	21.598	Tr-2-Octene	1522	0.017
49	22.905		1891	0.021
50	23.137		1802	0.020
51	23.269		1098	0.012
52	23.702		13849	0.153
53	24.278		441	0.005
54	24.570		9000858	99.447
55	24.859		311	0.003
56	25.082	Octadienes 01	1448	0.016
57	25.981	Octadienes 02	2592	0.029
58	26.438	Octadienes 03	1229	0.014
59	26.866		3257	0.036
60	30.888		524	0.006
Total			9050954	100.000

Figure A4. GC chromatogram processed results continuation for BaGa-NaY[AL] (liquid)

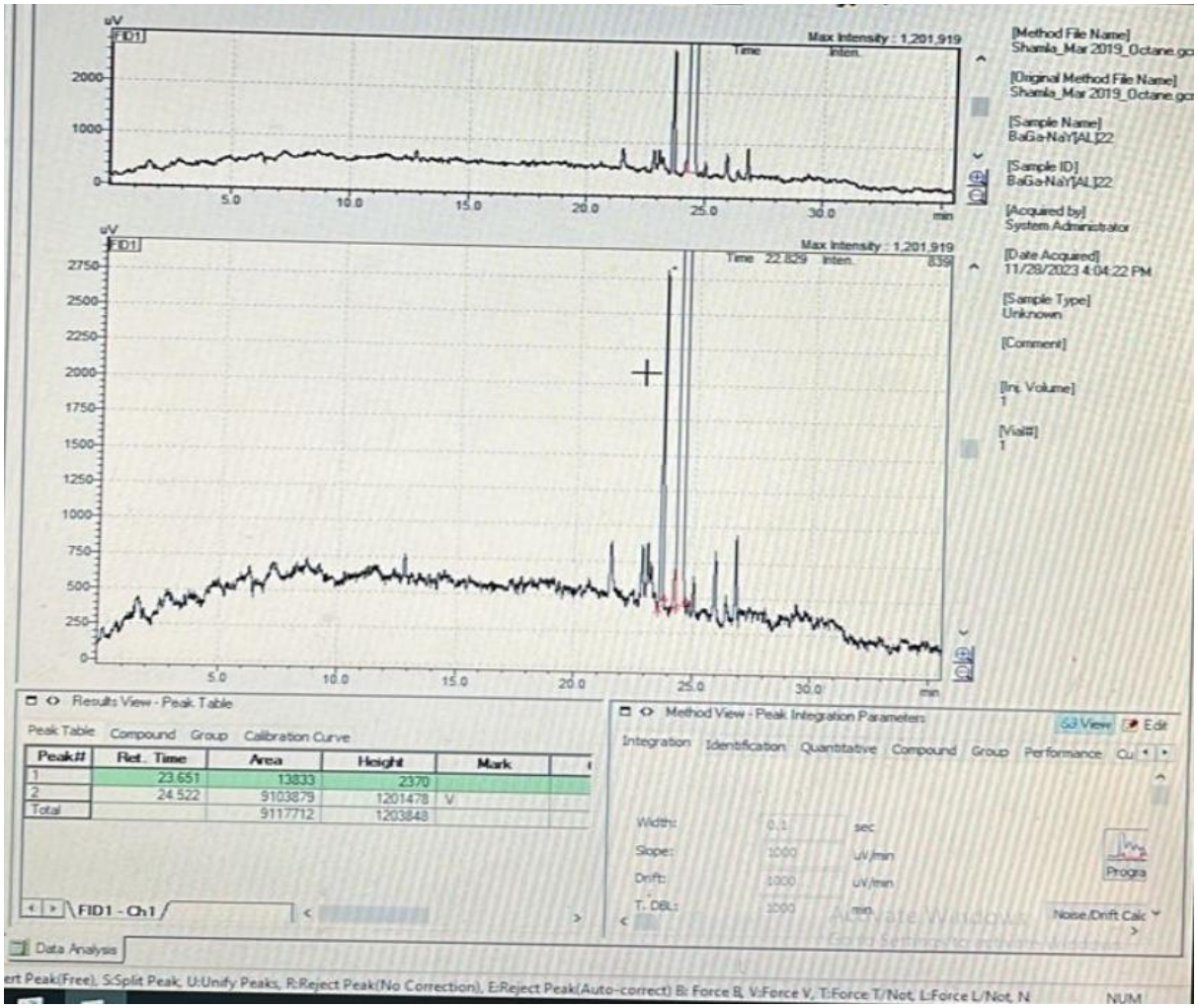

Figure A5. GC chromatogram for BaGa-NaY[AL] (liquid)

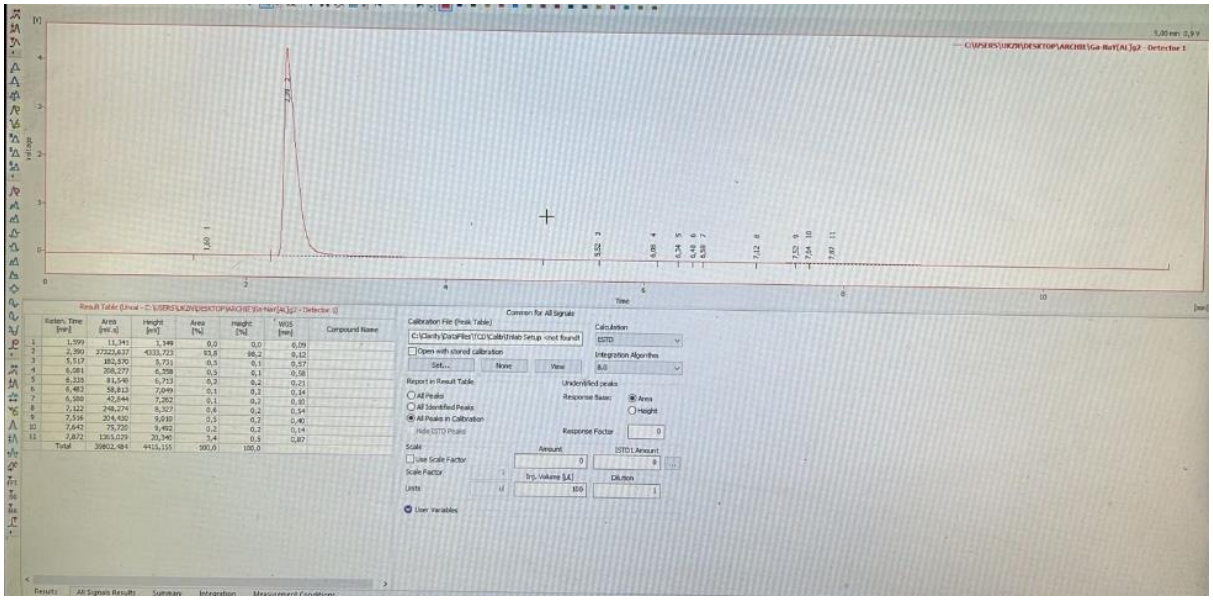

Figure A6. FID chromatogram for Ga-NaY[AL] (gas)